VARIATIONS IN THE ATMOSPHERIC METHANE BUDGET AFTER THE MOUNT PINATUBO ERUPTION

Narcisa Laura Bândă

Narcisa Laura Bândă
Institute for Marine and Atmospheric research Utrecht (IMAU)
Atmospheric Physics and Chemistry group

Current address:
Institute for Marine and Atmospheric research Utrecht (IMAU)
Utrecht University
P.O. Box 80005, 3508 TA Utrecht, The Netherlands
N.L.Banda@uu.nl

ISBN: 978-90-393-6363-8
Printing: Ridderprint, the Netherlands
Cover design: Valeriu Nechita

VARIATIONS IN THE ATMOSPHERIC METHANE BUDGET AFTER THE MOUNT PINATUBO ERUPTION

Variaties in het atmosferisch methaanbudget na de uitbarsting van Mount Pinatubo
(met een samenvatting in het Nederlands)

Variaţii ale bugetului metanului în atmosferă după erupţia vulcanului Pinatubo
(cu rezumat în română)

Proefschrift

ter verkrijging van de graad van doctor aan de Universiteit Utrecht op gezag van de rector magnificus, prof.dr. G.J. van der Zwaan, ingevolge het besluit van het college voor promoties in het openbaar te verdedigen op

woensdag 1 juli 2015 des middags te 12.45 uur

door

NARCISA LAURA BÂNDĂ

geboren op 23 juni 1986
te Satu Mare, Roemenië

PROMOTOREN:	Prof.dr. M. C. Krol
	Prof.dr. T. Röckmann
COPROMOTOREN:	Dr. T. P. C. van Noije
	Dr. M. van Weele

This thesis was accomplished with financial support from the NWO program 'Feedbacks in the Climate System', grant number 829.09.008.

CONTENTS

SUMMARY

Methane is the second most important anthropogenic greenhouse gas. Methane concentrations in the atmosphere have been increasing rapidly since the 18th century due to increasing anthropogenic emissions. The increase of methane concentrations slowed down in the past three decades, and the atmospheric growth rate showed variations that are not fully understood. This thesis aims to improve our understanding of the processes driving methane burden changes in the atmosphere by analyzing the variations in the methane growth rate in the years following the eruption of Mt. Pinatubo on 15 June 1991. This period was marked by anomalous climate conditions and perturbed atmospheric photochemistry caused by the eruption, which led to variations in both the methane emissions and the methane chemical removal from the atmosphere.

The eruption of Mt. Pinatubo was the largest eruption in the past century, and so far the only eruption of this size that has been monitored by both ground based and satellite instruments. The NOAA network of continuous methane measurements observed a slight increase in the global mean growth rate, followed by a sharp decrease by more than 10 ppb/yr over the first year after the eruption, and a partial recovery in the next year.

Variations in atmospheric methane concentrations can be caused by variations in either sources or sinks. Methane is emitted from natural and anthropogenic sources, with a significant contribution from natural emissions from wetlands. The main removal mechanism of methane from the atmosphere is its reaction with the hydroxyl radical (OH) in the troposphere. OH concentrations are determined by complex photochemistry, sensitive to levels of Ultra-Violet (UV) radiation and water vapour.

In contrast to more frequent minor volcanic eruptions, the plume of the explosive eruption of Mt. Pinatubo reached the stratosphere. The eruption emitted about 20 Tg of sulfur dioxide (SO_2), forming sulfate aerosols that remained in the stratosphere for a few years. Due to the size of the eruption, as well as the location of Pinatubo in the tropics, the eruption significantly perturbed the global climate. The Pinatubo sulfate aerosols caused a prolonged reduction in the amount of sunlight reaching the troposphere, a 0.5°C decrease in the global mean temperature near the surface, and enhanced stratospheric ozone depletion. The stratospheric aerosols and the increased ozone depletion caused changes in the amount of UV radiation, which affected OH concentrations and the methane removal rate in the troposphere. Moreover, the global cooling decreased both the methane emission rates from wetlands and the rate of methane removal by reaction with OH, both processes being temperature dependent. The OH production further responded to the decrease in wa-

ter vapour associated with the temperature reduction. Other potential effects of the eruption on the methane budget include changes in the transport between the troposphere and the stratosphere, inhibition of wetland emissions due to sulfur deposition and changes in natural emissions of other compounds that react with OH.

Methane concentrations in the period after the Pinatubo eruption were also affected by other factors of natural variability, such as the El Nino Southern Oscillation (ENSO) and biomass burning events. A decrease in anthropogenic emissions of methane after the collapse of the Soviet Union was also hypothesized as a cause for the decrease in methane growth rate in the time period after the eruption.

This thesis quantified the combined effect that the above processes had on methane variability in the first years following the eruption. In Chapter 3 we first investigated the drivers of methane variability after the eruption from a global perspective, using a one-dimensional chemistry model representative for the global tropospheric column. The changes in UV radiative fluxes were inferred by coupling the chemistry model to a radiative transfer model. Global mean perturbations in SO_2, sulfate, ozone column and temperature were applied to evaluate their impact on methane concentrations.

In this one-dimensional study, we found that the overall effect of natural processes after the eruption on the methane growth rate was dominated by the reduction in methane lifetime due to stratospheric ozone depletion. However, all the other processes also had non-negligible effects. The effect of the climate and photochemical changes after the eruption was an initial increase of 2 to 3 ppb/yr in the methane growth rate, followed by a sharp decrease in the growth rate of about 7 ppb/yr by mid-1993. When changes in anthropogenic emissions were taken into account according to emission inventories, an additional decrease of about 5 ppb/yr was obtained between the years 1991 and 1993. While the magnitudes of these changes are similar to observations, the decrease in the methane growth rate was simulated about 9 months later in the model than observed.

Using a one-dimensional model to represent global tropospheric chemistry, such as described in Chapter 3, had several shortcomings. It was not possible to take into account atmospheric transport and regional differences in the drivers of methane variability after the eruption. Clean and polluted regions with different chemical regimes could not be distinguished, nor the local sensitivity of OH chemistry to a particular driver. These issues were addressed in Chapters 4 and 5 through the use of a three-dimensional global chemistry and transport model (TM5).

As a first step in investigating the impact of the Pinatubo eruption with TM5, we simulated the evolution of stratospheric SO_2 and sulfate aerosols from the eruption. In Chapter 4, their effect on tropospheric photolysis frequencies and concentrations of OH and methane were quantified for the first time using the three-dimensional model. In order to obtain a good performance in reproducing satellite observations of SO_2 and sulfate after the eruption, the number of vertical layers in the model had to be increased from 34 to 60, and the representation of the aerosol size distribution had to be adjusted for typical stratospheric conditions. To further assess their impact

on methane, the simulated SO_2 concentrations and aerosol optical properties were coupled to the radiative transfer calculations used to determine photolysis frequencies.

Stratospheric sulfur from Pinatubo was found to decrease the photolysis frequencies of both ozone and nitrogen dioxide by about 2% globally. These photolysis reactions are involved in producing and recycling atmospheric OH, therefore we also found a 2% decrease in global OH concentrations in the first two years after the eruption. The effect of stratospheric sulfur on global OH and methane was dominated by the effect of scattering of UV radiation by aerosols, while absorption of UV radiation by SO_2 contributed 12.5% to the overall effect in the first year after the eruption. The reduction in OH concentrations caused an increase in the methane growth rate of 4 and 2 ppb/yr in the first and second year after the eruption, respectively, explaining 11 Tg of the 27 Tg observed methane burden change in late 1991 and early 1992.

In Chapter 5 we revisited the processes driving methane variability after the Pinatubo eruption using TM5. Seven potential drivers of variability were taken into account: stratospheric sulfur from the eruption, changes in stratospheric ozone, meteorology, emissions of methane from wetlands, biomass burning and anthropogenic activity, and emissions of other species (carbon monoxide, non-methane volatile organic compounds (NMVOCs), nitrogen oxides). We find that variations in the atmospheric methane growth rate during the period 1990 to 1995 were primarily determined by stratospheric aerosols from the eruption, and by changes in stratospheric ozone levels, temperature and humidity, methane emissions from wetlands, biogenic NMVOC emissions, and biomass burning emissions. Each of these processes caused variations of the order of 2 to 6 ppb/yr in the methane growth rate, and the effects were found to partly counteract each other. UV absorption by volcanic SO_2, changes in the exchange between the stratosphere and the troposphere, and in anthropogenic emissions were estimated to have a smaller impact on the global methane variability in the early 1990s, of less than 1 ppb/yr each. Overall we were able to reproduce a decrease in the methane growth rate of about 10 ppb/yr in the years after the Pinatubo eruption.

As in the case of the one-dimensional study, the minimum methane growth rate in the model occurred about 6 to 9 months later than in the observations. An additional decrease of about 20 Tg/yr in the methane burden in the atmosphere in the northern tropical region would be needed in our simulations during 1991 to 1994 to match the observed methane concentrations. Potential reasons for this mismatch are unaccounted methane emission variations in tropical wetlands, in combination with uncertainties in biogenic NMVOC emissions and chemistry, and not well-constrained biomass burning emissions. Two state-of-the-art inventories were used for methane emissions from wetlands, derived from the ORCHIDEE and LPJ dynamic vegetation models, to investigate the role of uncertainties in these emissions. Although the higher climate sensitivity of ORCHIDEE improves the simulated methane growth rate change after

the Pinatubo eruption, neither of the wetland emission inventories properly captured the observed timing of methane variations in this period.

The results presented in this thesis show that we have a good understanding of the most important processes driving methane variability in the time period after the Pinatubo eruption. Large uncertainties remain in the sensitivity of the methane emissions from wetlands and biogenic NMVOC emissions to the climate perturbation after the eruption. In Chapter 6, we summarized our recommendations for future research to further improve our understanding of the impact of a major volcanic eruption on methane concentrations, and of the drivers of atmospheric methane variability and trends in general.

SAMENVATTING

Methaan is het op één na belangrijkste antropogene broeikasgas. Ten gevolge van een aanhoudende groei in antropogene emissies sinds de 18^{e} eeuw zijn de methaanconcentraties in de atmosfeer snel toegenomen. Gedurende de laatste dertig jaar nemen de concentraties echter minder snel toe en laat de groeisnelheid variaties zien die nog niet goed worden begrepen. Dit proefschrift probeert meer inzicht te verkrijgen in de verschillende processen die tot veranderingen in de hoeveelheid methaan in de atmosfeer leiden. Hiertoe analyseren we de fluctuaties in de groeisnelheid van de methaanconcentraties in de jaren na de uitbarsting van Mt. Pinatubo op 15 juni 1991. Deze tijdsperiode werd gekenmerkt enerzijds door veranderende klimaatcondities ten gevolge van de eruptie en anderzijds door gerelateerde verstoringen van de fotochemie in de atmosfeer. Hierdoor traden veranderingen op in zowel de methaanemissies als de chemische afbraak van methaan in de atmosfeer.

De eruptie van Mt. Pinatubo in 1991 was de grootste vulkaanuitbarsting in de 20^{e} eeuw en tot nu toe de enige eruptie van een dergelijke orde die zowel door grond- als door satellietwaarnemingen is waargenomen. Het mondiale NOAA-netwerk van grondstations met continue methaanwaarnemingen laat een kleine toename zien in de wereldgemiddelde groeisnelheid die in het eerste jaar na de eruptie sterk afnam met meer dan 10 ppb en vervolgens zich deels weer herstelde in het tweede jaar na de eruptie.

Fluctuaties in de atmosferische methaanconcentraties kunnen zowel door variaties in de bronnen als in de verliesprocessen worden veroorzaakt. Methaan wordt door natuurlijke en door antropogene bronnen uitgestoten, waarbij de natuurlijke emissies van wetlands een belangrijke bijdrage leveren. Het belangrijkste verwijderingsmechanisme voor atmosferisch methaan is de chemische reactie met het hydroxylradicaal (OH) in de troposfeer. De OH-concentraties in de atmosfeer worden bepaald door ingewikkelde atmosferische chemie in interactie met waterdamp en de ultraviolette (UV) straling van de zon.

In tegenstelling tot de veelvuldig voorkomende kleinere vulkaanuitbarstingen bereikte de pluim van de explosieve eruptie van Mt. Pinatubo in 1991 de stratosfeer. De uitbarsting bracht ongeveer 20 Tg zwaveldioxide (SO_2) in de atmosfeer, waarbij sulfaatdeeltjes (aerosolen) werden gevormd die gedurende enkele jaren in de stratosfeer aanwezig bleven. De eruptie verstoorde tijdelijk het klimaat wereldwijd, enerzijds door de grootte van de uitbarsting en anderzijds door de locatie van Mt. Pinatubo in de tropen. De sulfaataerosolen gevormd na de uitbarsting veroorzaakten een langdurige afname van de hoeveelheid zonlicht die de troposfeer kon bereiken, wat leidde tot een afname van 0.5°C in de wereldgemiddelde temperatuur nabij het

aardoppervlak en daarnaast tot een toename van de chemische afbraak van ozon in de stratosfeer. Zowel de aerosolen als de extra ozonafbraak leidden tot veranderingen in de hoeveelheid UV-straling in de troposfeer, waardoor de concentraties van OH en dus ook de verwijderingssnelheid van methaan veranderden. Daarnaast verminderde de wereldwijde afkoeling de mate waarin wetlands methaan emitteerden en ook de verwijderingssnelheid van methaan door de reactie met OH, doordat beide processen temperatuurafhankelijk zijn. De chemische aanmaak van OH-radicalen reageerde verder ook op de afname van waterdamp in de atmosfeer als gevolg van de afkoeling. Andere mogelijke invloeden van de eruptie op het methaanbudget in de atmosfeer zijn o.a. veranderingen in het transport tussen de troposfeer en de stratosfeer, de eventuele beperking van methaanemissies van wetlands ten gevolge van zwaveldepositie en veranderingen in de natuurlijke emissies van andere gassen in de atmosfeer die met het OH-radicaal reageren.

De methaanconcentraties in de periode na de uitbarsting reageerden ook op andere natuurlijke variaties in het klimaatsysteem zoals de *El Niño Southern Oscillation* (ENSO) en grootschalige verbranding van biomassa ten gevolge van aanhoudende droogte. Een andere hypothese die in het verleden is geopperd om de afname van de groeisnelheid van methaan in de periode direct na de uitbarsting te verklaren, is een afname van de antropogene methaanemissies na de ineenstorting van de Sovjet-Unie.

In dit proefschrift hebben we het gecombineerde effect dat de hierboven genoemde processen hebben gehad op de methaanvariaties in het eerste jaar na de eruptie gekwantificeerd. In Hoofdstuk 3 hebben we eerst vanuit een mondiaal perspectief onderzoek gedaan naar de oorzaken van de methaanfluctuaties die optraden na de eruptie, waarbij we gebruik hebben gemaakt van een eendimensionaal chemiemodel dat representatief is voor de mondiale troposfeer. De veranderingen in de UV-stralingsfluxen zijn afgeleid door een koppeling van het chemiemodel met een stralingstransportmodel. Hierbij hebben we wereldgemiddelde verstoringen in SO_2, sulfaat, ozonkolom en temperatuur aangebracht om de effecten van deze verstoringen op de methaanconcentratie in het model te evalueren.

Aan de hand van deze eendimensionale studie hebben we gevonden dat het gecombineerde effect van natuurlijke processen op de groeisnelheid van methaan na de vulkaanuitbarsting werd gedomineerd door de afname in de methaanlevensduur als gevolg van ozonafbraak in de stratosfeer. Tegelijkertijd waren ook de effecten van elk van de andere bestudeerde processen niet verwaarloosbaar. Volgens het model was het gecombineerde effect van de veranderingen in het klimaat en de fotochemie na de uitbarsting eerst een toename in de groeisnelheid met 2 tot 3 ppb/jaar, gevolgd door een sterke afname in de groeisnelheid met ongeveer 7 ppb/jaar halverwege 1993. Indien we ook veranderingen in de antropogene emissies meenamen in het model - in lijn met state-of-the-art-emissie-inventarisaties - verkregen we in de jaren 1991 tot 1993 een extra afname in de groeisnelheid met ongeveer 5 ppb/jaar. Alhoewel de orde van grootte van de gevonden veranderingen overeenkomt

met de waarnemingen vindt de afname in de groeisnelheid in het model ongeveer 9 maanden later plaats dan de waarnemingen aangeven.

Het gebruik van een eendimensionaal model voor de mondiale troposferische chemie zoals beschreven in Hoofdstuk 3 heeft verschillende beperkingen. Het was bijvoorbeeld niet mogelijk om transport in de atmosfeer en regionale verschillen in de oorzaken van de methaanvariabiliteit in de periode na de uitbarsting mee te nemen. Schone en vervuilde regio's met verschillende chemische regimes konden niet worden onderscheiden, net zo min als de lokale gevoeligheid van de OH-chemie voor een specifieke factor. Deze tekortkomingen hebben we vervolgens geadresseerd in de Hoofdstukken 4 en 5 door gebruik te maken van een driedimensionaal chemie- en transportmodel (TM5).

Als eerste stap in het onderzoek naar de gevolgen van de uitbarsting met behulp van TM5 hebben we het verloop van de concentraties van stratosferisch SO_2 en de sulfaataerosolen na de uitbarsting gesimuleerd. In Hoofdstuk 4 hebben we, voor de eerste keer door gebruik te maken van een 3D-model, het effect hiervan op de fotolysesnelheden in de troposfeer en op de concentraties van OH en methaan gekwantificeerd. Om de kwaliteit van de modelsimulaties te verbeteren in vergelijking met satellietwaarnemingen van SO_2 en sulfaat na de uitbarsting moest het aantal verticale lagen in het model worden vergroot van 34 naar 60. Ook moest de representatie van de grootteverdeling van de sulfaataerosolen worden aangepast aan de specifieke stratosferische omstandigheden. De gesimuleerde SO_2-concentraties en aerosoleigenschappen zijn vervolgens gekoppeld met de stralingstransportberekeningen in TM5 die worden gebruikt voor de bepaling van de fotolysesnelheden.

De zwavelverbindingen die door de eruptie in de stratosfeer zijn gebracht hebben wereldwijd tot een afname van ongeveer 2% geleid in de fotolysesnelheden van ozon en stikstofdioxide, met als gevolg een vergelijkbare reductie in de wereldwijde OH-concentraties gedurende de eerste twee jaar na de uitbarsting. Het grootste effect van de zwavelverbindingen op OH en methaan konden we toeschrijven aan de extinctie van zonlicht door aerosolen, terwijl de absorptie van UV-straling door SO_2 volgens het model 12.5% heeft bijgedragen aan het totale effect in het eerste jaar. De afname in OH-concentraties hebben geleid tot een toename in de methaangroeisnelheid met respectievelijk 4 en 2 ppb/jaar in het eerste en tweede jaar na de uitbarsting. Deze effecten verklaren hiermee 11 Tg van de waargenomen verandering in de hoeveelheid methaan in de atmosfeer van 27 Tg in de laatste helft van 1991 en de eerste helft van 1992.

In Hoofdstuk 5 hebben we de oorzaken van de methaanvariaties in de jaren na de uitbarsting opnieuw onderzocht met TM5. Hierbij hebben we zeven mogelijke factoren onderscheiden, te weten: stratosferische zwavelverbindingen afkomstig van de uitbarsting, veranderingen in stratosferisch ozon, meteorologie, methaanemissies van wetlands, grootschalige verbranding van biomassa en antropogene activiteiten, en tenslotte emissies van andere stoffen (koolstofmonoxide (CO), vluchtige organische stoffen (NMVOCs) en stikstofoxiden). We hebben gevonden dat gedurende de

periode 1990 tot 1995 de groeisnelheid van methaan vooral gedreven is door de aanwezigheid van sulfaataerosolen en veranderingen in stratosferisch ozon, temperatuur en waterdamp, methaanemissies van wetlands, biogene NMVOC-emissies en emissies door verbranding van biomassa. Elk van deze processen heeft geleid tot veranderingen in de groeisnelheid van methaan van de orde van 2 tot 6 ppb/jaar waarbij de verschillende effecten elkaar deels tegen hebben gewerkt. Voor respectievelijk de absorptie van UV-straling door SO_2, veranderingen in de uitwisseling tussen de stratosfeer en de troposfeer en veranderingen in antropogene emissies vonden we een kleiner effect van minder dan 1 ppb/jaar in het begin van de jaren 90. Met alle effecten gecombineerd zijn we in staat om met het model de waargenomen afname in de groeisnelheid van methaan van ongeveer 10 ppb/jaar na de uitbarsting van Mt. Pinatubo te reproduceren.

Net als in de eendimensionale modelstudie vonden we ook met het 3D-model een minimum in de methaangroeisnelheid dat 6 tot 9 maanden later optreedt dan het waargenomen minimum. Om tot overeenstemming te komen met de waargenomen methaanconcentraties zou in de simulaties tussen 1991 en 1994 een extra afname nodig zijn van de hoeveelheid methaan in de noordelijke tropen van ongeveer 20 Tg/jaar. Mogelijke oorzaken van deze discrepantie zijn niet meegenomen veranderingen in methaanemissies van tropische wetlands, in combinatie met onzekerheden in biogene NMVOC-emissies en -chemie en in de emissies die verband houden met de verbranding van biomassa. Om de rol van onzekerheden in de emissies van wetlands nader te analyseren hebben we twee verschillende state-of-the-artinventarisaties gebruikt afkomstig van de dynamischevegetatiemodellen ORCHIDEE en LPJ. Hoewel de hogere klimaatgevoeligheid van ORCHIDEE een verbetering geeft voor de gesimuleerde groeisnelheid van methaan na de uitbarsting, hebben we het waargenomen tijdsverloop van de variaties in methaan in deze periode met geen van beide inventarisaties kunnen reproduceren.

De resultaten van het onderzoek in dit proefschrift laten zien dat we een goed begrip hebben van de belangrijkste processen die de methaanvariaties in de periode na de uitbarsting van Mt. Pinatubo hebben veroorzaakt. Desondanks blijven er grote onzekerheden bestaan met betrekking tot de gevoeligheid van de methaanemissies van wetlands en biogene NMVOC-emissies voor de verstoring van het klimaat na de uitbarsting. In Hoofdstuk 6 geven we een samenvatting van onze aanbevelingen voor toekomstig onderzoek naar het effect van een grote vulkaanuitbarsting op de methaanconcentraties in de atmosfeer en de oorzaken van de variabiliteit en trends in methaan in zijn algemeenheid.

REZUMAT

Metanul este cel mai important gaz cu efect de seră antropogen după dioxidul de carbon. Începând cu secolul al XVIII-lea, concentraţia de metan din atmosferă este in creştere datorită creşterii emisiilor antropogene. Rata de creştere metanului a scazut în ultimele trei decenii, prezentând variaţii care nu sunt complet înţelese. Scopul aceastei teze este de a îmbunătăţi înţelegerea proceselor care controlează schimbările care au loc în cantitătea de metan din atmosferă prin analiza variaţiilor ratei de creştere a metanului atmosferic din anii de după erupţia vulcanului Pinatubo pe 15 iunie 1991. Datorită erupţiei vulcanice, această perioadă a fost marcată de perturbăţii ale climei şi fotochimiei atmosferice care au determinat variaţii atât ale emisiilor de metan, cât şi ale proceselor chimice care elimină metanul din atmosferă.

Erupţia vulcanului Pinatubo din Filipine a fost cea mai mare erupţie vulcanică din ultimul secol. Până în prezent, este singura erupţie de această magnitudine care a putut fi monitorizată atât de instrumente de măsură de la sol cî şi din satelit. Reţeaua NOAA de măsurători continue ale concentraţiilor de metan a observat o uşoară intensificare a ratei de creştere globală după erupţie, urmată de o diminuare puternică de peste 10 ppb/an în cursul primului an de după erupţie şi o redresare partială în urmatorul an.

Variaţiile concentraţiei de metan din atmosferă pot fi generate de variaţii ale surselor sau ale pierderilor de metan. Metanul este emis din surse naturale şi antropogene, o contribuţie importantă având emisiile naturale din mlaştini. Procesul principal prin care metanul este eliminat din atmosfera este reacţia acestuia cu radiacalul hidroxil (OH) în troposferă. Concentraţia de OH este determinată de procese complexe de fotochimie atmosferică, care e sensibilă la nivelul de radiaţii ultraviolete şi de vapori de apă.

Spre deosebire de erupţiile vulcanice minore frecvente, norul erupţiei explozive al vulcanului Pinatubo a ajuns până în stratosferă. Erupţia a emis 20 Tg de dioxid de sulf (SO_2), formând particule de sulfat care au rămas timp de căţiva ani în atmosferă. Datorită mărimii erupţiei, cât şi a locaţiei în zona tropicală, erupţia lui Pinatubo a afectat semnificativ clima globală. Particulele de sulfat produse în stratosferă au determinat scăderea a intensităţii radiaţiei solare de la suprafaţa pământului, scăderea cu 0.5°C a temperaturii globale medii şi diminuarea accentuată a stratului de ozon. Sulfatul vulcanic şi diminuarea stratului de ozon au determinat schimbări în cantitatea de radiaţii ultraviolete care ajung in troposferă, care au afectat producţia de OH şi, implicit, eliminarea metanului din atmosferă prin reacţia cu OH. Răcirea globală de după erupţie a diminuat atât rata de emisie a metanului din mlaştini, cât şi eliminarea metanului prin reacţia cu OH, ambele procese fiind dependente de temperatură.

Producţia de OH a răspuns de asemenea la scăderea concentraţiei de vapori de apă asociată cu scăderea temperaturii. Alte efecte potenţiale ale erupţiei asupra bugetului de metan sunt schimbări în transportul dintre troposferă şi stratosferă, inhibarea emisiilor de metan datorită depunerii de sulf, şi schimbări în emisiile naturale ale altor compuşi care reacţionează cu OH.

Concentraţia de metan în perioada de după erupţia vulcanului Pinatubo a fost de asemenea afectată de alţi factori de variabilitate naturală, precum Oscilaţia Sudică El Niño şi incendiile de pădure şi de stepă. O alta ipoteză pentru cauza diminuării ratei de creştere a metanului în perioada de după erupţie este scăderea emisiilor antropogene ca urmare a prăbuşirii Uniunii Sovietice.

În cadrul aceastei teze, am cuantificat pentru prima dată efectul de ansamblu al proceselor de mai sus asupra variabilităţii metanului în anii de după erupţie. În Capitolul 3 am investigat factorii care determină variabilitatea metanului după erupţie dintr-o perspectivă globală, folosind un model uni-dimensional al chimiei atmosferice reprezentativ pentru coloana troposferică globală medie. Modificări ale nivelului de radiaţii ultraviolete au fost deduse prin cuplarea modelului chimic cu un model de transfer radiativ. Au fost aplicate perturbaţii în SO_2, sulfat, coloana de ozon şi temperatură pentru a evalua impactul acestora asupra concentratiei de metan.

Din acest studiu uni-dimensional a rezultat că efectul de ansamblu al proceselor naturale de după erupţie asupra ratei de creştere a metanului a fost dominat de scăderea timpului de rezidenţă al metanului în atmosferă datorită diminuării stratului de ozon. Cu toate acestea, toate celelalte procese au avut efecte non-neglijabile. Efectul schimbărilor climatice şi fotochimice de după erupţie a fost o intensificare iniţială de 2 până la 3 ppb/an a ratei de creştere a metanului, urmată de o diminuare puternică de aproximativ 7 ppb/an pană în vara anului 1993. Când variaţiile în emisiile antropogene au fost de asemenea luate în considerare, s-a obţinut o diminuare adiţională de 5 ppb/an între anii 1991 şi 1993. Deşi amplitudinea acestor variaţii este similară cu observaţiile, diminuarea ratei de creştere a metanului a fost simulată cu aproximativ 9 luni mai târziu decât a fost observată.

Utilizarea unui model uni-dimensional pentru a reprezenta chimia troposferică globală în Capitolul 3 a avut unele limitări. Nu a fost posibil să luăm în considerare transportul atmosferic şi diferenţele regionale în factorii de variabilitate ai metanului după erupţie. Nu au putut fi distinse regiuni curate şau poluate cu regim chimic diferit şi nici sensibilitatea locală a chimiei OH la un anumit factor. Aceste aspecte au fost adresate în Capitolele 4 şi 5 prin folosirea unui model tri-dimensional global de chimie şi transport atmosferic (TM5).

Într-o primă etapă de investigare a efectelor erupţiei lui Pinatubo în TM5, am simulat evoluţia norului de SO_2 şi de particule de sulfat de la erupţie. În capitolul 4, am cuantificat pentru prima dată folosind un model tri-dimensional efectul acestora asupra frecvenţelor de fotoliză în troposferă şi asupra concentraţiilor de OH şi metan. Pentru a obţine o performanţa bună în reproducerea observaţiilor de SO_2 şi sulfat din satelit, a trebuit mărit numărul de niveluri verticale ale modelului de la 35 la 61, iar

reprezentarea distribuţiei în mărime a particulelor a trebuit ajustată pentru condiţii tipice stratosferei. Pentru a evalua impactul acestora asupra metanului, concentraţiile de SO_2 şi proprietăţile optice ale aerosolilor au fost cuplate cu calculul transferului radiativ folosit pentru a determina frecvenţele de fotoliză.

Rezultatele noastre arată că sulful stratosferic provenit de la erupţia vulcanică a diminuat frecvenţa globală de fotoliză ale ozonului şi dioxidului de azot cu aproximativ 2%. Aceste reacţii de fotoliză sunt implicate în producerea şi reciclarea OH în atmosferă. În consecinţă, am obţinut o diminuare a concentraţiei globale de OH de 2% în primii doi ani de după erupţie. Acest efect al sulfului stratosferic asupra OH şi asupra metanului a fost dominat de efectul împrăştierii radiaţiei ultraviolete de către particule de sulfat, în timp ce absorbţia de ultraviolete a SO_2 a contribuit cu 12.5% în primul an de după erupţie.

În Capitolul 5 am reevaluat procesele care controlează variabilitatea metanului după erupţia vulcanului Pinatubo folosind TM5. Au fost luaţi în considerare şapte potenţiali factori de variabilitate: sulf stratosferic provenit de la erupţie, schimbări în stratul de ozon, meteorologie, emisii de metan din mlaştini, incendii şi activităţi antropice, emisii ale altor compuşi (monoxid de carbon, compuşi organici volatili nemetanici (COVnm), oxizi de azot). Rezultatele obţinute arată că variaţiile ratei de creştere a metanului în atmosferă în perioada 1990-1995 au fost determinate în principal de către particule de sulfat de la erupţia vulcanică, schimbări în nivelul de ozon stratosferic, temperatură şi umiditate, emisii de metan din mlaştini, emisii naturale de COVnm şi emisii din incendii. Fiecare din aceşti factori au determinat variaţii de 2 până la 6 ppb/an în rata de creştere a metanului, parţial compensându-se reciproc. Am estimat că absorbţia de ultraviolete de către SO_2, schimbările în transportul dintre troposferă şi stratosferă, şi schimbările emisiilor antropogene au avut un efect mai mic asupra variabilităţii globale a metanului în această perioadă, de mai putin de 1 ppb/an fiecare. Am putut să reproducem diminuarea ratei de creştere a metanului în atmosferă de aproximativ 10 ppb/an în anii de după erupţia vulcanului Pinatubo.

Precum în cazul studiului uni-dimensional, rata minimă de creştere a metanului a fost simulată 6 pană la 9 luni mai târziu decât a fost observată. O scădere adiţională de aproximativ 20 Tg/an în cantitatea de metan din atmosferă în regiunea tropicală nordică ar fi fost necesară în perioada 1991-1994 în simulările noastre pentru a obţine concentraţiile de metan observate. Posibile motive pentru această neconcordantă sunt variaţii ale emisiilor din mlastini din reginea tropicală care nu au fost luate in considerare, în combinaţie cu incertitudini ale emisiilor naturale şi a chimiei COVnm-lor, şi posibile erori în emisiile din incendii de păduri şi stepă.

Rezultatele prezentate în aceasta teză arată că deţinem o bună înţelegere a celor mai importante procese care au determinat variaţiile metanului în atmosferă în perioada de dupa erupţia lui Pinatubo. Rămân însă incertitudini semnificative privind sensibilitatea emisiilor de metan din mlastini şi ale emisiilor naturale de NMVOC la perturbaţia climatică de după erupţie. Capitolul 6 cuprinde recomandările noastre

pentru cercetări viitoare care ar îmbunătăţi în continuare înţelegerea impactului erupţiilor vulcanice asupra concentraţiilor de metan, şi a factorilor care controleaza în general variabilitatea şi tendinţele metanului atmosferic.

1

INTRODUCTION

1.1 ATMOSPHERIC METHANE AND TROPOSPHERIC PHOTOCHEMISTRY

1.1.1 *Relevance and past evolution of atmospheric methane*

Solar shortwave (SW) radiation, between about 100 nm and 4μm, is absorbed by the Earth's surface and atmosphere. The absorbed energy is then re-emitted as longwave (LW) radiation between about 5 and 100 μm. Atmospheric gases that absorb LW radiation re-emit the absorbed radiation partly back towards the surface, preventing it from leaving the Earth's atmosphere. This creates the 'greenhouse effect', which leads to a warming of the Earth's surface. Anthropogenic emissions of greenhouse gases since the industrial revolution have disturbed the natural radiative balance of the atmosphere. Global warming due to human activity has become apparent in recent decades, and is expected to continue throughout this century. A good understanding of the atmospheric budget of greenhouse gases is necessary in order to predict future concentrations and to assess what emission reductions would be most effective in limiting global warming.

Methane (CH_4) is the most important anthropogenic greenhouse gas after carbon dioxide (CO_2). Methane mole fractions in the past 800 thousand years oscillated between roughly 350 ppb during glacial periods and about 700 ppb during interglacial periods (Figure 1.1). Since the year 1750, CH_4 mole fractions have increased due to anthropogenic emissions from 700 ppb to nearly 1800 ppb in the present-day atmosphere. Although in the present-day atmosphere CH_4 has a mole fraction 200 times smaller than the mole fraction of CO_2, its efficiency in absorbing LW radiation is much larger than that of CO_2. The Intergovernmental Panel on Climate Change (IPCC) estimated that the radiative forcing related to the increased mole fraction of CH_4 between the years 1750 and 2011 is 0.48±0.05 W/m^2, contributing significantly to the 2.3 (1.1 to 3.3) W/m^2 total anthropogenic radiative forcing (Myhre et al. 2013). The radiative forcing attributed to the increase in CH_4 emissions since the year 1750 is about twice as large when feedbacks between CH_4 and other greenhouse gases are taken into account.

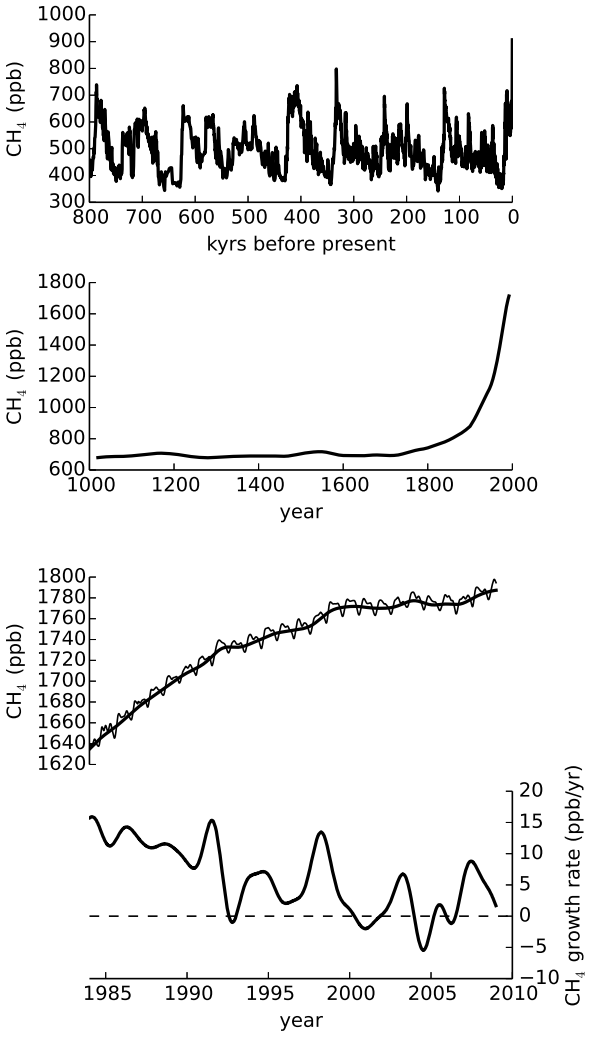

Figure 1.1: Evolution of atmopheric global mean methane mole fractions over different time scales: a) over the last 800 thousand years (800 kyrs) measured in ice cores (Loulergue et al. 2008); b) over the last millennium measured in firn air (Etheridge et al. 1998); c) over the past 26 years measured by the NOAA surface network (GLOBALVIEW-CH4 2009). d) Growth rate corresponding to c).

The record of continuous atmospheric measurements available since the 1980s shows a slow-down in the methane increase from 14 ppb/yr in the early 1980s to almost zero in the early 2000s and a renewed increase of 5 ppb/yr since 2007. Several processes have been proposed to explain the evolution of CH_4 mole fractions in the 1990s and 2000s, related to anthropogenic and natural emissions, and changes in the removal rate of CH_4 (Holmes et al. 2013; Kirschke et al. 2013; Monteil et al. 2011; Pison et al. 2013). However, the relative roles of CH_4 emissions and chemistry in both the long- and short-term evolution of CH_4 mole fractions are not well understood.

From the bottom panel of Figure 1 it is clear that large fluctuations in the CH_4 growth rate occurred in 1991-1993 and 1997-1998. The first event is related to the eruption of Mount Pinatubo in 1991, and the second one to a large El Niño event. The focus of this thesis is to investigate the processes causing the observed fluctuations in CH_4 concentrations in 1991-1993. We assess to what extent these fluctuations can be attributed to the eruption, which affected chemistry and climate for several years. Explaining the causes for the observed CH_4 fluctuations can help us better understand the processes driving CH_4 concentrations in the atmosphere, and improve our ability to predict the sensitivity of CH_4 concentrations to future changes in climate and chemistry.

1.1.2 *Sources and sinks*

CH_4 is emitted to the atmosphere from natural and anthropogenic sources. Figure 1.2 shows an overview of the emission categories and removal processes, and the associated source and sink strengths. It is estimated that half of the CH_4 is emitted from natural sources. Most of these CH_4 emissions are produced by organic matter decomposition by archaea microorganisms in anaerobic environments in wetland areas. The CH_4 is then emitted to the atmosphere by diffusion through the water column, ebullition or transport through plants. Part of the CH_4 is oxidized to CO_2 before reaching the atmosphere. The amount of CH_4 that is produced and emitted from wetlands depends on many environmental factors, such as temperature, water column depth and organic matter availability. It has been shown that the relationship between temperature and emissions can be approximated by an exponential function $E(T) = E(T_0) * Q_{10}^{(T-T_0)/10}$. The constant Q_{10} is the factor of emission rate increase for a 10-degree increase in temperature. Measured values for Q_{10} vary between 1.2 and 16 depending on the archaea species and substrate conditions at the different measurement locations (Dunfield et al. 1993; Ringeval et al. 2010; Valentine et al. 1994).

CH_4 is produced by similar processes in rice cultivation and landfills. Archaea in the stomach of ruminants cause additional CH_4 production from wild ruminants and agriculture. Other natural sources of CH_4 include production by termites and wild

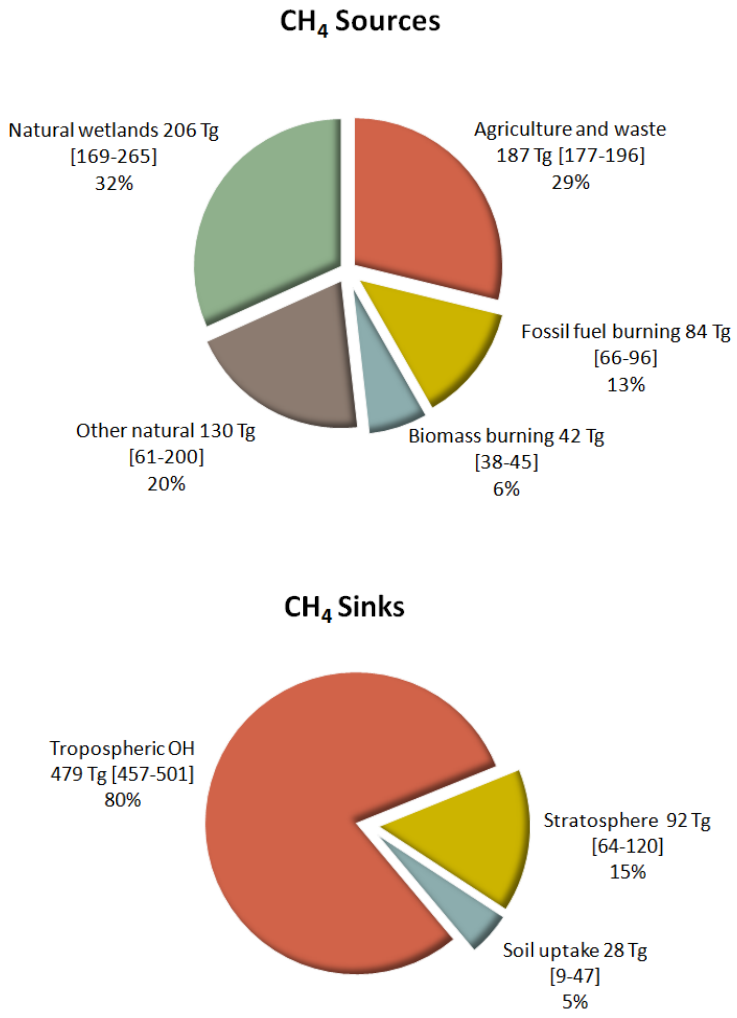

Figure 1.2: Methane source and sink categories. Numbers and uncertainty ranges as given by the bottom-up estimates from the IPCC 5th Assessment Report (Ciais et al. 2013).

animals, emissions from oceans and fresh-water bodies other than wetlands, and CH_4 from deep sediments released to the atmosphere from mud volcanoes and gas seeps. CH_4 produced under high pressure and temperature conditions in the deep sediments is also emitted to the atmosphere by leaks in gas extraction and distribution systems. Another source of CH_4 is incomplete combustion during forest fires and biofuel use.

The main CH_4 sink is the reaction with the hydroxyl radical (OH) in the troposphere, which removes about 80% of the atmospheric CH_4. The remaining 20% is removed by bacteria in the soil and by the reactions with OH, excited oxygen atoms ($O(^1D)$) and chlorine (Cl) in the stratosphere. The uncertainty in the absolute value of the total methane source and the total methane sink is of the order of 20%. Natural emissions determine a large part of the uncertainty in the CH_4 emissions. The small annual increase in CH_4 mole fractions of the order of 0-15 ppb/yr shows that the imbalance between its sources and sinks is less than 10%.

1.1.3 *Atmospheric chemistry*

The main mechanism of CH_4 removal from the atmosphere is its reaction with OH in the troposphere, which in turn is determined by complex photochemistry (Figure 1.3, Lelieveld et al. 2002). OH is primarily produced by ozone (O_3) photolysis that is initiated by UV radiation of wavelengths up to 320 nm, followed by the reaction of $O(^1D)$ with water vapour:

$$O_3 + h\nu \longrightarrow O_2 + O(^1D)$$

$$O(^1D) + H_2O \longrightarrow 2OH$$

Recycling between OH and HO_2 determines secondary OH production. Under low pollution conditions recycling of OH involves O_3 destruction:

$$OH + O_3 \longrightarrow HO_2 + O_2$$

$$HO_2 + O_3 \longrightarrow OH + 2O_2$$

The removal of HO_X (OH and HO_2) in this case mainly occurs through the self-reaction of HO_2 that produces H_2O_2, which is then removed by wet deposition.

OH also reacts with carbon monoxide (CO), CH_4 and non-methane volatile organic compounds (NMVOC), under both polluted and unpolluted conditions, to produce, among other species, HO_2. Under high NO_X pollution, OH is formed back in the following reaction:

$$NO + HO_2 \longrightarrow NO_2 + OH$$

The above reaction together with the photolysis of nitrogen dioxide (NO_2) form the recycling of NO_X (NO and NO_2), which leads to the formation of O_3:

$$NO_2 + h\nu \longrightarrow NO + O,$$

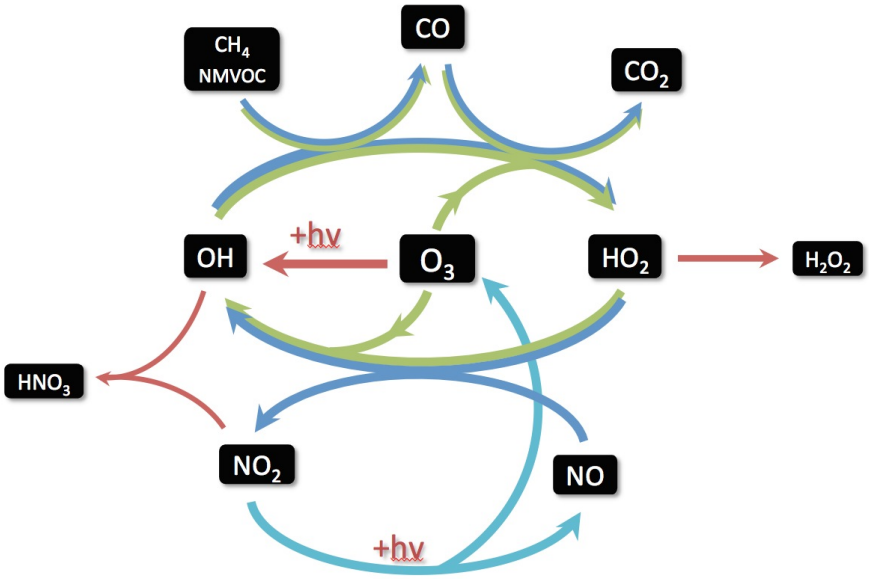

Figure 1.3: Simplified scheme of tropospheric OH chemistry. The red arrows represent sources and sinks of HO_X; dark blue and green arrows highlight the recycling mechanism of HO_X under polluted and unpolluted conditions, respectively. Light blue arrows represents NO_2 photolysis, which is part of the NO_X recycling mechanism.

$$O + O_2 + M \longrightarrow O_3 + M$$

Both HO_X and NO_X are removed by the following reaction:

$$OH + NO_2 \longrightarrow HNO_3$$

Because of its short lifetime of the order of one second, OH reacts rapidly to changes in atmospheric composition. Determining global OH from atmospheric measurements would therefore need very high spatial and temporal coverage, which is not feasible given the low concentrations of OH. Estimates of global OH can be made from inverse modelling of longer-lived species which react with OH. Methyl chloroform is particularly suitable for this, because it has a lifetime of 5 years and is only emitted by anthropogenic activity. However, the amount of information that can be extracted from measurements of methyl chloroform is limited by the number of measurement stations and emission uncertainties. Estimated global mean OH concentrations based on methyl chloroform range from 9.4 to 10.7 10^{-5}molec cm^{-3} (Bousquet et al. 2005; Krol and Lelieveld 2003; Prinn et al. 2001). The magnitude of the inferred interannual variability (IAV) in OH differs substantially between studies. The studies of Prinn et al. (2005) and Bousquet et al. (2005) an IAV in OH of

about 7-9% for the periods 1978-2003 and 1980-2000, respectively. The more recent study of Montzka et al. (2011a) shows an OH IAV of only 2.3±1.5% for the period 1998-2007, arguing that estimates for the earlier periods are affected by uncertainties in methyl chloroform emissions. Emissions have been low since 1998 due to the inclusion of methyl chloroform in the Montreal protocol to protect the O_3 layer.

1.1.4 *Radiative transfer*

As shown above, the photolysis reactions of O_3 and NO_2 are important for producing and recycling OH. A molecule is photolysed when it dissociates in the interaction with radiation. These photolysis reactions are dependent on the amount of radiation in the atmosphere, which can be described by the actinic flux F (photons $s^{-1}nm^{-1}cm^{-2}$). F is amount of incoming radiation from all directions of a certain wavelength, including the direct radiation from the sun and the radiation reflected by the surface and scattered by atmospheric constituents.

Two processes can influence the amount of solar radiation reaching during its passage through the atmosphere: absorption and scattering by atmospheric constituents. For LW radiation, the additional process of emission of radiation by the atmosphere is also important. However, emission of SW radiation, which is the most relevant for atmospheric photochemistry, is negligible.

Particles and molecules can absorb SW radiation. The absorbed energy can be reemitted in the form of LW radiation or can be converted into thermal energy, leading to the heating of the atmospheric layer. Absorption of radiation may also lead to the breakdown of molecules, in which case a photolysis reaction occurs. The process of scattering of radiation occurs when the incoming radiation changes direction of propagation due to the interaction with molecules or particles. Both absorption and scattering are wavelength-dependent processes.

The radiation transmitted through an absorbing or scattering layer of the atmosphere can be determined by the Beer-Lambert law:

$$F = F_0 e^{-\sigma N l}$$

where F_0 is the incident radiation flux, F the radiation flux transmitted through the atmospheric layer, σ ($cm^2 molec^{-1}$) is the extinction (the sum of absorption and scattering) cross section, N (molec cm^{-3}) is the density of scatterers or absorbers, and l (cm) is the path length of radiation through the layer. If d is the depth of the layer and θ is the angle between the direction of the incoming radiation and the vertical, then the path length through the atmospheric layer is $l = d / \cos\theta$. The Beer-Lambert law can thus be rewritten as

$$F = F_0 e^{-\tau / \cos\theta}$$

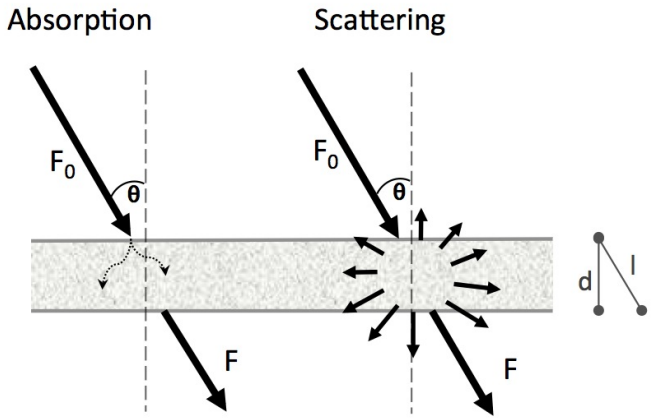

Figure 1.4: Absorption and scattering processes in the atmosphere.

where $\tau = \sigma N d$ is called the optical depth of the layer. When both absorption and scattering occur within the same layer then $\tau = \tau_a + \tau_s$, with τ_a and τ_s the absorption and scattering optical depths of the layer.

The direct radiation at each level of the atmosphere can be determined by the above formula. In addition to direct radiation, the actinic flux also has a diffuse component, consisting of radiation from all directions that has been scattered by molecules, particles or cloud droplets. Radiative transfer models generally divide the atmosphere in a certain number of vertical layers and calculate the radiative fluxes at each level based on the known properties of incoming radiation and atmospheric composition. Models used in this thesis are based on the two-stream method of calculating radiative fluxes for light propagation in two directions. The computed actinic fluxes are then used to calculate photolysis frequencies for different species, including O_3 and NO_2.

1.1.5 *Photolysis*

The frequency of a photolysis reaction is determined by the absorption cross section, or the probability of a molecule to absorb a photon of a certain wavelength, by the quantum yield, or the probability to dissociate with a certain outcome of the pho-

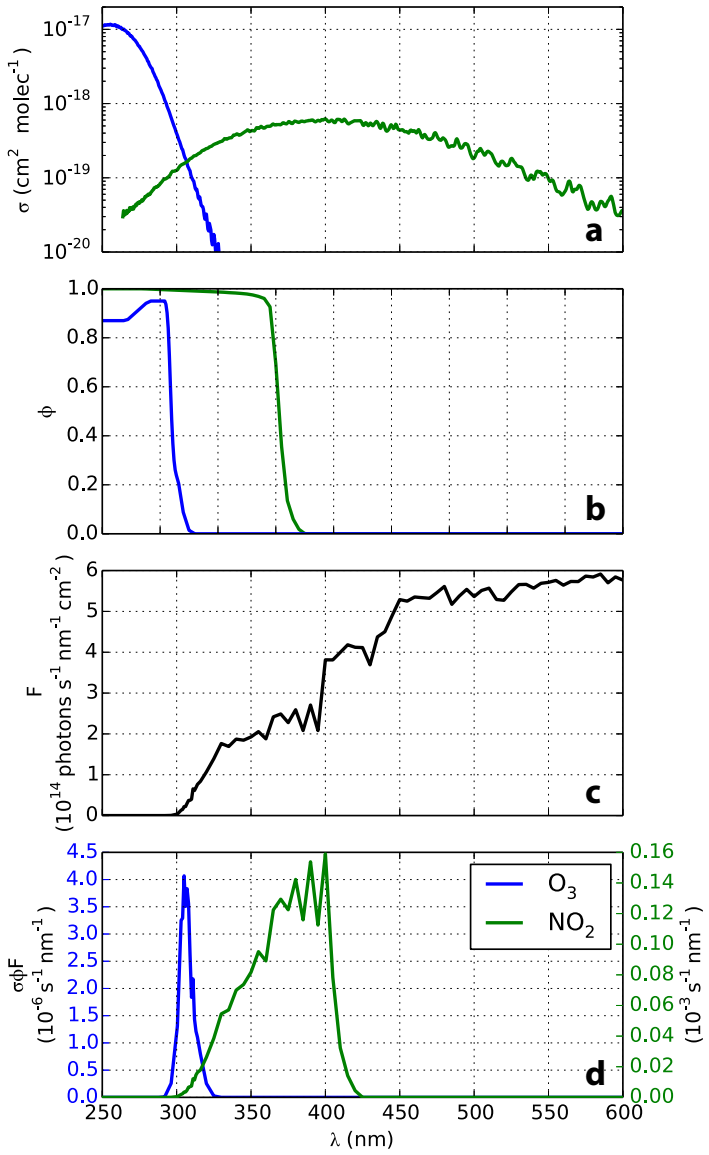

Figure 1.5: Wavelength dependence of the parameters used to calculate the photolysis frequencies of O_3 to $O(^1D)$ (blue) and of NO_2 (green) as a function of wavelength: a) absorption cross sections, b) quantum yields, c) surface actinic flux, and d) photolysis rate coefficients $\sigma\phi F$. Surface actinic flux and photolysis rate coefficients were taken from the TUV model output on 15 March 1991 at noon at the equator.

tolysis reaction, and by the actinic flux, which is the amount of photons available, according to:

$$J_X = \int \sigma_X(\lambda)\phi_X(\lambda)F(\lambda)d\lambda$$

where J_X (s^{-1}) is the photolysis frequency of the compound X, σ_X (cm^2molec^{-1}) the absorption cross section, ϕ_X is the quantum yield, and λ the wavelength. The absorption cross section and quantum yield depend on the molecular structure of the compound and are determined from laboratory experiments. In some cases a photolysis reaction can have more than one outcomes, and a quantum yield is defined for each outcome. For example, the photolysis of O_3 produces O_2 and either a ground state oxygen atom ($O(^3P)$) or an excited state oxygen atom ($O(^1D)$). F (photons $s^{-1}nm^{-1}cm^{-2}$) is the actinic flux.

Figure 1.5a and 1.5b present σ and, respectively, ϕ for NO_2 photolysis, and the photolysis of O_3 to $O(^1D)$ as a function of wavelength between 250 and 600 nm. The absorption cross section of O_3 decreases with wavelength over this interval, while the absorption cross section of NO_2 has a maximum at 370 to 400 nm. The quantum yield of $O(^1D)$ from O_3 photolysis and that of NO+O from NO_2 photolysis are also shown. They show that $O(^1D)$ is is the dominating photolysis channel for O_3 photolysis for wavelengths smaller than 300 nm. Although NO_2 is able to absorb wavelengths of up to 600 nm, it only dissociates below 420 nm.

Figure 1.5c shows the amount of radiation reaching the surface at noon on 15 March 1991 at the equator, as calculated by the TUV model (Madronich 1993). Radiation coming from the Sun spans the UV range, of 100 to 400 nm, the visible range of 400 to 700 nm, and the infrared of 700 nm to 1 mm. SW radiation in the UV and visible part of the spectrum represents the most important component of solar radiation for atmospheric photolysis. The actinic flux increases over the interval shown in Figure 1.5c, having a peak at 550-600 nm. In addition, wavelengths below 290 nm are absorbed by O_3 and oxygen in the stratosphere and therefore do not reach the surface. As a result, the photolysis rate coefficient of O_3 at the surface (Figure 1.5d) is significant only in the region 290 to 330 nm, with a maximum at 305 nm. Photolysis of NO_2 occurs for wavelengths of 300 to 420 nm, with a maximum rate at 400 nm.

1.2 THE ERUPTION OF MOUNT PINATUBO

1.2.1 *The largest eruption of the past century*

The eruption of Mt. Pinatubo on 15 June 1991 ejected between 8.4 and 10.4 km^3 of pumice in the form of rock, ash and magma, and 18±4 Tg gaseous sulfur dioxide (SO_2) (Guo et al. 2004a; Scott et al. 1996; Sheng et al. 2015). With a volcanic eruption index (VEI) of 6, it was the largest eruption since that of Novarupta in 1912 in

terms of erupted mass, and determined the largest stratospheric disturbance of the 20th century.

Mount Pinatubo is situated on the island of Luzon, the largest and most populated island of the Philippines. The eruption in 1991 caused large damage to properties and agricultural land in the area, killing almost 1000 people (Bautista 1996). Before the eruption in June 1991, no volcanic activity was detected on Mt. Pinatubo for about 500 years (Newhall et al. 1996). This made the eruption surprising and difficult to predict. Hints of an upcoming eruption became apparent about three months before the eruption, in the form of earthquakes, ground fracturing and steaming. Small ash eruptions and increasing volcanic unrest motivated the Philipine Institute of Volcanology and Seismology (PHIVOLCS) to issue an alert on 5 June and to start evacuating the population. Ash and steam emissions started to occur on 7 June and continued until 12 June, when the first explosive eruption occurred. Between 12 June and 15 June several explosive events created ash clouds reaching 20 km. The climactic eruption started at 14:00 on 15 June and ended at 22:30, having the largest intensity in the first three hours (Wolfe and Hoblitt 1996).

The volcanic eruption affected the lives of one million people, damaging over 1000 km^2 of agricultural land (Bautista 1996; Mercado et al. 1996). The eruption threat was detected early enough that PHILVOLCS was able to conduct efforts to educate the local officials and population about its danger. More than 60.000 people were evacuated and thousands of lives were saved. Damage to property and agriculture continued in the following years due to mudflows or lahars of erupted material during the monsoon season into densely populated areas.

This was the first volcanic eruption of this magnitude that could be monitored in detail, both in terms of geological processes and its atmospheric effects. It was the first eruption of this size to be detected by satellite measurements, and its effects could be monitored by ground-based continuous measurements of atmospheric composition. The eruption provided many new insights into geological and atmospheric processes. Emissions from the eruption caused a significant climate perturbation, providing a useful climate sensitivity test for global climate models. As new developments are made in process understanding and modelling tools, measurements done at the time of the Pinatubo eruption continue to provide useful information. Almost 25 years after the eruption, the present thesis aims to get additional insight into tropospheric chemistry, in particular how atmospheric CH_4 concentrations were affected by the eruption.

1.2.2 *Pinatubo aerosols*

Explosive volcanic eruptions emit particle and gas compounds to the atmosphere. In terms of the climate impact of a volcanic eruption, the most important emissions are

those of gaseous SO_2. The following reaction sequence occurs, converting SO_2 to sulfuric acid (H_2SO_4) (Pinto et al. 1989):

$$SO_2 + OH + M \longrightarrow HSO_3 + M$$
$$HSO_3 + O_2 \longrightarrow SO_3 + HO_2$$
$$SO_3 + H_2O + M \longrightarrow H_2SO_4 + M$$

H_2SO_4 then condenses onto existing particles or forms new sulfate particles. These particles can have a lifetime of the order of one year in the stratosphere, producing significant effects on climate and chemistry for a few years after the eruption (McCormick et al. 1995). Ash particles injected directly by the eruption can also have a local effect on atmospheric dynamics and form a threat to aviation safety. However, these particles sediment within a few days due to their mass, therefore their global climate impact is negligible (Guo et al. 2004b; Niemeier et al. 2009).

The SO_2 emitted by the Pinatubo eruption was removed by the reaction with OH, resulting in an average lifetime of about a month (Guo et al. 2004a; Read et al. 1993). The Total Ozone Mapping Spectrometer (TOMS) and TIROS (Television Infrared Observation Satellite) Optical Vertical Sounder (TOVS) satellite instruments measuring at the time of the eruption reported elevated column densities of SO_2 and tracked the plume evolution in the first weeks after the eruption. Based on the TOMS and TOVS data, the lifetime of SO_2 in the first two weeks after the eruption was estimated at 23 to 25 days. The SO_2 columns dropped afterwards below the detection limit of the two instruments. SO_2 from Pinatubo was detected again by the Microwave Limb Sounder (MLS) launched in September 1991 (Read et al. 1993). MLS found a peak in SO_2 at 26 km in the tropics in October 1991, and arrived at estimate of the lifetime of SO_2 of about 33 days. The differences between the two estimates of SO_2 lifetime might be related to instrument uncertainty, or to the different time of measurement. Emissions of water vapour by the eruption and catalytic reactions on ice and ash particles might have enhanced the SO_2 removal in the first stages of the development of the volcanic plume (Guo et al. 2004a, see also Section 4.4).

Sulfate aerosols formed from SO_2 scatter SW radiation and absorb LW radiation, therefore they can be detected by satellite instruments measuring in these ranges. Sulfate aerosols from Pinatubo were detected by the SAGE II (Stratospheric Aerosol and Gas Experiment II) instrument, which was measuring stratospheric aerosols at the time of the eruption using the solar occultation technique. The amount of solar radiation coming directly from the sun is measured after passing through the upper layers of the atmosphere, at several wavelengths in the range 380-1020 nm. Therefore these measurements are able to infer information about the vertical profile of aerosols. High extinction by volcanic aerosol often exceeded the measurement range of the instrument in the first year after the eruption, leading to instrument saturation. Data from ground-based lidar measurements was used to augment the SAGE II data

and to provide a gap-filled product (Thomason and Peter Eds). The AVHRR (Advanced Very High Resolution Radiometer) retrieves the column integrated AOD by measuring the amount of radiation reflected from the Earth surface and by the atmosphere. The measured AOD is in general overwhelmed by the tropospheric aerosols. However, the stratospheric AOD anomaly after Pinatubo was of the same order of magnitude as the tropospheric AOD in the first two years after the eruption. Therefore the Pinatubo AOD can be inferred by making an estimate of the background tropospheric component and subtracting that contribution from the total AOD (Long and Stowe 1994). Data from the two satellites showed that aerosols from the eruption spread to both hemispheres. The global mean aerosol optical depth reached 0.1-0.15, with values of more than 0.4 in the tropics during the first months after the eruption. Stratospheric AOD values remained elevated for a few years, returning to background values around 1995 (Bauman et al. 2003).

Volcanic aerosols were also detected by ground-based lidar instruments. These instruments send out a beam of light of a certain wavelength. By measuring then the amount of light scattered back to the instrument as a function of time, an aerosol vertical profile can be determined. After the eruption, elevated aerosol backscatter signals were found between the tropopause and up to 25-30 km by many lidar instruments around the world. Depending on location, the aerosol lifetime was estimated between 9 months and 1.4 years based on lidar data (Barnes and Hofmann 1997; Deshler 2008; Jayaraman et al. 1995; Nagai et al. 2010).

By using information on the wavelength-dependence of the aerosol optical depth, information on aerosol size can be retrieved from the SAGE II measurements. The SAGE II data showed that the stratospheric aerosol size increased from an effective radius, or area-weighted mean radius, of 0.1-0.2 μm to more than 0.4 μm in the first half year after the eruption. The larger aerosol particles were removed from the atmosphere by gravitational settling, and the aerosol size gradually decreases to background values by mid-1996 (Bauman et al. 2003). Other estimates for the particle size of Pinatubo sulfate aerosols using lidar and balloon-borne measurements at tropical and midlatitude locations in the Northern Hemisphere showed effective radii of up to 0.4-0.6 μm (Ansmann et al. 1997; Deshler et al. 1993; Dutton et al. 1994).

1.2.3 *Impacts on climate and stratospheric chemistry*

Pinatubo aerosols caused changes in the radiative balance of the atmosphere, leading to climate anomalies in the following two years. Scattering of SW radiation by sulfate particles caused an increased of up to 10 W/m^2 in the SW radiation at the top of the atmosphere in the tropics in the first year after the eruption (Bender et al. 2010; Stenchikov et al. 1998). Global tropospheric temperatures decreased in the following two years, with a more pronounced decrease in the upper layers of the

troposphere than close to the surface (Free and Angell 2002; Graf et al. 1996). After removing the effect of a coinciding El Niño event, which partly offset the temperature decrease from the eruption, a decrease of 0.3-0.45 K was found from measurements at the surface and 0.6-0.8 K in the lower troposphere (Santer et al. 2001). General circulation models also find a decrease of about 0.5 K at the surface in response to the changes in the shortwave radiative flux one year after the eruption (Bender et al. 2010). Sulfate absorption of LW radiation emitted by the Earth surface caused a significant heating of the stratosphere. Rawinsonde data and satellite measurements from the Microwave Sounding Unit (MSU) found an increase in stratospheric temperatures reaching 2-3 K in the northern tropics in the first year after the eruption, and a global mean increase of about 1 K at 50 hPa (Spencer and Christy 1993). This stratospheric heating was shown to have increased the Brewer-Dobson circulation and planetary wave activity in the first year after the eruption (Aquila et al. 2013; Tie et al. 1994), possibly affecting the exchange of chemical species between the troposphere and the stratosphere.

The presence of aerosol particles altered the chemistry of the stratosphere, leading to one of the lowest values in global stratospheric O_3 recorded in history. A global O_3 decrease of 3-5% was observed by TOMS between 1991 and 1993 (Chipperfield et al. 2003). This pronounced decrease in O_3 after the Pinatubo eruption was caused by several processes (Aquila et al. 2013; Kinnison et al. 1994; Telford et al. 2009; Tie et al. 1994). First, the dynamical perturbation caused by stratospheric heating led to increased transport of O_3 from the tropics to the high-latitudes, where O_3 is broken down more efficiently by heterogeneous chemistry. Second, the aerosol particles provided additional surface for heterogeneous reactions. The heterogeneous conversion of N_2O_5 to HNO_3 led to the depletion of stratospheric NO_2, and caused enhanced breakdown of O_3 by chlorine. Finally, both the aerosol scattering and the increase in stratospheric temperatures might have affected O_3 photochemical production and loss.

1.2.4 *Potential impacts on tropospheric photochemistry and methane*

The above changes in climate and stratospheric chemistry after the Pinatubo eruption also caused perturbations in the chemistry of the troposphere and the CH_4 budget. The processes through which the Pinatubo eruption could have affected CH_4 concentrations are listed in Table 1.1. Changes in radiation after the eruption affected the chemistry of the troposphere. As described in Section 1.1.2, the removal of CH_4 from the atmosphere mainly occurs by the reaction with OH in the troposphere. OH production from O_3 photolysis is dependent on the amount of UV radiation reaching the troposphere. Therefore changes in UV radiation triggered by volcanic SO_2, sulfate, and by stratospheric O_3 depletion affected the lifetime of CH_4. SO_2 absorbs UV radiation between 290 nm and 330 nm and sulfate aerosols scatter solar radiation,

Table 1.1: Potential effects of the Pinatubo eruption on CH_4 sources, sinks and concentrations.

Process	CH_4 emissions from wetlands	Tropospheric UV	Tropospheric OH	CH_4+OH	CH_4
UV absorption by SO_2		−	−	−	+
UV scattering by sulfate aerosols		−	−	−	+
Stratospheric O_3 depletion		+	+	+	−
Sulfur deposition	−				−
Temperature effect on CH_4+OH reaction rate				−	+
Water vapour decrease			−	−	+
Temperature effect on wetland emissions	−				−
Temperature effect on NMVOC emissions			+	+	−
Increased stratosphere-troposphere exchange					−

leading to a reduction of photolysis frequencies in the troposphere, thus to a longer CH_4 lifetime. In contrast, stratospheric O_3 depletion would lead to an increase of UV radiation in the troposphere, and thus to a higher OH abundance and a shorter CH_4 lifetime.

The eventual fate of the volcanic sulfur is deposition to the surface. Deposition of large amounts of sulfur over wetland areas was shown to increase the population of sulfate-reducing bacteria and inhibit methanogens (Gauci et al. 2004; 2008). The modelling results of Gauci et al. (2008) indicate that deposition of 122 Tg SO_2 emitted by the Laki eruption in the years 1783 to 1784 led to a decrease of 8.8 Tg yr^{-1} in CH_4 emissions from wetlands in the two years following the eruption. As a rough estimate assuming linearity, the SO_2 emitted from the Pinatubo eruption would lead to a decrease in CH_4 emissions about 1 Tg yr^{-1}. We consider this effect to be small and do not investigate it further here.

The global temperature perturbation after Pinatubo triggered changes in the chemical composition of the atmosphere, as well as in natural sources related to biogenic activity. A decrease in temperature would generally slow down photochemical transformations. In particular, the slowdown of the reaction between CH_4 and OH would lead to higher tropospheric CH_4 concentrations (Bekki and Law 1997). Soden et al. (2002) found that the cooling after the eruption is associated with a maximum global decrease of 3% in the water vapour column in both observations and model simulations. Less water vapour in the troposphere would imply less OH formation by photolysis of O_3, because the reaction between $O(^1D)$ and water becomes less likely. This would increase the CH_4 lifetime, leading to CH_4 build-up in the atmosphere.

Natural emissions from wetlands are sensitive to changes in temperature and soil moisture (Spahni et al. 2011). Furthermore, natural emissions of NMVOC are known to be temperature dependent (Guenther et al. 1993). A decrease in the surface temperature would result in reductions in both CH_4 emissions from wetlands (Section 1.1.2) and biogenic NMVOC emissions. Biogenic emissions of NMVOC are also dependent on the amount of photosynthetically active radiation (PAR) reaching the surface (Guenther et al. 1993). A decrease in PAR fluxes due to enhanced aerosol scattering would further decrease these emissions, although the more diffuse character of the solar radiation after the Pinatubo eruption was shown to increase plant productivity and isoprene emissions (Mercado et al. 2009; Wilton et al. 2011). While a reduction in CH_4 emissions directly impacts CH_4 concentrations, a change in NMVOC emissions may affect OH, and thus impose an indirect impact on the CH_4 lifetime.

The eruption of Pinatubo also changed the dynamics of the atmosphere, which might have influenced OH and CH_4 concentrations. It was inferred in the 4-box modelling study of Schauffler and Daniel (1994) that heating of the stratosphere may have increased the exchange between the stratosphere and the troposphere, leading to a decrease in tropospheric CH_4 concentrations. Lowe et al. (1997) suggest that a large effect of enhanced stratosphere-troposphere exchange would be inconsistent with the decrease in observed $\delta^{13}C$ in this period. However, other isotope data from

this period do not support a strong decrease in $\delta^{13}C$ between 1991 and 1992 (Quay et al. 1999).

The list presented above includes the main global-scale effects of radiation and climate changes after the eruption on CH_4 concentrations, based on our current understanding of CH_4 processes. Most previous studies using forward models investigated the effect of one or two of the above processes, without attempting simulate the observed CH_4 concentrations. Dlugokencky et al. (1996) showed that the evolution of CH_4 and CO in 1991 and early 1992 is consistent with a decrease in OH for up to one year after the eruption. They qualitatively related this decrease in OH to an attenuation of the UV flux due to the presence of SO_2 and sulfate in the stratosphere. The study of Bekki and Law (1997) investigated temperature-related effects on the growth rate of CH_4 in 1991-1992, and found that reduced emissions from wetlands may partly or fully explain the reduced growth rate in 1992. Using a two-dimensional model, Bekki et al. (1994) concluded that half of the CH_4 growth rate reduction in 1992 could be attributed to decreased stratospheric O_3. Telford et al. (2010) found that a decrease in natural isoprene emissions due to Pinatubo cooling led to an increase in CH_4 removal. In addition to the Pinatubo-related processes, the collapse of the Soviet Union in late 1991 might also have affected CH_4 emissions. Law and Nisbet (1996) postulate that gas leak fixes in the former Soviet Union shortly after its collapse contributed to the decrease in CH_4 growth rate in 1992.

The inverse modelling studies of Bousquet et al. (2006), Pison et al. (2013) and Wang et al. (2004) estimated the variations in the CH_4 emissions needed to explain the evolution of CH_4 concentrations in the period after the Pinatubo eruption. Their results depend on the assumed OH variability. However, the OH fields used in these studies do not take into account all the effects presented above. Wang et al. (2004) use parameterised OH concentrations based on stratospheric O_3, climate variables, and modelled concentrations of CO and NMVOC, but do not take into account volcanic SO_2 and sulfate. The OH fields in Bousquet et al. (2006) and the prior OH fields in Pison et al. (2013) are taken from inversions of methyl chloroform observations, and have a large uncertainty in this period due to uncertainties in methyl chloroform emissions. Additionally, their inverse modelling setup does not allow to determine the causes of OH variations. In this thesis we aim to investigate the contribution of the effects listed in Table 1.1 to observed CH_4 concentration changes after the eruption, using a common forward modelling framework.

1.3 THIS THESIS

The perturbed climate and radiation conditions after the eruption of Mount Pinatubo provide an interesting test case for investigating the mechanisms driving temporal variations in CH_4 concentrations. In the present thesis, we address the following research questions:

- What processes related to the Pinatubo eruption affected the CH_4 budget and what are their individual contributions to the observed CH_4 growth rate?
- What other processes than the volcanic eruption contributed to the observed CH_4 variability in the post-Pinatubo period?
- Are we able to simulate the observed CH_4 growth rate variations after the Pinatubo eruption?

An important aspect of modelling the impact of the Pinatubo eruption on CH_4 is simulating the effect of stratospheric sulfate aerosol on photolysis frequencies. For this purpose, aerosols in the TM5 global chemistry and transport model were coupled to the radiation scheme used in the calculation of photolysis frequencies. The aerosol representation in TM5, together with other aspects of our modelling framework, are described in Chapter 2. Results on the impact of tropospheric aerosols on radiation and photolysis frequencies are also presented.

The effect of the Pinatubo eruption on global CH_4 concentrations is analysed in Chapter 3. A column chemistry model coupled to the column radiative transfer model TUV is used to investigate the various effects from a global perspective. We address most of the processes in Table 1.1, except for the effect of NMVOC and of stratosphere-troposphere exchange, which are difficult to assess using a column chemistry model.

In Chapter 4, the stratospheric SO_2 and sulfate aerosols from the Pinatubo eruption are modelled using the global chemistry and transport model TM5, and results are validated against observations. We assess their impact on tropospheric photolysis frequencies, driven by UV radiation changes, and the corresponding effects on OH and CH_4 concentrations.

In Chapter 5 we investigate the possible reasons for CH_4 variability in the early 1990s using TM5. We include in our analysis both processes related to the eruption (Table 1.1), as well as other factors controlling CH_4 variability in the atmosphere.

The main conclusions of this thesis are discussed in Chapter 6, together with proposed recommendations for future study.

2

MODELLING THE IMPACT OF AEROSOLS ON TROPOSPHERIC PHOTOLYSIS FREQUENCIES

2.1 MODELLING SETUP

2.1.1 *The TM5 chemistry and transport model*

The global chemistry and transport model TM5 (Huijnen et al. 2010; van Noije et al. 2014) is used in this thesis to model tropospheric photochemistry. The model includes the aerosol microphysics module M7 (Aan de Brugh et al. 2011; Vignati et al. 2004). The default TM5 model setup uses 34 hybrid sigma-pressure vertical layers, and a resolution of 3 x 2 degrees (longitude x latitude) globally, except for the polar region, where a reduced grid is used for advection in the zonal direction. For modelling the dispersion of SO_2 and sulfate aerosols from Pinatubo in the stratosphere this vertical resolution was found to produce large numerical diffusion errors (see Appendix Chapter 4). Therefore 60 hybrid sigma-pressure vertical layers were used in Chapters 4 and 5. TM5 is driven by meteorological data from the ERA-Interim reanalysis (Dee et al. 2011) from the European Centre for Medium-Range Weather Forecasts (ECWMF). The gas-phase chemistry is represented by 24 gas-phase transported chemical species, 15 gas-phase non-transported chemical species and 99 chemical reactions, based on a modified and updated version of the carbon bond mechanism 4 (CBM4, Houweling et al. 1998). Aerosol composition and size is described by 28 additional tracers. TM5 does not include a comprehensive stratospheric O_3 chemistry scheme, therefore stratospheric O_3 concentrations are nudged to the multi-sensor reanalysis data (van der A et al. 2010) above 45 hPa in the tropics and above 90 hPa in the extratropics. To constrain the stratospheric loss of CH_4 by OH, Cl and $O(^1D)$, CH_4 is also nudged above these pressure levels using climatological values from Grooß and Russell III (2005).

Photolysis frequencies are determined by the parameterisation scheme based on Williams et al. (2006), using on-line radiative transfer calculations for wavelengths between 202 nm and 695 nm. The wavelength interval 202-695 nm is divided into seven wavelength intervals, using different sets of intervals for small and large solar zenith angles (SZAs). The actinic flux, which includes both direct and diffuse radi-

ation, is calculated for seven wavelengths representative for each interval, using a two-stream radiative transfer method. The direct radiation flux, taking into account only absorption, is calculated on a much higher wavelength resolution, using 122 wavelengths. The actinic flux is then evaluated for all 122 wavelengths, assuming that the ratio between the absorption-only direct flux and the actinic flux is constant within each of the seven wavelength intervals. The performance of this method in representing tropospheric photolysis frequencies was tested in Williams et al. (2006), and its implementation in TM5 in Williams et al. (2012). To model scattering and absorption of UV radiation by aerosols interactively, the radiation transfer scheme used for the photolysis calculation was coupled to the M7 module. Aerosol absorption and scattering properties are calculated in M7 using a lookup table generated by the Generic Aerosol Optics Toolbox (GAOT, Aan de Brugh 2013).

2.1.2 *Aerosol modelling*

The aerosol module M7 simulates the following aerosol types: sulfate (SO_4), black carbon (BC), organic carbon (OC), sea salt, and mineral dust. In addition, TM5 simulates ammonium and nitrate using the Equilibrium Simplified Aerosol Model (EQSAM, Metzger et al. 2002), and methyl sulfonic acid (MSA).

The aerosol dynamics in the atmosphere is governed by aerosol formation, growth and removal, processes that are all modeled in TM5 (Aan de Brugh et al. 2011; Vignati et al. 2004). Aerosols can be either emitted to the atmosphere, or can be formed in the atmosphere by nucleation and condensation. Gas molecules with low volatility, such as sulfuric acid (H_2SO_4), can cluster to form new particle through the process of nucleation. Further condensation of gas molecules onto existing particles and collision between particles, are processes responsible for particle growth. The removal of aerosols in the atmosphere occurs through sedimentation, or gravitational settling, and deposition to the Earth surface. Aerosols can also be removed from the troposphere by wet deposition by rain or snow droplets.

Aerosols can be grouped in four categories depending on their size:

- *nucleation aerosols* – newly formed particles from the condensation of gases;
- *Aitken aerosols* – black carbon and organic carbon particles are emitted to the atmosphere from anthropogenic activity and biomass burning. Both nucleation-mode and Aitken-mode particles are are small in size and large in number, and rapidly grow into bigger particles;
- *accumulation aerosols* – particles formed from the coagulation of Aitken particles, and by condensation of H_2SO_4 onto existing particles. A small amount of the dust and sea salt particles is also directly emitted in this size range. These particles are smaller in number, therefore they do not coagulate easily. Due to their relatively small size, the removal by gravitational settling is slow for these

particles. The main removal process is wet deposition. Accumulation particles have the longest residence time in the atmosphere of the order of one week;

- *coarse aerosols* – mainly representing large dust and sea salt particles emitted to the atmosphere. Other chemical components can be incorporated by condensation and coagulation onto sea salt and dust particles. Coarse particles have a short residence time due to gravitational fall-out.

Aerosols in M7 are represented by a superposition of several lognormal distributions, or modes, each representing a size category (Whitby 1978; Willeke and Whitby 1975). In a lognormal distribution, the aerosol number $N(r)$ as a function of aerosol radius r is given by the following relationship:

$$N(r) = \frac{N_i}{r \ln\sigma\sqrt{2\pi}} \exp\left(\frac{(\ln r - \ln r_i)^2}{2\ln^2\sigma_i}\right),$$

where r_i is the median radius of the distribution, σ_i is the distribution width, and N_i is the total aerosol number in the distribution, labelled by the mode index i. The aerosol total volume and surface for a lognormal distribution are:

$$V_i = \frac{4}{3}\pi N_i r_i^3 \exp\left(\frac{9}{2} ln^2\sigma_i\right),$$

$$A_i = 4\pi N_i r_i^2 \exp(2ln^2\sigma_i).$$

A parameter for aerosol size often retrieved from measurements is the effective radius, or the mean radius weighted by the surface:

$$R_{\text{eff},i} = 3V_i/A_i = r_i \exp\left(\frac{5}{2}\ln^2\sigma_i\right)$$

The M7 module uses 7 modes to describe the size distribution and composition of aerosols. Three modes are used for insoluble particles (Aitken, accumulation, and coarse) and four modes for soluble particles (nucleation, Aitken, accumulation, and coarse). Each mode is represented by a lognormal size distribution with a fixed width of σ=2.0 for coarse mode particles and σ=1.59 for the other modes.

M7 has been developed for simulating tropospheric aerosols, and the size distributions used have been optimised for tropospheric aerosols. For simulating the Pinatubo eruption, some adjustments were needed. In Kokkola et al. (2009) the performance of the M7 scheme was tested in a box model setup for stratospheric conditions with elevated aerosol loads that occur after a large volcanic eruption. The authors postulate that the coarse mode, representative for large tropospheric sea salt and dust particles, should not be used for modeling stratospheric sulfate, as this would lead to an overestimated particle size and a too short lifetime due to fast sedimentation. Furthermore, a decreased width of the particle distribution has been observed after large volcanic eruptions (Bauman et al. 2003). The results of Kokkola et al. (2009)

show that removing the soluble coarse mode, and reducing the width of the soluble accumulation mode to σ=1.2 significantly improves the model performance in such situations. Niemeier et al. (2009) and Toohey et al. (2011) used this setup to simulate the Pinatubo eruption within the global climate model MAECHAM5, and obtained realistic results. Therefore in Chapter 4 and 5 we use the setup recommended in Kokkola et al. (2009) above 300 hPa, and the standard M7 setup below 300 hPa to model tropospheric aerosols. As a consequence, tropospheric coarse mode particles are restricted to the part of the atmosphere below 300 hPa. As stratospheric accumulation-mode particles sediment below 300 hPa they are redistributed into the tropospheric accumulation and coarse modes. This redistribution might cause some unphysical changes in their radiative properties. As outlined above, particles have a short residence time in the troposphere of about one week. Therefore we expect the resulting error on the radiative effect of volcanic sulfate particles to be marginal. The nucleation scheme in M7 was also adapted to handle high H_2SO_4 concentrations typical for volcanic conditions, according to Kokkola et al. (2009).

M7 tropospheric aerosols and their impact on photolysis frequencies of O_3 and NO_2 during three months in 1990 are shown further in this chapter, to illustrate the effect of the coupling between M7 and photolysis. Results on Pinatubo aerosols and their effect on photolysis and CH_4 will be presented and discussed in Chapter 4.

2.2 THE IMPACT OF AEROSOLS ON PHOTOLYSIS FREQUENCIES

2.2.1 *Background tropospheric aerosols*

To test the coupling between aerosols and radiation, and the impact of aerosols on photolysis frequencies, two simulations were performed for the first half of the year 1990, using the default TM5 setup of 34 layers. Aerosols were modelled in both simulations, however, in the first simulation no aerosols were considered in the radiative transfer code that calculates photolysis frequencies. In the second simulation aerosol properties from M7 were used in the radiative transfer calculation. The last three months of the simulation, April-May-June 1990 (AMJ), are analysed here.

Anthropogenic and biomass burning aerosol emissions were used from the AC-CMIP and the Coupled Model Intercomparison Project (CMIP5, Lamarque et al. 2010). Natural emissions of organic carbon, and aerosol precursors of ammonia (NH_3) and SO_2 were taken from the Monitoring Atmospheric Composition and Climate (MACC) project, as described in van Noije et al. (2014). Anthropogenic emissions of SO_2 and NH_3 were taken from the EDGAR 4.1 inventory (European Commission and Joint Research Centre (JRC)/Netherlands Environmental Assessment Agency (PBL) 2011). Sea salt and dust emissions are calculated online within TM5.

Figures 2.1a and 2.1b show the modelled column integrated aerosol optical depth at 310 nm and 370 nm during AMJ 1990, wavelengths at which the photolysis of

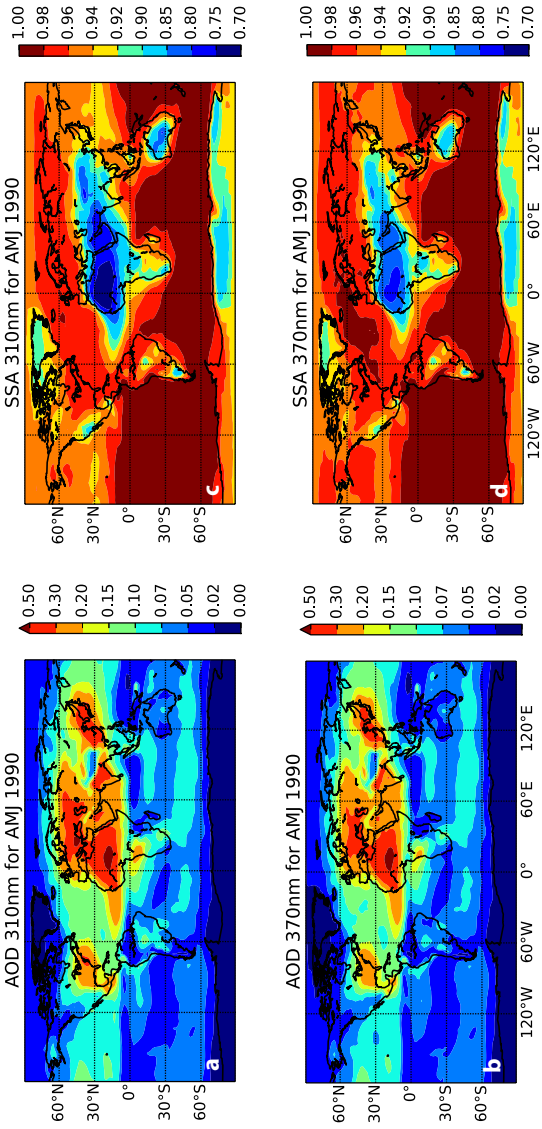

Figure 2.1: Mean aerosol optical depth at a) 310 nm and b) 370 nm, c) and d) the corresponding single scattering albedo for April-May-June (AMJ) 1990.

ozone (O_3) and, respectively, of nitrogen dioxide (NO_2) occur in the troposphere. The AOD values are somewhat larger than the values for the more recent period obtained by van Noije et al. (2014), due the lower wavelengths chosen here. At 525 nm we find a global mean AOD of 0.075, in line with findings in van Noije et al. (2014). TM5 simulates the largest AOD over Saharan region, where large emissions of dust occur. AOD values above 0.3 are also found over Europe, India, Southeast China, and eastern United States, where significant amounts of aerosols and precursors are emitted by anthropogenic activity. AOD values below 0.05 are found in remote areas of the Southern Hemisphere and the northern high-latitudes. Aerosols in TM5 were validated against station and satellite data in van Noije et al. (2014) and Aan de Brugh et al. (2011), and were generally found to be underestimated. Some tests performed in Aan de Brugh et al. (2011) using reduced wet deposition were shown to improve the comparison with European station data. However, the reasons for the low AOD in TM5 are still unclear and under investigation, and might be related to either emissions or the tropospheric aerosol lifetime.

The single scattering albedo (SSA), or the ratio of scattering to the total aerosol extinction, is shown in Figures 2.1c and 2.1d. The SSA is generally larger for 370 nm than for 310 nm. Desert dust over the Saharan region, although it is an efficient scatterer for visible light, is the most absorbing aerosol for UV radiation, with SSA of 0.75-0.85. Aerosols with SSA close to 1, signifying almost purely scattering aerosols, are found over the oceans in the Southern Hemisphere, where the aerosol composition is dominated by sea salt. High SSA are also found over eastern United States, the North Atlantic region, Europe and northern Asia. Over Europe and eastern Unites States, aerosols are dominated by anthropogenic sulfate and ammonium nitrate aerosols, which are mainly scattering aerosols. Over Southeast Asia, large emissions of absorbing black carbon and organic carbon occur, leading to SSA values of 0.85 to 0.9 in this region.

2.2.2 *Effect on photolysis frequencies of O_3 and NO_2*

The interactive coupling between aerosols and radiation affects our modelled photolysis frequencies. We show here results on the impact of the tropospheric aerosols from TM5 on the photolysis frequencies of O_3 and NO_2. Modelled photolysis frequencies of O_3 and NO_2, averaged over the tropospheric column during AMJ are presented in figures 2.2a and 2.2b. The tropopause height was defined as a function of latitude as recommended in Lawrence et al. (2001), and the vertical averaging was done by weighting with the air mass. More sunlight is received on the Northern Hemisphere over the three-month period analysed here, which leads to asymmetric behaviour of the NO_2 and O_3 photolysis frequencies. The photolysis frequency of NO_2, which occurs at wavelengths of up to 420 nm (see Section 1.1.5), decreases from North

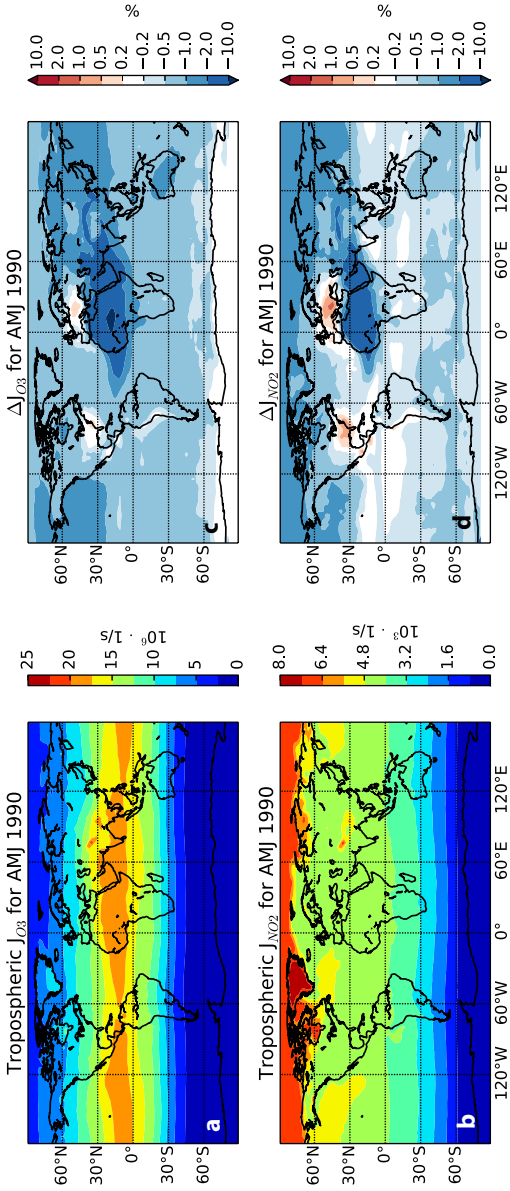

Figure 2.2: Tropospheric mean photolysis frequencies of a) O_3, b) NO_2 during AMJ 1990, c) and d) the impact of tropospheric aerosols on these photolysis frequencies relative to a hypothetical aerosol-free case. The tropopause height was defined as a function of latitude as recommended in Lawrence et al. (2001).

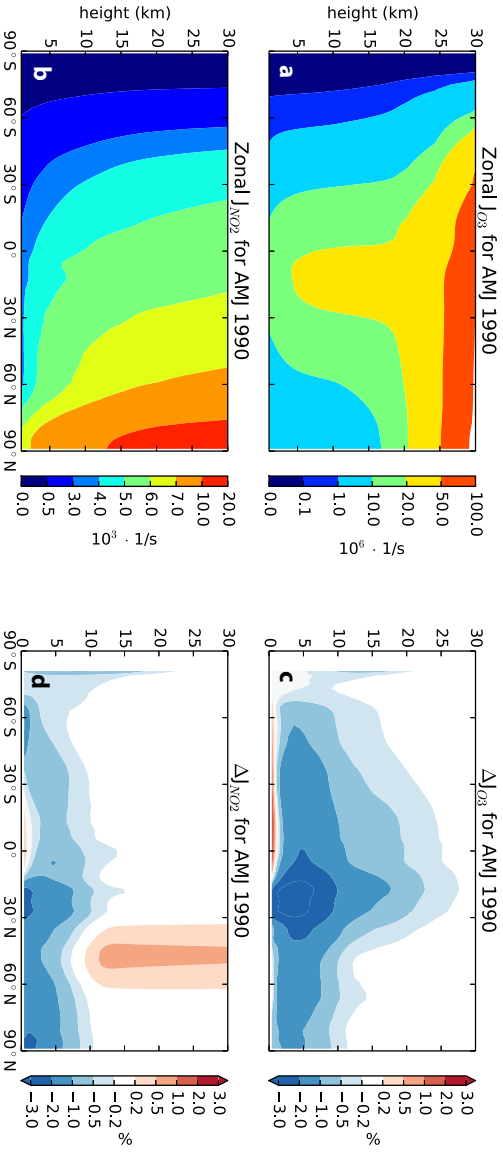

Figure 2.3: Similar to Figure 2.2 for the zonally averaged height distributions.

to South together with the amount of light. The photolysis of O_3, at wavelengths of up to 330 nm, is highest in the tropics, due to a high sensitivity of O_3 photolysis to the SZA. At large SZA, the slant path of direct light through the O_3 layer is larger, leading a stronger attenuation of UV radiation. Therefore the photolysis of O_3 in the troposphere mainly takes place at small SZA, which occurs predominantly in the tropics.

Figures 2.2c and 2.2d show the relative difference in J_{O_3} and J_{NO_2} between the two simulations with and without the aerosol effect on radiation. A decrease of more than 0.5% in J_{O_3} occurs throughout the global troposphere, except over Antarctica, Central Europe and the western United States. The most pronounced decrease is found over North Africa, where UV-absorbing Saharan dust leads to a decrease of up to 10% in J_{O_3}. A decrease of 1 to 2% also occurs over the northern midlatitudes, where absorbing black carbon and organic carbon aerosols are found. The impact of aerosols on the tropospheric mean J_{NO_2} is somewhat smaller, with decreases of 0.5 to 1% in the mid-latitudes, and decreases of 1 to 2% in the northern high-latitudes. A decrease of 2 to 10% over North Africa also occurs for J_{NO_2}. Both tropospheric mean J_{O_3} and J_{NO_2} increase by up to 1% over the western United States and Central Europe, where aerosols are predominantly scattering.

The impact of tropospheric aerosols on J-values for different levels in the atmosphere is presented in Figure 2.3, where the zonal mean J_{O_3} and J_{NO_2}, and the relative effect of aerosol coupling are plotted as a function of altitude. Due to tropospheric aerosols, zonal mean J_{O_3} decreases by 1% to 2% in the troposphere at tropics and at mid-latitudes, except near the surface. A decrease of 1% to 3% is found from the surface up to 10 km in the northern tropics, a zonal band that includes North Africa with absorbing Saharan dust aerosols. In the first 1 km from the surface J_{O_3} increases in the southern tropics and mid-latitudes due to increased scattering near the surface.

A somewhat smaller impact of aerosols is found on zonal J_{NO_2}. A decrease of 1% to 2% is found in the Northern Hemisphere from the surface up to 5 km. An increase of less than 0.5% is also found for J_{NO_2} in the equatorial region near the surface. Additionally, an increase of up to 1% is found in the northern midlatitudes above 10 km due to an increase in diffuse radiation.

The effect of aerosols on photolysis frequencies can be explained by their impact on the actinic flux. Figure 2.4 shows the actinic flux and the contribution of direct radiation to the total actinic flux at 310 nm and 370 nm at different SZAs as a function of altitude. These radiative fluxes were derived for an aerosol-free atmosphere from simulations of the TUV radiative transfer model at the equator on 15 September (SZA=3° and SZA=46°) and 15 December 1990 (SZA=77°). At 310 nm, the amount of radiation rapidly decreases with SZA. For a SZA of 77° the amount of radiation at 310 nm below 20 km is very small. At 370 nm radiation gradually decreases throughout the troposphere for large SZA, with about a third of the radiation reaching the surface. The contribution of direct radiation to the actinic flux at 310 nm decreases

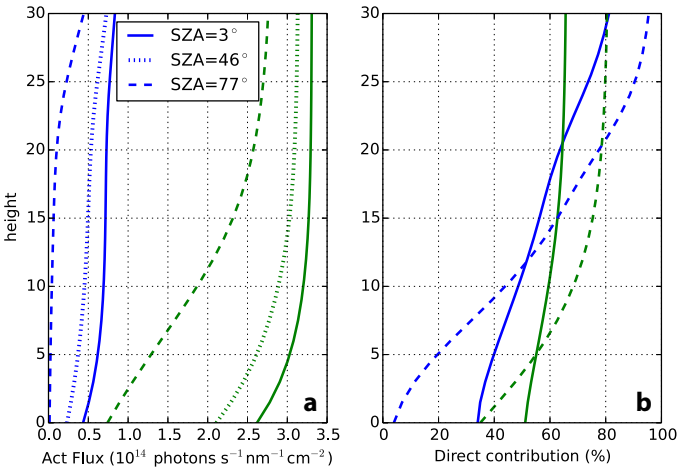

Figure 2.4: a) Actinic flux at 310 (blue) and 370 nm (green) at the equator for SZA=3°, SZA=46°, and SZA=77°. b) Contribution of direct radiation to the total actinic flux for SZA=3° and SZA=77°.

with altitude. The increase in diffuse radiation near the surface is due to Rayleigh scattering by air molecules, which is more pronounced at 310 nm than at 370 nm. The actinic flux above the tropopause at 310 nm is more than 60% direct radiation, while diffuse radiation contributes about 65% close to the surface. At 370 nm, direct radiation contributes for small SZAs by 55 to 60% throughout the troposphere. At larger SZA the contribution of diffuse radiation strongly increases near the surface.

In general, the presence of aerosols in the atmosphere leads to an increase in diffuse radiation and a decrease in direct radiation. The overall effect of aerosols on the actinic flux is a complex function of aerosol abundance, aerosol height, SSA, surface albedo, SZA, and available direct and diffuse radiation at each wavelength and height. For large amounts of absorbing aerosols, such as over the Saharan region, the effect is dominated by the reduction is direct radiation both at wavelengths around 310 nm, relevant for O_3 photolysis, and near 370 nm, relevant for NO_2 photolysis.

Due to the significant amount of diffuse radiation at 310 nm near the surface, additional scattering by aerosols increases the radiation at 310 nm less strongly than at 370 nm. The increase in diffuse radiation generally has a larger impact at 370 nm, explaining the fact that the relative decrease in J_{NO_2} is smaller than that in J_{O_3}. At northern midlatitudes the relatively large amounts of scattering aerosols above Europe and the western United States lead to an overall increase in actinic flux at both wavelengths throughout the troposphere. This increase is more pronounced at 370 nm, resulting in a zonal mean increase in J_{NO_2} above 10 km. The increase in

J_{NO_2} at high altitudes shows that scattering by tropospheric aerosols can influence stratospheric chemistry.

Large SZAs at high-latitudes increase the path length of radiation through the aerosol layer, enhancing the decrease in direct radiation and leading to a decrease in the amount of radiation reaching the surface. The surface albedo and cloud cover can additionally influence the effect of aerosol scattering by increasing the amount of diffuse radiation. The decrease in actinic flux due to aerosols at large SZA, together with high surface albedo explains the decreases in J-values at high-latitudes.

We can compare our calculations of the impacts of tropospheric aerosols on photolysis rates with results from other modelling studies. A thorough investigation of the above processes is presented in He and Carmichael (1999), where the impact of aerosols on the photolysis of NO_2 and on O_3 concentrations in Chongqing, China (106.9°E, 27.48°N) is shown as a function of several atmospheric parameters, including AOD, aerosol type, SZA and time of the year. It is found that maritime aerosols with AOD=0.13 at 380 nm increase surface J_{NO_2} by 3.44%, and rural aerosols with AOD=0.06 increase J_{NO_2} by 1.38%. Decreases in J_{NO_2} are found for absorbing urban and dust aerosols. Furthermore, He and Carmichael (1999) show that in the summer and spring months, scattering aerosols increase surface J_{NO_2} for an AOD of up to 0.1, and decrease J_{NO_2} for larger AOD. In the winter months, aerosols are shown to decrease J_{NO_2} irrespective of the AOD. This is a result of the larger SZA in winter months. Scattering aerosols of AOD=0.37 are found to increase J_{NO_2} at the surface by up to 9% at SZA smaller than 45°, and to decrease J_{NO_2} by similar amounts at larger SZA. The above results are similar to the results of our sensitivity study.

The global effect of clouds and aerosols on tropospheric photolysis was quantified in Wild et al. (2000). Clouds are very efficient scatterers of radiation, having optical depth values in the range of 1 to 100. Due to the global cloud cover, Wild et al. (2000) found increases of 10% and 8% for J_{NO_2} and J_{O_3}, respectively, in the upper troposphere and decreases of similar magnitude near the surface. This resulted in an overall increase of 3% in the global CH_4 removal by the reaction with tropospheric OH. Krol and Van Weele (1997) also found compensating effects in the upper and lower troposphere, and a resulting decrease in CH_4 lifetime of 2.4%. Wild et al. (2000) showed that scattering aerosols with an AOD of 0.1 increase tropospheric J-values by 4.5% for a SZA=0°, and that this effect is reduced to 1% in the presence of deep clouds, giving a similar magnitude to our findings. At large SZA, both positive and negative effects were found in Wild et al. (2000). Other literature studies assessed the impacts of aerosol pollution on photolysis frequencies using AOD values of 0.5 to 2 (Dickerson et al. 1997; Liao et al. 1999; Reuder and Schwander 1999). Due to the large differences in AOD between these studies and ours, a quantitative comparison with their results is difficult. However, a few similar features are identified. Liao et al. (1999) found that tropospheric photolysis rates are increased by sulfate aerosol pollution and decreased by absorbing soot aerosols. Using a radiative transfer model, Reuder and Schwander (1999) obtained a decrease of 20 to 30% in

the surface actinic flux due to an increase in AOD from 0.1 to 0.8 at 400 nm at Hoher Preissenberg in Germany. They found more significant decreases in total actinic flux at large SZA and at lower wavelengths, similar to our findings. Dickerson et al. (1997) investigated the effect of aerosol pollution for AODs at 380 nm between 0.5 and 2 on the photolysis frequency of NO_2. They obtained decreases in photolysis frequencies near the surface, and increases above and in the upper part of the aerosol layer, with stronger effects at large SZA.

In conclusion, our results on the effect of tropospheric aerosols are in good agreement with results from previous studies on this subject. The coupling between aerosols and photolysis frequencies presented here is used in this thesis to investigate the effect of stratospheric aerosols from the Pinatubo eruption on tropospheric photochemistry. Results on the changes in tropospheric photolysis frequencies and in the CH_4 removal by the reaction with OH due to stratospheric sulfate aerosols from the eruption are shown in Chapters 4 and 5.

3

ANALYSIS OF GLOBAL METHANE CHANGES AFTER THE PINATUBO ERUPTION

The global methane (CH_4) growth rate showed large variations after the eruption of Mount Pinatubo in June 1991. Both sources and sinks of tropospheric CH_4 were altered following the eruption by feedback processes between climate and tropospheric photochemistry. Such processes include Ultra Violet (UV) radiative changes due to the presence of volcanic sulfur dioxide (SO_2) and sulfate aerosols in the stratosphere, and due to stratospheric ozone (O_3) depletion. Changes in temperature and water vapour in the following years caused changes in tropospheric chemistry, as well as in natural emissions. We present a sensitivity study that investigates the relative effects that these processes had on tropospheric CH_4 concentrations, using a simple one-dimensional chemistry model representative for the global tropospheric column. To infer the changes in UV radiative fluxes, the chemistry model is coupled to a radiative transfer model. We find that the overall effect of natural processes after the eruption on the CH_4 growth rate is dominated by the reduction in CH_4 lifetime due to stratospheric O_3 depletion. However, all the other processes are found to have non-negligible effects, and should therefore be taken into account in order to obtain a good estimate of CH_4 concentrations after the eruption. We find that the overall effect was a small initial increase in the CH_4 growth rate after the eruption, followed by a decrease of about 7 ppb yr^{-1} by mid-1993. When changes in anthropogenic emissions are employed according to emission inventories, an additional decrease of about 5 ppb yr^{-1} in the CH_4 growth rate is obtained between the years 1991 and 1993. The results using the simplified single column model are in good qualitative agreement with observed changes in the CH_4 growth rate. Further analysis, taking into account changes in the dynamics of the atmosphere, variations in emissions from biomass burning, and in biogenic emissions of non-methane volatile organic compounds (NMVOC), requires the use of a full three-dimensional model.

This chapter has been published as:

Bândă, N., Krol, M., van Weele, M., van Noije, T., and Röckmann, T.: *Analysis of global methane changes after the 1991 Pinatubo volcanic eruption*, Atmos. Chem. Phys., 13, 2267-2281, doi:10.5194/acp-13-2267-2013, 2013.

3.1 INTRODUCTION

CH_4 is the second most abundant anthropogenic greenhouse gas in the atmosphere after CO_2. Its concentration in the atmosphere has increased since preindustrial times by a factor of 2.5 (Dlugokencky et al. 2011). A good understanding of the processes responsible for variations in the CH_4 concentration is needed for making future predictions and developing mitigation strategies. However, the evolution of the CH_4 concentrations observed in the background atmosphere in the past three decades is not fully understood (Montzka et al. 2011a). The growth rate of CH_4 was generally positive and showed a decreasing trend during the 80s and 90s, with year to year fluctuations (Dlugokencky et al. 2003). As shown in Figure 3.7, particularly large fluctuations were observed in the years following the eruption of Mount Pinatubo in 1991 (Bekki and Law 1997; Bousquet et al. 2006; Butler et al. 2004; Dlugokencky et al. 1994; 1996). After a peak of about 16 ppb yr^{-1} near the time of the eruption, the globally averaged CH_4 growth rate dropped to -2 ppb yr^{-1} in late 1992, remaining negative for the second half of the year 1992 (Dlugokencky et al. 2003). A subsequent recovery of the growth rate to 7 ppb yr^{-1} was observed by the end of 1993.

Changes in the global CH_4 concentration are determined by either changes in CH_4 emissions or by changes in the CH_4 lifetime. CH_4 is emitted from both natural sources (e.g. wetlands, oceans and geological seeps) and anthropogenic sources (e.g. agriculture, fossil fuel exploitation, waste treatment and biomass burning). The lifetime of CH_4 in the atmosphere is determined by the reaction of CH_4 with the hydroxyl radical (OH) in the troposphere, by the uptake of CH_4 by soils and by the destruction of CH_4 in the stratosphere. The main sink is, however, the reaction with OH, the other processes contributing by only 10-20% to the CH_4 loss (Prather et al. 2001; Spahni et al. 2011). Atmospheric levels of OH are determined by tropospheric photolysis reactions driven by the incident solar UV radiation, by water vapour levels, and by non-linear tropospheric chemistry. Because OH reacts with these species, its abundance is sensitive to atmospheric concentrations of CH_4, nitrogen oxides (NO_X), carbon monoxide (CO) and NMVOC. Montzka et al. (2011b) showed by inversions of methyl chloroform that the global tropospheric OH is relatively stable to perturbations, having an interannual variability of 2.3±1.5% for the period 1998 to 2007. Such a small variability was shown to be consistent with the small interannual variability in CH_4 concentrations. In a previous study, Prinn et al. (2005) found an interannual variability in tropospheric OH of 7 to 9% for the period 1978 to 2004. On a decadal timescale, a possible small positive trend in OH of the order of 0.2% yr^{-1} for the period 1985 to 2000, and higher after the year 2000, has been suggested by inversions of CH_4 and δ^{13}C-CH_4 (Monteil et al. 2011, scenario P2).

The eruption of Mount Pinatubo triggered a multitude of photochemical effects (McCormick et al. 1995), including feedbacks between climate and atmospheric photochemistry, which contributed to the observed evolution of the CH_4 concentrations.

The different processes had both positive and negative impacts on the CH_4 growth rate, affecting CH_4 emissions and the CH_4 lifetime. From satellite observations it is estimated that the eruption emitted about 18 ± 4 Tg SO_2 (Guo et al. 2004a). Volcanic SO_2 absorbs UV radiation between 290nm and 330nm, thus its presence in the stratosphere would lead to a decrease in O_3 photolysis in the troposphere (Dlugokencky et al. 1996). Since OH formation in the troposphere depends on the photolysis of O_3 to $O(^1D)$, the UV absorption by SO_2 would lead to a longer CH_4 lifetime. SO_2 stayed in the stratosphere for a few months, forming sulfate aerosols with an e-folding time of 23-25 days (Guo et al. 2004a). Enhanced sulfate aerosols were observed by the SAGE II satellite instrument for up to 4 years after the eruption at heights between 15 and 30 km with a maximum globally averaged aerosol optical depth (AOD) at 550 nm of approximately $\tau = 0.15$ about 7 months after the eruption (Russell et al. 1996; Thomason et al. 1997). Scattering of solar radiation by sulfate aerosols would lead to a further reduction of photolysis frequencies in the troposphere, thus to a longer CH_4 lifetime. Particles of ash emitted directly by the eruption would also absorb and scatter solar radiation, determining a similar effect on CH_4 lifetime. However, because of their lifetime of only a few days, they are considered to have a negligible global impact (Guo et al. 2004b; Niemeier et al. 2009) and are not included in our study.

Another secondary effect on the CH_4 lifetime is triggered by the destruction of stratospheric O_3 on sulfate aerosols. A maximum global O_3 depletion of 5% was observed by TOMS about two years after the eruption (Chipperfield et al. 2003). Changes of similar magnitude have been obtained in modelling studies (Bekki and Pyle 1994; Kinnison et al. 1994), and were attributed to enhanced heterogeneous O_3-depleting reactions on sulfate aerosols and changes in circulation due to stratospheric aerosol heating. Stratospheric O_3 loss would lead to an increase of UV radiation in the troposphere, and thus to a higher OH abundance and a shorter CH_4 lifetime.

The eventual fate of the volcanic sulfur is deposition to the surface. The modelling results of Gauci et al. (2008) indicate that deposition of 122 Tg SO_2 emitted by the Laki eruption led to a decrease of 8.8 Tg yr^{-1} in CH_4 emissions from wetlands in the two years following the eruption. As a rough estimate assuming linearity, the Pinatubo eruption would lead to 1.3 Tg decrease in the emissions. We consider this effect to be small and do not investigate it further here.

Other effects of the eruption on CH_4 concentrations have occurred because of temperature changes after the eruption (Bekki and Law 1997). The scattering of shortwave radiation by aerosols led to an increase in the reflected solar radiation of up to 10 W m^{-2} at the top of the atmosphere (Bender et al. 2010). This affected tropospheric temperatures, leading to an observed global cooling of up to 0.45 K in the two years following the eruption (Free and Angell 2002). Bender et al. (2010) show that ten general circulation models give a maximum decrease of 0.5 K in response to the observed changes in the shortwave radiative flux after the eruption. They attribute the 0.05 K difference between models and observations to the coinciding El Niño event.

Temperature perturbations trigger changes in the chemical composition of the atmosphere, as well as in natural sources related to biogenic activity. A decrease in temperature would generally slow down photochemical transformations. In particular, the slowdown of the reaction between CH_4 and OH would lead to higher tropospheric CH_4 concentrations (Bekki and Law 1997). Soden et al. (2002) found that the cooling after the eruption is associated to a maximum global decrease of 3% in the water vapour column in both observations and model simulations. Less water vapour in the troposphere would imply less OH formation by photolysis of O_3, because the reaction between $O(^1D)$ and water becomes less likely. This would increase the CH_4 lifetime, leading to CH_4 build-up in the atmosphere.

Natural emissions from wetlands, accounting for about 30% of the total emissions in the year 2004 (Spahni et al. 2011), are sensitive to temperature and soil moisture changes. Furthermore, natural emissions of NMVOC are known to be temperature dependent (Guenther et al. 1993). A decrease in the surface temperature would result in reductions in both CH_4 emissions from wetlands and biogenic NMVOC emissions. Biogenic emissions of NMVOC are also dependent on the amount of photosynthetically active radiation (PAR) reaching the surface (Guenther et al. 1993). Decrease in PAR fluxes because of enhanced aerosol scattering would further decrease these emissions. While a reduction in CH_4 emissions directly impacts CH_4 concentrations, a decrease in NMVOC emissions may affect OH, and thus impose an indirect impact on the CH_4 lifetime.

The eruption of Pinatubo also changed the dynamics of the atmosphere, which might have influenced OH and CH_4 concentrations. It was inferred in the 4-box modelling study of Schauffler and Daniel (1994) that heating of the stratosphere may increase the exchange between the stratosphere and the troposphere, leading to a decrease in tropospheric CH_4 concentrations. Lowe et al. (1997) suggest that a large effect of enhanced stratosphere-troposphere exchange would be inconsistent with the decrease in observed $\delta^{13}C$ in this period. However, other isotope data from this period do not support a strong decrease in $\delta^{13}C$ between 1991 and 1992 (Quay et al. 1999).

Although the processes presented above are known to have contributed to the evolution of the CH_4 growth rate after the Pinatubo eruption, their relative magnitudes are not yet totally resolved. CH_4 observations show the net outcome of these processes and other processes not related to the eruption, such as changes in anthropogenic emissions. The growth rate changes after the eruption have been attributed in other studies to changes in either sources or sinks. Dlugokencky et al. (1996) show that the evolution of CH_4 and CO in 1991 and early 1992 is consistent with a decrease in OH for up to one year after the eruption. They relate this decrease in OH to an attenuation of the UV flux due to the presence of SO_2 and sulfate in the stratosphere. Additionally, Dlugokencky et al. (1994) relate the decrease in CH_4 growth rate in 1992 to a decrease in anthropogenic emissions due to the collapse of the Soviet Union. The modelling study of Bekki and Law (1997) shows that temperature-

related effects had a significant impact on the growth rate of CH_4 in 1991-1992. They find that reduced emissions from wetlands may partly or fully explain the reduced growth rate in 1992. The inverse modelling study of Butler et al. (2004) reveals a global source-sink imbalance of +27 Tg CH_4 for the year 1991 and -19 Tg for the year 1992. In their inverse modelling studies, Bousquet et al. (2006) and Wang et al. (2004) both find a decrease in wetland emissions of 20-25 Tg between 1991 and 1993. Bousquet et al. (2006) also find reductions in the biomass burning and anthropogenic emissions, as well as in the OH sink for this period. In contrast, Wang et al. (2004) postulate an increase in OH due to reduced stratospheric O_3. Using a two-dimensional model, Bekki et al. (1994) also conclude that half of the CH_4 growth rate reduction in 1992 can be attributed to the effect of decreased stratospheric O_3. In the modelling study of Telford et al. (2010) it is found that natural isoprene emissions have a minimum in early 1993, yielding an increase in the CH_4 sink of 5 Tg yr^{-1}. Telford et al. (2010) also show that variations in meteorology lead to a decrease in the CH_4 sink of up to 14 Tg yr^{-1}, mainly due to changes in temperature and water vapour following the eruption. To our knowledge, no complete study has been made to include all competing effects of the Pinatubo eruption and to analyse the processes responsible for OH and CH_4 growth rate variations. Quantifying these processes may help us gain a better understanding of the CH_4 budget and, consequently, to make better predictions of the future atmospheric burdens.

In this sensitivity study we will use a simplified tropospheric column chemistry model as a first step to assess the changes in the CH_4 growth rate after the Pinatubo eruption and the relative contributions of the various processes. First, we will analyse how the equilibrium state of the chemical system changes when varying individual conditions (emissions, photolysis frequencies, water vapour). The impact on the tropospheric steady state gives us an idea about the drivers of CH_4 and OH concentrations, and about the relative magnitude of different processes. Next, we allow the system to respond to transient perturbations. The response of CH_4 concentrations to natural changes after the eruption will be contrasted to their response to changes in anthropogenic emissions. Due to obvious limitations of a single column model, the effect of changes in the dynamics of the atmosphere cannot be studied here. Additionally, because of the high sensitivity of OH to isoprene emissions in our model (see Section 3.3.1.1), we do not include the effect of changes in NMVOC emissions.

A detailed description of the column chemistry model is presented in Section 3.2. In Section 3.3.1 we show sensitivities of the model, and evaluate its performance in representing the global atmosphere in the period 1890-2005. We show our results on steady-state and transient CH_4 changes after Pinatubo in Section 3.3.2, and conclusions are drawn in Section 3.4.

3.2 MODEL SETUP

The model used in this study is a one-dimensional column chemistry model, coupled to the radiation model TUV (Madronich (1993), http://cprm.acd.ucar.edu/Models/TUV/). The chemistry model can be used both in steady-state and transient versions. The effects of atmospheric perturbations on photolysis frequencies are calculated with the radiative transfer model TUV, and then employed in the chemistry model.

3.2.1 *The column chemistry model*

In this exploratory study we use a strongly simplified model that represents the troposphere in 10 vertical layers of 1.5 km thickness each. The chemical scheme employs 8 chemical species, of which 5 are transported between adjacent layers (O_3, NO_X, CH_4, CO, RH). OH, HO_2 and RO_2 are not transported, but calculated in steady state with the longer-lived transported species. Here RH stands for NMVOC, and RO_2 for peroxy-radicals formed from NMVOC and CH_4 oxidation.

Vertical transport is defined by vertical diffusion coefficients of 10 m^2s^{-1} between the first two layers (at 1.5 km), 5 m^2s^{-1} between the second and 3rd layers (at 3 km) and 2 m^2s^{-1} higher up. No flux to the stratosphere is considered except for O_3 and CH_4. For O_3, we fix the concentration in the upper layer (at 13.5 km) at 148 ppb. A flux of 40 Tg yr^{-1} to the stratosphere is considered for CH_4, following Prather et al. (2001).

The chemical reactions included are presented in Table 3.1. We run the model with all-day all-year averaged reaction rate coefficients and photolysis frequencies. The 0.9 CO yield from CH_4 oxidation is comparable to that found by complex 3D global chemistry models (Shindell et al. 2006). The yield of CO from the oxidation of NMVOC varies strongly between species (Grant et al. 2010). We use here a global CO yield from NMVOC of 0.35. CH_4 oxidation produces CH_3O_2, which may react with NO, yielding at least one molecule of HO_2 through all the reaction pathways. CH_3O_2 is included in the model as RO_2, together with other compounds produced from NMVOC oxidation. Thus we consider an HO_2 yield y from the reaction of RO_2 and NO, equal to the ratio between the CH_3O_2 production from CH_4 and the total RO_2 production. For computational reasons, we use a global yield determined from a steady-state assumption. The rate of production of CH_3O_2 from CH_4 oxidation is equal to the rate of loss of CH_4 in this reaction. Assuming steady state, this is equal to the emission rate of CH_4 (E_{CH4}). Similarly, the rate of RO_2 production from NMVOC is equal to the emission rate of NMVOC (E_{RH}). Therefore the HO_2 yield y from the reaction of RO_2 and NO is taken as $\frac{E_{CH4}}{E_{CH4}+E_{RH}}$.

Reactants	Products
$O_3 + h\nu$	$2 \times OH$
$NO_2 + h\nu$	$O_3 + NO$
$O_3 + NO$	NO_2
$O_3 + OH$	HO_2
$O_3 + HO_2$	OH
$HO_2 + HO_2$	
$HO_2 + OH$	
$HO_2 + NO$	$OH + NO_2$
$NO_2 + OH$	
$CO + OH$	HO_2
$CH_4 + OH$	$0.9 \times CO + RO_2$
$RH + OH$	$0.35 \times CO + RO_2$
$RO_2 + NO$	$NO_2 + y \times HO_2$
$RO_2 + HO_2$	
$RO_2 + RO_2$	

Table 3.1: Reactions included in the model. Reaction rate coefficients are the ones described in Huijnen et al. (2010), except for photolysis rates, which are computed using TUV.

Dry deposition of O_3 and NO_2 are included with a deposition velocity of 1.0×10^{-3} m s^{-1}. An additional loss of NO_2 through heterogeneous reactions is considered, with a deposition velocity of 1.5×10^{-4} m s^{-1} throughout the column.

A time-dependent version of the chemistry model performs transient simulations using the Euler Backward Iterative scheme with a time step of one hour.

3.2.2 *Photolysis frequencies*

The TUV model version 4.1 is used to calculate the effects of SO_2, aerosols and O_3 column on tropospheric photolysis frequencies. Yearly averaged photolysis frequencies are calculated by averaging daily mean photolysis frequencies at 30°N for the 15th of the months of March, June, September and December. This latitude band is used because photochemistry is most active in the tropics, and is chosen such that CH_4 concentrations and lifetime are realistically reproduced.

For the base scenario, the climatological aerosol profile of Elterman (1968) is used, with an aerosol single scattering albedo of 0.99.

Simulation name	Changes implemented in TUV	Changes implemented in the column chemistry model
SO_2	2.54 DU of SO_2 between 15 and 30 km altitude	Changes in photolysis frequencies from TUV
Aerosol	0.15 AOD due to Pinatubo between 15 and 30 km altitude	Changes in photolysis frequencies from TUV
Ozone	5% O_3 column decrease	Changes in photolysis frequencies from TUV
Temp Rates		Changed reaction rate coefficients due to temperature
H_2O		Changes in water vapour profile due to changed temperature profile
CH_4 Emis		Changes in CH_4 emissions from wetlands due to temperature
Temp All		Changes in reaction rate coefficients, water vapour and CH_4 emissions due to temperature

Table 3.2: Setup of the Pinatubo simulations. AOD = aerosol optical depth; DU = Dobson Unit.

3.2.3 *Emissions and atmospheric parameters*

Global anthropogenic emissions for NO_X, CO, CH_4 and NMVOCs are taken from EDGAR 4.1 yearly values for the years 1970 - 2005 (European Commission and Joint Research Centre (JRC)/Netherlands Environmental Assessment Agency (PBL) 2011), and EDGAR-HYDE decadal emissions for the years 1890 - 1970 (Van Aardenne et al. 2001). Natural emissions used are described in Huijnen et al. (2010), except for CH_4 emissions, which are taken from Spahni et al. (2011) posterior values for the year 2004. The evolution of CH_4 emissions implemented in the model is shown in Figure 3.4. In addition to surface NO_X emissions, we add yearly 6.3 Tg N of NO_X from lightning (Huijnen et al. 2010), evenly distributed throughout the column in terms of mixing ratios.

Profiles of temperature, water vapour, O_3, and air density for 30°N were derived from the global 3D chemistry transport model TM5 (Huijnen et al. 2010) driven by ERA-Interim meteorological fields (Dee et al. 2011) for the year 2005. These are applied both in TUV and in the column chemistry model. The O_3 columns for the four months used here are respectively 302, 294, 283 and 270 Dobson Units (DU).

3.2.4 *Implementation of Pinatubo perturbations*

We define two sets of simulations. First, we evaluate the change in the model state due to individual natural perturbations after the eruption, in order to distinguish the most important drivers of CH_4 concentrations. In the second set of simulations we also include variations in anthropogenic CH_4 sources, with the aim to reproduce the evolution of the global CH_4 concentration in the early 1990s.

In the first set of simulations, we define the base simulation as the 1990 equilibrium situation. Next, the change in the model state due to the natural perturbations after Pinatubo is evaluated as a steady-state and as a transient response. The perturbations implemented in TUV and the column chemistry model are summarised in Table 3.2. In these sensitivity experiments, we assume constant anthropogenic and biomass burning emissions.

To compute the perturbations in photolysis frequencies after Pinatubo in TUV, we implement single forcings of 5% decrease in O_3 column, 2.54 DU increase in SO_2, equivalent to 18.5 Tg SO_2, and 0.15 increase in AOD. SO_2 and aerosols are considered to be evenly distributed in our atmospheric column between 15 and 30 km altitude. In the column chemistry model, the perturbations in photolysis frequencies are then scaled with the magnitudes of the forcings, thus assuming that the effects of these processes are linear. In addition, we assume additivity between the different processes by adding the perturbations in photolysis frequencies when more than one process is considered. We tested the effect of this assumption on our results by performing two simulations: one in which we used photolysis rates calculated with TUV by implementing all the forcings at the same time, and one in which we implemented each forcing separately and assumed additivity. The difference in the CH_4 steady-state concentration between the two simulations is 0.5 ppb, which is small compared to the magnitude of the perturbations related to the eruption.

The time evolution of the forcings assumed in the column chemistry model is based on observed values, and is shown in Figure 3.1. For SO_2, an exponential decay with an e-folding time of 24 days is considered, as found by Guo et al. (2004a), and a starting global mean concentration of 2.54 DU directly after the eruption. For the aerosol optical thickness, we use the Goddard Institute for Space Studies (GISS) monthly averaged values (Hansen et al. 2005), based on SAGE II satellite data. Surface temperature is taken from GISS analysis data (Hansen et al. 2010). The global mean GISS data for AOD and temperature are interpolated in the 4.5 and 3.5 years following the eruption, respectively. The resulting evolutions have a peak at approximately 7 and 15 months after the eruption, respectively, and then a smooth decay, which is extrapolated for 10 years. To a 0.5 K temperature decrease at the surface, we associate a tropospheric temperature change of 0.5 K decrease below 214.4 hPa, and a 1 K increase at 87.7 hPa, following the observations from Free and Angell (2002), and interpolate between these values. These profile changes are then scaled with the magnitude of the surface temperature change. For O_3 decrease, we use an evolution that has a peak of 4.5% 2 years after the eruption and then decays to 0, following the results of Randel et al. (1995).

The water vapour profile as a function of temperature change is evaluated using the Clausius-Clapeyron equation, assuming constant relative humidity. Variations in emissions of CH_4 from wetlands due to temperature are calculated using the Q_{10} temperature dependence relation (Dunfield et al. 1993), with a Q_{10} value of 2. For

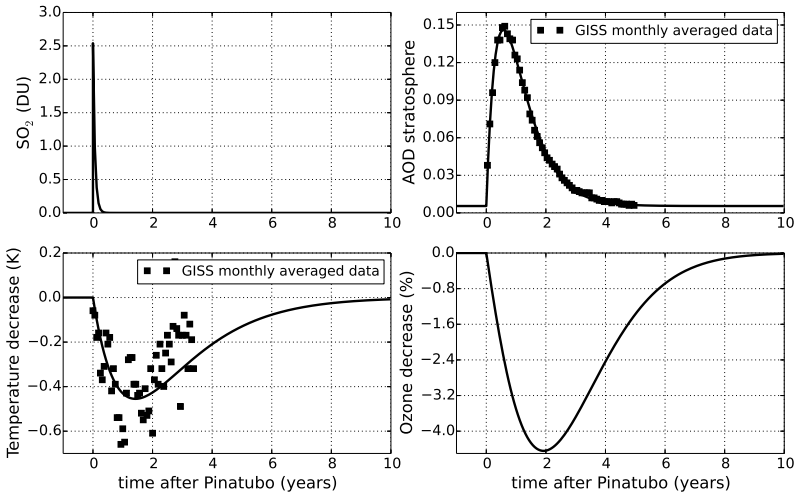

Figure 3.1: Time evolution of the forcings, as implemented in the model. Squares represent monthly averaged GISS data (Hansen et al. 2005; 2010).

a temperature decrease of 0.5 K, we find that CH_4 wetland emissions decrease from 171.8 Tg yr^{-1} to 165.9 Tg yr^{-1}.

The second set contains two additional transient simulations, which enable us to compare the magnitude of natural effects after the eruption to that of variations in anthropogenic sources. In both simulations we employ yearly anthropogenic emissions from EDGAR 4.1, while keeping the biomass burning emissions constant at 1990 values. In the first simulation, natural emissions and atmospheric parameters are kept constant. In the second one we also include the natural forcings after the eruption. These simulations are performed starting from the steady state in the year 1890, using EDGAR-HYDE and EDGAR 4.1 emissions for the spin-up period between 1890 and 1990.

3.2.5 *Methyl chloroform model*

For validating the transient OH concentrations obtained with our column chemistry model, we perform an offline simulation of methyl chloroform (MCF) for the period 1988 to 2005. We use the same column model, with only one chemical tracer, MCF.

The MCF emissions used are the same as described in Montzka et al. (2011b). The main sink of MCF is the reaction with OH in the troposphere. We use OH fields from each time step of the transient simulation for the period 1890 to 2005 (the

Species (unit)	1890	1990
CH_4 ($Tg\,yr^{-1}$)	278	512
NO_X ($Tg\,N\,yr^{-1}$)	22.7	47.6
CO ($Tg\,yr^{-1}$)	460	1177
NMVOC ($Tg\,C\,yr^{-1}$)	707	808

Table 3.3: Yearly emissions for 1890 and 1990 implemented in the model. Emission units are given in parentheses.

first simulation of the second set), and a temperature-dependent reaction rate as given in JPL 2011 (Sander et al. 2011). Additional stratospheric and ocean sinks are considered with lifetimes of 38 and 80 years, respectively. These are in the range of values found by Krol and Lelieveld (2003).

We use an initial condition in 1988 of 115 ppt throughout the column.

3.3 RESULTS AND DISCUSSION

3.3.1 *Model evaluation*

Even though the model presented above contains many simplifications, we will show that it performs reasonably well in representing the global state of the troposphere.

Figurere 3.2 presents the steady-state profiles for CH_4, O_3, NO_X, and CO obtained by the column chemistry model for the years 1890 and 1990. The yearly emission values used are shown in Table 3.3. CH_4 decreases with altitude by about 100 ppb throughout the troposphere in the year 1990. CO mixing ratios for the same year decrease with altitude from 125 ppb at the surface to 30 ppb near the tropopause. The NO_X profile has the typical C-shape due to the production of NO_X by lightning throughout the column and the longer lifetime of NO_X in the upper troposphere. Ozone mixing ratios decrease with altitude in the first few kilometers, and then increase towards the stratosphere.

Between the years 1890 and 1990, we find increases in O_3, CO and CH_4, which are more pronounced near the surface due to increases in emissions of O_3 precursors, CO and CH_4. For NO_X we find increases both near the surface, because of increased emissions, as well as near the tropopause, due to an increase in the NO_X lifetime at this altitude. This is consistent with a decrease in OH in the upper troposphere due to higher CH_4 concentrations. In the study of Wang and Jacob (1998), zonal averaged profiles for O_3, OH, NO_X and CO are computed using a three-dimensional model of tropospheric chemistry for preindustrial and year 1990 conditions. Concentrations

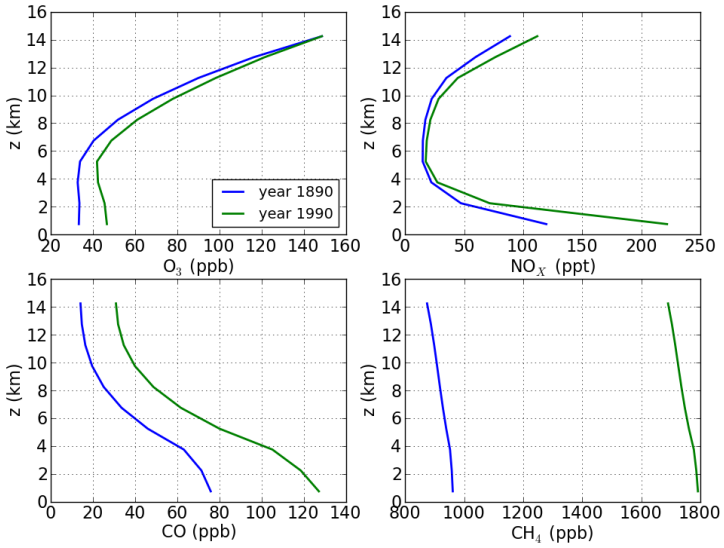

Figure 3.2: Vertical profiles of O_3, NO_X, CO, and CH_4 obtained with the one dimensional model for the years 1890 and 1990.

of O_3 and NO_X near the surface are somewhat higher in our model, possibly due to the fact that no differentiation is made between land and ocean in our simplified single column model. Our model finds a higher CO variability throughout the column, which may be caused by the fact that we did not formulate a convective redistribution of the column. In terms of changes in concentrations between the preindustrial setup and the year 1990, our model finds generally lower relative changes than the study of Wang and Jacob for O_3, NO_X and CO, possibly due to the different emission sets that are used. However, the 30% increase in OH that we find in the lowest 1.5 km of the model, and about 20% decrease between 6 and 12 km altitude compare well with their study.

In Table 3.4, we compare the O_3, OH and CO budgets given by our model for the year 1990 to global budgets found by several 3-dimensional chemistry transport models presented in Shindell et al. (2006); Stevenson et al. (2006); Williams et al. (2012). Overall, our model falls within the uncertainties of these models in terms of OH and CO burdens and budgets. CO and CH_4 lifetimes are also modeled realistically, certainly when one considers the huge simplifications of the chemical system and the simplified representation of the global atmosphere. Ozone burden, production, and deposition are high compared to full 3D models. These are more representative of

	Stevenson et al. (2006) S1 scenario	Shindell et al. (2006)	Williams et al (2012)	One-dimensional model
Ozone chemical production	5110 ± 606		4729	6117
Ozone chemical loss	4668 ± 727			5009
Ozone deposition	1003 ± 200		863	1349
Ozone stratospheric exchange	552 ± 168		274	241
Ozone burden (Tg)	344 ± 39		320	448
Ozone lifetime (days)	22.3 ± 2		23.4	25.7
OH (molec cm^{-3})		11.3 ± 1.7		9.5
OH production from photolysis			1663	2061
OH chemical production			3522	3519
CO chemical production		1505 ± 236	1314	1400
CO burden (Tg)			322	368
CO lifetime (days)			48.3	52.1
CH_4 lifetime (yrs)	8.76 ± 1.32	9.7 ± 1.7	8.35	8.2

Table 3.4: Comparison of trace gas budgets for the global troposphere obtained with our one-dimensional model, with the results from other models. Numbers in Tg yr^{-1}, unless otherwise specified.

tropical values than global ones, likely due to the choice of tropical conditions to represent the global troposphere. For the same reason, O_3 stratospheric inflow is quite low. This is because most O_3 inflow occurs in the extratropics (Gettelman et al. 2011), while our model column is in the tropics.

3.3.1.1 *Model sensitivities*

We further evaluate the sensitivity of the model to parameters involved in this study, i.e. to CH_4 and isoprene emissions, O_3 column, temperature and water vapour (Table 3.5). We compare the sensitivities of our model to sensitivities of 2D and 3D models present in literature. Except for the sensitivity to CH_4 emissions, these studies evaluate other sensitivities while keeping CH_4 concentrations fixed, or by looking at timescales of a few years. Because of the CH_4 lifetime of about 8 years, the feedback of CH_4 concentrations on its own lifetime is ineffective on such a short period. Therefore we also calculate these sensitivities while keeping CH_4 concentrations fixed.

The effect of CH_4 emission changes on the CH_4 concentrations is enhanced by the feedback via the CH_4 lifetime. To describe this process, a feedback factor a is defined as $a = 1/(1 - \frac{d\ln\tau}{d\ln CH_4})$, following Voulgarakis et al. (2012). Here τ stands for the CH_4 lifetime, and the small offsets $d\ln CH_4$ and $d\ln\tau$ are determined by a small perturbation in CH_4 emissions. We find that a has a value of 1.45 for the year 1990, which compares well with the best estimate of the Third Assessment Report

Sensitivity	1D model	Value in literature	Study
Feedback factor between CH_4 emissions and CH_4 concentrations	1.45	1.4	IPCC TAR, Prather et al. (2001)
		1.23 - 1.69	Voulgarakis et al. (2012)
Change in tropospheric OH due to a 6% increase in O_3 column (%)	6.4	6	Bekki and Pyle (1994)
Change in CH_4 lifetime due to a 1 K increase in global temperature (yr K^{-1})	- 0.49	- 0.31±0.14	Voulgarakis et al. (2012)
Change in tropospheric OH due to a 9% decrease in isoprene emissions (%)	1.9	1.	Telford et al. (2010)

Table 3.5: Sensitivities and feedback factors of our column chemistry model and comparison to literature.

of the IPCC (Prather et al. 2001), and falls well in the range found in the model intercomparison study of Voulgarakis et al. (2012).

Another sensitivity that is important to our study is the sensitivity of CH_4 to changes in the O_3 column. In the two-dimensional modelling study of Bekki and Pyle (1994), a 6% increase in OH is found due to a 6% decrease in stratospheric O_3 between the years 1991 and 1993. We find that a 6% decrease in O_3 column leads to a 6.4% enhancement in OH, which compares well to their results. Other studies that assess the sensitivity of CH_4 and OH to O_3 column changes find lower sensitivities (Camp et al. 2001; Fuglestvedt et al. 1994). However, the O_3 perturbations in these studies are dominated by the middle and high latitudes, where O_3 photolysis and CH_4 oxidation are less important. After the Pinatubo eruption, both low and high latitude O_3 columns were affected (Chipperfield et al. 2003). Therefore we consider it more appropriate to compare our results to Bekki and Pyle (1994).

To test the sensitivity of our model to climate, we used a temperature increase of 1 K throughout the column, and computed the corresponding change in humidity using the Clausius-Clapeyron equation. The CH_4 lifetime change of -0.49 yrK^{-1} in our model is somewhat larger than the multimodel mean of -0.31±0.14 yrK^{-1} found in Voulgarakis et al. (2012). However, we do not include changes in stratospheric O_3 related to temperature. We use observed changes in stratospheric O_3, and the effect of temperature on O_3 concentrations is included in the observations. The two models used in Voulgarakis et al. (2012) that also do not include this feedback give higher sensitivities to temperature, of -0.4 and -0.57 yrK^{-1}. Therefore we consider our model to respond to temperature changes in a similar manner as global chemistry models.

Telford et al. (2010) found a maximum decrease in isoprene emissions of 9% due to lower temperature and lower PAR fluxes in the year 1992 due to the presence of aerosols in the stratosphere. They find a corresponding 1% increase in OH tropospheric burden. We test the sensitivity of our model to such a perturbation in iso-

prene emissions, and find that our model is two times more sensitive. We attribute this again to our one-column approach, in which we cannot account for horizontal transport. Isoprene reacts rapidly with OH, and regions with large and small isoprene emissions are present in the true atmosphere. Furthermore, our simplified chemistry scheme is not well suited to explore the sensitivity to changing NMVOC emissions. A more recent study shows that the effect of aerosols on isoprene emissions is smaller if diffuse and direct radiation is treated separately (Wilton et al. 2011). We conclude therefore that the calculated feedback of NMVOC emissions on OH is highly uncertain, and we decide not to include it in further simulations. We simply note that decreases (increases) in NMVOC emissions probably lead to more (less) OH and a shorter (higher) CH_4 lifetime.

3.3.1.2 *Evaluation of CH_4 and methyl chloroform concentrations*

The results on MCF surface and tropospheric mean mixing ratios are shown in Figure 3.3. We compare our simulation results to the observations-based global mean mixing ratios, computed by averaging the GAGE/AGAGE data at the stations Mace Head, California, Barbados, Samoa, and Cape Grim. The modelled total lifetime of MCF is 4.6 yr and the lifetime with respect to OH is 5.7 yr, in agreement with other studies (Krol and Lelieveld 2003; Prinn et al. 2005). When we sample the model at the surface in the period in which MCF emissions were significant (1988-1998), the model is seen to overestimate the observed mixing ratios. This is related to differences in

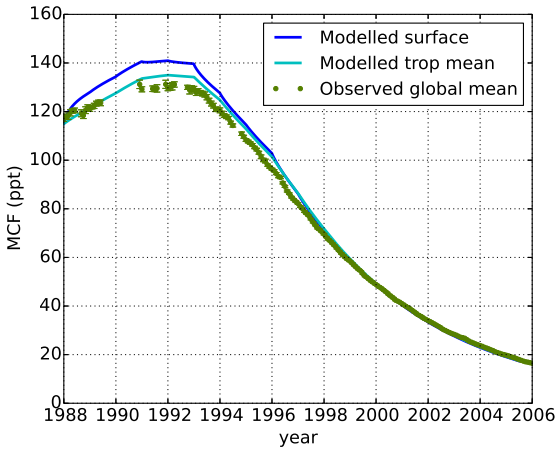

Figure 3.3: Observed and modeled evolution of methyl chloroform surface and tropospheric mean mixing ratios between 1988 and 2006.

the sampling of the model and the observations. Observations are generally taken in remote areas, away from the emissions, in order to be representative for the global burden. In our one-dimensional model, the sampling is done in the surface grid box, where the emissions are also put in. Therefore a tropospheric mean sampling of the model is in better correspondence with the observations. This is confirmed by the fact that our modelled tropospheric mean MCF mixing ratios are in very good agreement with GAGE/AGAGE observations. A tropospheric mean sampling of the model will be used in the rest of the paper.

The results for CH_4 concentrations from the first simulation of the second set, as defined in Section 3.2.4, are shown in Figure 3.4. They are compared to global means for the period 1890 to 1990, calculated from ice core measurements in Etheridge et al. (1998). Following the same procedure as used in Etheridge et al. (1998), we estimate global mean mixing ratios for the period 1985 to 2005 based on the monthly means from the GLOBALVIEW-CH4 (2009) data from the stations Alert and South Pole. The global mean is therefore computed as the mixing ratio at South Pole plus 37% of the interpolar difference. Modelled CH_4 mixing ratios generally follow the decadal trends in CH_4 emissions, with a delay of about 10 years due to the CH_4 lifetime. The stabilization of the concentrations towards the end of the simulation period is a phenomenon that is also present in the observations (Dlugokencky et al. 2003).

Compared to the observations, our model follows quite well the trends in CH_4 mixing ratios, but generally overestimates CH_4 mixing ratios by up to 50 ppb. We expect this to happen in the first decades of the simulation, because the starting point represents a steady state, while the system might not have been in equilibrium in the year 1890. The concentration continues to be overestimated until 1990, pointing either to an overestimation of the CH_4 emissions or of the CH_4 lifetime in this period. These results are only based on changing anthropogenic emissions (NO_X, CO, CH_4, NMVOC) for the simulated period, and there are several possible explanations for the differences between modelled and observed concentrations. Firstly, processes not included here, such as changes in stratospheric O_3, temperatures and possible trends in natural and biomass burning emissions can have a significant impact on CH_4 concentrations. Secondly, we are not able to represent high and low NO_X regions in our column chemistry model. For this reason, our model might misrepresent the sensitivity of CH_4 concentrations to NO_X and NMVOC emissions. Finally, we use a fixed CO yield from NMVOC oxidation for the simulated period. This yield varies among species and among NO_X pollution environments, therefore we would expect it to change on a centennial scale. However, the chosen model setup captures the observed range of CH_4 concentrations in the period 1990-2005, which is the period we are interested in.

We conclude that our model properly represents the global budgets and lifetimes of the different species, and is able to reproduce the mean state of the atmosphere in the 1990s. The sensitivities relevant for this study are reasonably represented. However,

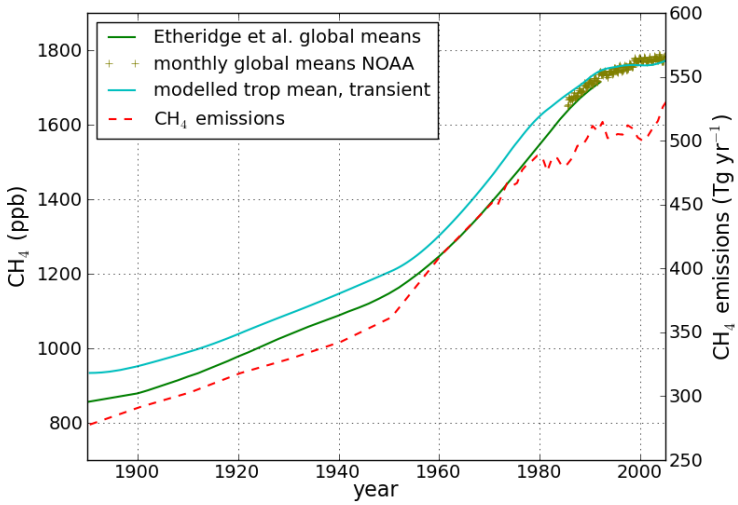

Figure 3.4: Observed and modeled evolution of CH_4 mixing ratios between 1890 and 2005. Observation-based global means are calculated by Etheridge et al. (1998) based on ice-core data (green line), and more recent global means are calculated using measurements at South Pole and Alert NOAA stations (green crosses). CH_4 emissions implemented in the model are also shown (red dotted line, with scale on the right axis) (Spahni et al. 2011; Van Aardenne et al. 2001).

the model is too simplified to capture variations of CH_4 on a centennial scale, or vertical profiles of different species present in the model. Our sensitivity tests also show that the sensitivity of the model to NMVOC emissions is overestimated.

3.3.2 *The Pinatubo Eruption*

3.3.2.1 *Steady-state perturbations*

We first examine the effect of each of the forcings of the Pinatubo eruption described in Table 3.2 on the CH_4 equilibrium concentration, using the maximum magnitude of each forcing. The differences in tropospheric CH_4 and OH between each simulation and the 'base' simulation are shown in Figure 3.5.

We find that the 5% reduction in O_3 column has the largest effect on the tropospheric mean CH_4 equilibrium mixing ratio, decreasing it by 125 ppb. SO_2, aerosol and water vapour changes all increase the CH_4 steady-state by 48 to 55 ppb. The

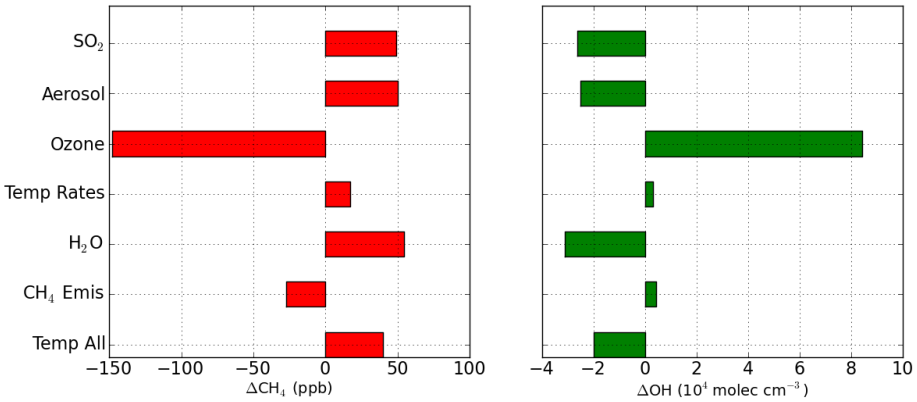

Figure 3.5: CH_4 and OH steady-state changes due to various Pinatubo forcings.

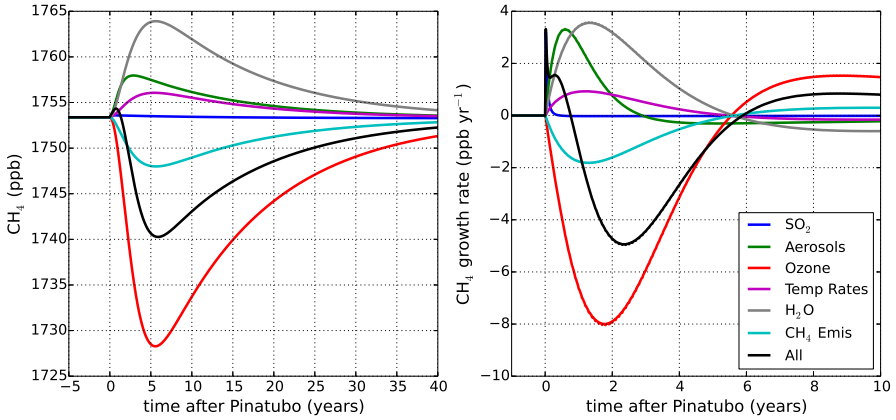

Figure 3.6: Effect of the different Pinatubo forcings on the temporal evolution of the tropospheric mean CH_4 mixing ratio and growth rate.

effects of temperature decrease on CH_4 emissions and reaction rates have smaller impacts on the simulated steady-state mixing ratios, of 27 and 17 ppb respectively. The temperature-related processes, that is 'Temp Rates', 'H_2O' and 'CH_4 Emis', partly cancel each other, resulting in an overall increase of 40 ppb.

Except for the effects of changed CH_4 emissions and changed reaction rates, the effects on CH_4 are strongly correlated to effects on OH of the same relative magnitude and of opposite sign. The OH response to decreasing CH_4 emissions reflects

the effectiveness of the feedback factor introduced in the previous section. Changed reaction rates due to tropospheric cooling lead to a small increase in OH, because of the slower oxidation rate of CH_4.

3.3.2.2 *Evolution of transient concentrations and growth rate*

The modelled transient evolution of CH_4 mixing ratios due to individual natural perturbations following the eruption, and including their overall effect, are shown in Figure 3.6a. When all natural effects are included, the tropospheric mean CH_4 mixing ratio slightly increases for 9 months after the eruption. Afterwards it decreases, reaching a maximum decrease of 13 ppb about 6 years after the eruption. The magnitudes of the perturbations in transient concentrations are smaller than the effect on the steady states, occurring at different moments in time after the eruption and on different timescales. Because the CH_4 lifetime is about 8 years, the concentration at one moment in time shows an integrated effect of its source-sink imbalance in the previous years. Therefore not only the magnitude, but also the duration of the perturbation plays an important role in determining its effect on CH_4 concentrations. The recovery time to the initial concentration is much longer compared to the recovery time of the perturbations applied. The SO_2 effect is hardly observed in the transient concentrations, because of its short duration. All the other processes affect the CH_4 concentration for up to 40 years after the eruption.

We calculate the CH_4 growth rate by differentiating the transient mixing ratios. The overall effect of the natural forcings after Pinatubo on the tropospheric CH_4 growth rate (Figure 3.6b) is a positive jump of 3 ppb yr^{-1} due to UV absorption by SO_2 immediately after the eruption. The effect decreases, but remains positive for about 9 months after the eruption, due to the presence of SO_2 and sulfate aerosols in the stratosphere. After that, the effect on the CH_4 growth rate is dominated by the forcing exerted by O_3 depletion, partly counteracted by decreased water vapour. The overall effect of natural forcings on CH_4 growth rate experiences a minimum of -5 ppb yr^{-1} about 2 years after the eruption. The growth rate increases afterwards, reaching zero about 6 years after the eruption, when the effect on the transient CH_4 mixing ratios is at a minimum (Figure 3.6a). The slow recovery of the concentrations to the steady state is marked by a small positive growth rate of less than 1 ppb yr^{-1}. The shape of the growth rate evolution reflects the annual imbalance between CH_4 sources and sinks.

We find a positive CH_4 growth rate for about 9 months after the eruption. The effect of temperature on the reaction rates is small in this period, and the temperature effect on emissions leads to a negative growth rate. Therefore we can only relate this positive growth rate to a decrease in OH, as also suggested by Dlugokencky et al. (1996). The large effect of O_3 depletion which follows compares well with the results of Bekki et al. (1994). They report a 7 ppb yr^{-1} decrease in growth rate from spring 1991 to autumn 1992 due to O_3 depletion. The drop in CH_4 growth rate due to O_3

depletion in our model is associated with a 5% increase in OH. This is consistent with the findings of Wang et al. (2004) of a global drop in OH of 10^5 molec cm^{-3}, equivalent to 7%, between the end of 1991 and beginning of 1994. Using the same parametric model, but keeping stratospheric O_3 constant, they find much smaller variability in OH in this period, on the order of 1-2%. Similar to our results, Bousquet et al. (2006) find an increase in the OH sink until the beginning of 1992, and then a subsequent decrease in 1992 and 1993. However, they find different magnitudes of these changes compared to our study, leading to an overall increase in the OH sink between 1991 and 1993. The magnitude of the temperature-related effects that we find compares well with the estimate from in Bekki and Law (1997). We find a maximum of 6 Tg yr^{-1} change in wetland emissions after the eruption. This is similar to the bottom up estimate of about 5 Tg yr^{-1} shown in Spahni et al. (2011) Figure 8a, but a few times lower than the maximum anomaly of about 40 Tg yr^{-1} found in the inverse modelling study of Bousquet et al. (2006). Our lower estimate might be partly due to the fact that we considered changes in CH_4 emissions solely due to temperature. CH_4 emission changes also depend on spatial and temporal changes in soil moisture and precipitation, which have also been observed after the eruption (Spahni et al. 2011). Changes in wetland extent were also shown to have a large impact on the interannual variability in CH_4 emissions from wetlands (Ringeval et al. 2010), which is also not taken into account in the study of Spahni et al. (2011) for the years 1991 and 1992. In addition, we consider a global Q_{10} factor of 2, while this factor was shown to be dependent on ecosystem type, with a range of measured values between 1.6 and 16 (Dunfield et al. 1993; Valentine et al. 1994).

The results show that stratospheric O_3 changes had a large impact on CH_4 growth rate after the eruption. The WMO 2003 report (Chipperfield et al. 2003) shows that the total O_3 in the atmosphere decreased between the years 1991 and 1993 by about 5%. Similar numbers are found when excluding the high latitudes (for 60°S-60°N), or when looking only at the tropical region (25°S-25°N). This change was caused partly by natural variability, including an increase in the solar activity in this period, and partly by processes related to the eruption. Therefore, after removing the effects of the solar cycle and QBO, a decrease of 2% to 3% is found in the measured total O_3 between 1991 and 1993. CH_4 measurements are affected by changes in the O_3 column, irrespective of their cause. For this reason, we used here a maximum decrease of 4.5% in the O_3 column, representative for 60°S-60°N, which includes solar variability. To distinguish the change in CH_4 concentrations due to changes in O_3 related to the eruption, a smaller perturbation should be considered.

The modelled CH_4 growth rate from the second set of simulations, when varying anthropogenic emissions of CH_4, CO, NO_X and NMVOC, is shown in Figure 3.7. These simulations have a starting point in 1890, producing a more realistic growth rate at the moment of the eruption of 10 ppb yr^{-1}. Results for the full length of the simulation, without including the post-Pinatubo perturbations, are shown in Fig-

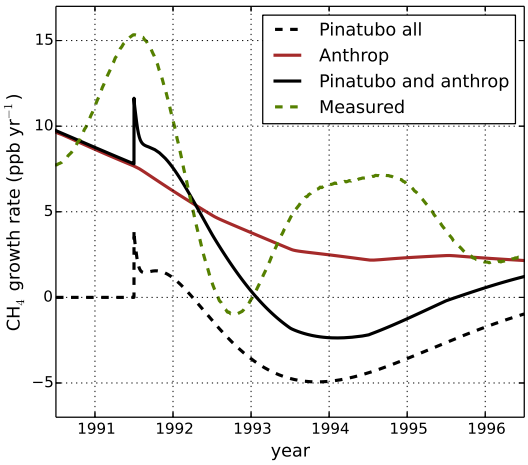

Figure 3.7: Modelled growth rate evolution after the Pinatubo eruption including variations due to anthropogenic emissions, and the combined signal from natural and anthropogenic changes. The black dotted line shows the growth rate evolution obtained in the first set of simulations, including all natural forcings (the same as the black line in Figure 3.6b). Also shown is the measured globally averaged growth rate obtained using the reference marine boundary layer matrix from GLOBALVIEW-CH4 (2009).

ure 3.4. We compare our results with the observations-based global mean growth rate, obtained by globally averaging the CH_4 reference marine boundary layer matrix from GLOBALVIEW-CH4 (2009), and deseasonalising it using the software provided by NOAA (based on Thoning and Tans (1989)). CH_4 anthropogenic emissions were relatively stable in the years 1990 to 2000, while anthropogenic NO_X emissions increased and CO emissions decreased. Therefore we find a generally decreasing trend in CH_4 growth rate due to a decrease in CH_4 lifetime, when only variations in anthropogenic emissions are taken into account.

When both variations in anthropogenic emissions and natural forcings are included in the model, a similar range of values is found for the modelled and observed growth rates in the years 1991 to 1996. These values vary between more than 10 ppb yr^{-1} and slightly negative values of up to -2 ppb yr^{-1}. Decreased anthropogenic CH_4 emissions between the years 1991 and 1993 are found to contribute by an additional 5 ppb yr^{-1} to the drop in CH_4 growth rate in this period, in agreement with previous studies (Bousquet et al. 2006; Dlugokencky et al. 1994). The timing of the minimum growth rate after the eruption is modelled about 15 months later than that observed. This minimum is found by a complex balance between the different forcings, being

later than the minimum in any of the individual forcings applied. Therefore the discrepancy between the timing of the modelled minimum and of the observed one might be related to the simplified evolution of the temperature and O_3 changes applied, or the fact that some sources of variability (see below) are not taken into account. This might also explain the fact that the increased growth rate in 1994 is not captured in our simplified simulations.

By comparing the sum of the 'Pinatubo all' and 'Anthrop' curves to the growth rate evolution when including both Pinatubo forcings and changes in anthropogenic emissions, we find that the effect of nonlinearity on growth rates is less than 10%.

Since our study is an idealised sensitivity study, there are many possible reasons for differences between the modelled and the observed growth rate. Firstly, many processes known to determine CH_4 variability are not included here. These include changes in biomass burning emissions (Bousquet et al. 2006), isoprene emissions (Telford et al. 2010) and variability in wetland emissions due to atmospheric changes related to the El Niño Southern Oscillation (ENSO) cycle (Hodson et al. 2011). Secondly, differences may result from the different sampling of the model and the observations, as already mentioned in Section 3.3.1.2. The interpolation procedure used to obtain the observed global CH_4 growth rate curve can also smoothen out some sudden variations in the CH_4 growth rate, such as the jump due to the SO_2 injected by the eruption. Finally, there are uncertainties related to our model setup, on which we elaborate further below.

In order to show that our results are robust with respect to the parameters used in the model, a series of sensitivity tests was performed. We tested different temperature and water vapour profiles, a higher value for the CO yield from the oxidation of NMVOC, including NMVOC recycling, and increased vertical mixing. Although the effect on the modelled CH_4 concentrations in the last century may be on the order of 100 ppb (results not shown), the effect on the growth rate evolution after the eruption is less than 10%. Changing the temperature by -2.5 K to +1 K and simultaneously changing the water vapour profile according to the Clausius-Clapeyron equation lead to changes in the CH_4 growth rate results of less than 0.1 ppb yr^{-1}. Similar results are obtained when changing the CO yield from NMVOC to 0.5 instead of 0.35, or when doubling the vertical mixing coefficients. Including a 0.25 yield of HO_2 from the oxidation of NMVOC in the presence of NO_X leads to a higher growth rate minimum after the eruption by 0.3 ppb yr^{-1}. We estimate therefore a maximum error of 10% in the modelled growth rate due to uncertainties in the model parameters.

Horizontal distributions of the modelled forcings can play an important role for the overall effect on the CH_4 growth rate, and cannot be simulated in our column model. This may cause additional uncertainties in our results. For example, we expect to overestimate the effect of SO_2, by inferring an instant homogenisation of the emissions. In reality, high concentrations were found close to the emission point after the eruption, and the short lifetime of SO_2 limited this effect to low latitudes (Guo et al. 2004a). Changes in stratospheric aerosol, O_3 and temperature have been observed

globally, but with different magnitudes at different latitudes. Since CH_4 oxidation is more important in the tropics, processes that are relatively stronger in the tropics will have a higher impact on the CH_4 lifetime.

3.4 CONCLUSIONS

We have implemented a column chemistry model, and tested its performance in representing the mean state of the atmosphere. Although we acknowledge that our model is simplified and difficult to apply in a globally-averaged fashion, it allowed us to quantify for the first time the combined effect of radiation and temperature-related effects after the Pinatubo eruption on the CH_4 growth rate, including feedbacks on the CH_4 lifetime. The results show that full recovery of transient CH_4 concentrations from these perturbations takes about 40 years.

Using this simple approach, we are able to explain a large part of the observed drop in CH_4 growth rate after the eruption of Pinatubo. We conclude that a multitude of emission and lifetime effects contributed to the observed growth rate variations following the eruption, as has been suggested by previous inverse modelling studies (Bousquet et al. 2006; Wang et al. 2004). We find that about 7 ppb yr^{-1} of the observed 17 ppb yr^{-1} can be explained by natural processes after the eruption. The dominating effects operate through tropospheric photolysis rates, with an important contribution from O_3 depletion. This shows the importance of stratospheric-tropospheric couplings, and that a good representation of stratospheric chemistry is needed in order to model accurately CH_4 concentrations. We also find that the decrease in anthropogenic emissions between 1991 and 1993 contributed by 5 ppb yr^{-1} to the decreased CH_4 growth rate in 1993. The remaining 5 ppb yr^{-1} of the observed drop in CH_4 growth rate remains unexplained, and might be related to changes in emissions from biomass burning or changes in biogenic NMVOC emissions.

Our model has the advantage of simplicity; however, there are processes that cannot be represented, such as horizontal transport and changes in the dynamics of the atmosphere. Additionally, we did not consider the spatial distribution of CH_4 emissions. Using a global vegetation model would allow better estimates of the response of natural emissions to changes in temperature, precipitation and radiation. Therefore, a three dimensional chemistry transport model coupled with a climate model will be used to perform future experiments.

4

THE EFFECT OF STRATOSPHERIC SULFUR FROM MOUNT PINATUBO ON TROPOSPHERIC OXIDIZING CAPACITY AND METHANE

The eruption of Mount Pinatubo in 1991 injected a large amount of SO_2 into the stratosphere, which formed sulfate aerosols. Increased scattering and absorption of UV radiation by the enhanced stratospheric SO_2 and aerosols decreased the amount of UV radiation reaching the troposphere, causing changes in tropospheric photochemistry. These changes affected the oxidizing capacity of the atmosphere and the removal rate of CH_4 in the years following the eruption. We use the three-dimensional chemistry transport model TM5 coupled to the aerosol microphysics module M7 to simulate the evolution of SO_2 and sulfate aerosols from the Pinatubo eruption. Their effect on tropospheric photolysis frequencies and concentrations of OH and CH_4 are quantified for the first time.

We find that UV attenuation by stratospheric sulfur decreased the photolysis frequencies of both O_3 and NO_2 by about 2% globally, decreasing global OH concentrations by a similar amount in the first two years after the eruption. SO_2 absorption mainly affects OH primary production by O_3 photolysis, while aerosol scattering also alters OH recycling. The effect of stratospheric sulfur on global OH and CH_4 is dominated by the effect of aerosol extinction, while SO_2 absorption contributes by 12.5% to the overall effect in the first year after the eruption. The reduction in OH concentrations causes an increase in the CH_4 growth rate of 4 and 2 ppb yr^{-1} in the first and second year after the eruption, respectively, contributing 11 Tg to the 27 Tg observed CH_4 burden change in late 1991 and early 1992.

This chapter has been published as:
Bândă N., Krol, M, van Noije, T., van Weele, M., Williams, J. E., Le Sager, P., Niemeier, U., Thomason, L., and Röckmann, T.: *The effect of stratospheric sulfur from Mount Pinatubo on tropospheric oxidizing capacity and methane*, J. Geophys. Res. Atmos., 120, 1202-1220, doi:10.1002/2014JD022137, 2015

4.1 INTRODUCTION

The hydroxyl radical (OH) is the main oxidant in the troposphere, controlling the removal of many atmospheric pollutants (Levy 1971). The atmospheric lifetime of methane (CH_4), the second most important anthropogenic greenhouse gas, is mainly determined by OH. About 70% of CH_4 is oxidized in the tropical troposphere, where photochemistry is most active (Lawrence et al. 2001). Large uncertainties still remain about the CH_4 budget in the past decades and the role of OH in controlling CH_4 concentrations (Kirschke et al. 2013; Naik et al. 2013). Chemistry and climate models (Naik et al. 2013) as well as a study simulating the isotopic composition of CH_4 isotopes (Monteil et al. 2011) infer a positive OH trend of up to 0.3%/yr in the past decades, while inverse modelling studies using methyl chloroform find a positive trend in OH in the 1980s, followed by a decline in the 1990s (Bousquet et al. 2005; Krol and Lelieveld 2003). These studies stress that the inferred OH trend is very sensitive to uncertainties in the assumed methyl chloroform emissions. Bousquet et al. (2005) estimated an inter-annual variability (IAV) of OH between 1980 and 2000 of 8.5±1.0%. A more recent study from Montzka et al. (2011a) finds a smaller IAV of 2.3±1.5% for the period 1998 to 2007.

The eruption of Mt. Pinatubo in June 1991 caused significant global scale radiative and climate changes which likely affected tropospheric CH_4 and OH concentrations. Dlugokencky et al. (1996) observed an anomalously high CH_4 growth rate during the second half of 1991, which they attributed to a decrease in the OH sink caused by changes in radiation. Subsequently, the CH_4 growth rate strongly decreased, becoming negative during late 1992, and then recovered by mid-1993 to 5 $\mathrm{ppb\,yr^{-1}}$ (Dlugokencky et al. 1996).

Global scale OH variability may be caused by variations in OH sources, sinks and recycling between OH and HO_2, which depend on multiple factors, such as climate and natural and anthropogenic emissions of reactants. Tropospheric OH is produced through the photolysis of ozone (O_3) by ultra-violet (UV) radiation and the subsequent reaction of $O(^1D)$ with water vapour. This primary production of OH by O_3 photolysis in the troposphere mainly occurs at wavelengths between 290 and 330 nm. Photolysis of nitrogen dioxide (NO_2) at wavelengths up to 420 nm also affects OH concentrations because it produces nitrogen oxide (NO), important for OH recycling (Lelieveld et al. 2002). Therefore the amount of OH in the troposphere is influenced by the amount of incoming UV radiation.

The Pinatubo eruption injected about 18.5 Tg sulfur dioxide (SO_2) into the stratosphere, which was converted to sulfate aerosols on a timescale of about 24 days (Guo et al. 2004a). Having a lifetime of one year, sulfate aerosols remained in the atmosphere for a few years after the eruption (Bauman et al. 2003). SO_2 absorbs UV radiation between 240 and 320 nm (Bogumil et al. 2003), while sulfate aerosols scatter radiation. Thus the presence of these species in the stratosphere led to a decrease in the UV radiation entering the troposphere.

Using a box model, Dlugokencky et al. (1996) found the decrease in OH due to the UV attenuation by SO_2 and sulfate consistent with the high CH_4 and carbon monoxide (CO) growth rates in the second half of 1991. In their inverse modelling study, Bousquet et al. (2006) inferred a reduction of the OH-based sink of 26 Tg CH_4 in the two years following the eruption, and attributed this reduction to changes in UV radiation. Previous studies have been carried out to assess the impact of Pinatubo sulfate aerosols on short and longwave radiation using 3D chemistry climate models (e.g. Andronova et al. 1999; Stenchikov et al. 1998; Timmreck et al. 1999). To our knowledge, none of these studies estimated the direct effect of stratospheric sulfate on UV radiation and tropospheric photochemistry. Furthermore, studies of the Pinatubo eruption generally do not include absorption by SO_2. In the two-dimensional studies of Bekki et al. (1993; 1996), SO_2 absorption was shown to be important for the stratospheric O_3 abundance after Pinatubo, and the volcanic plume lifetime of the Toba mega-eruption.

In this study we restrict our analysis to the effects of SO_2 and sulfate described above, which are significant in the first two years after the eruption. The three-dimensional model TM5 is used to simulate SO_2 and sulfate aerosols from the eruption, and the corresponding changes in UV radiation, OH and CH_4 concentrations. It is important to note that changes in climate are incorporated through the use of the ERA-Interim atmospheric reanalysis from the European Centre for Medium-Range Weather Forecasts (ECMWF), and that stratospheric O_3 changes are prescribed based on satellite observations. The perturbations in climate and stratospheric O_3 associated with the eruption (see Chapters 3 and 5) will thus be included in the model runs, but their effect on the CH_4 budget is not investigated here.

This chapter is organized as follows. The model setup is described in Section 4.2. In Section 4.3.1 we compare the modelled and observed evolution of the SO_2 and sulfate burdens. The results on tropospheric CH_4 and OH after the eruption are shown in Section 4.3.2. The results are discussed in Section 4.4, and conclusions are drawn in Section 4.5.

4.2 METHOD

The atmospheric chemistry and transport model TM5 (Huijnen et al. 2010; Williams et al. 2012) was used in this study to simulate tropospheric photochemistry and aerosols. Aerosol microphysics is modelled by the modal scheme M7 (Aan de Brugh et al. 2011; Vignati et al. 2004). In this section, the setup of the TM5 model is presented. We include a description of the changes implemented in TM5 and M7 useful for modelling volcanic SO_2 and sulfate and their effect on tropospheric chemistry. The performance of TM5 in simulating atmospheric chemistry was validated against observations in Huijnen et al. (2010) and van Noije et al. (2014) and the main con-

clusions of these studies remain valid under the current setup. At the end of Section 4.2 we define the simulations performed in this study.

4.2.1 *The TM5 chemistry transport model coupled to the M7 aerosol module*

The TM5 model was run on 60 hybrid sigma-pressure vertical layers, at a resolution of 3° x 2° (longitude x latitude) globally, except for the polar region, where a reduced grid was used. This vertical resolution was employed because the default model configuration of 34 layers was found to produce large numerical diffusion errors for stratospheric SO_2 (see Appendix A). The model was driven by meteorological data from the ECMWF ERA-Interim reanalysis (Dee et al. 2011). The gas-phase chemistry scheme is based on a modified and updated version of the carbon bond mechanism 4 (Houweling et al. 1998). The natural and anthropogenic emissions of gas-phase and aerosol species used are described in Appendix B. The photolysis frequencies were determined by the parameterisation scheme based on Williams et al. (2006), using on-line radiative transfer calculation for wavelengths between 202 nm and 695 nm.

Two setups for calculating CH_4 concentrations are possible in TM5: a 'free-running' setup and a 'nudged' setup. In the 'free-running' setup CH_4 concentrations are calculated from the balance between sources, sinks, and transport. To avoid a long term drift in the CH_4 concentration due to small imbalances in sources and sinks, in the 'nudged' setup monthly surface station data from background sites is used to constrain the CH_4 concentrations in the lowest 2 km of the model. The observed north-south gradient in CH_4 mixing ratios is obtained through latitudinal interpolation of the monthly-mean observations at the stations South Pole, Cape Grim, Mauna Loa, Niwot Ridge, Barrow, and Alert. The ratio f between the measured and modelled CH_4 mixing ratio at the dateline (0° longitude) is applied as a scaling for the modelled CH_4 in each zonal band, with a relaxation timescale of τ =3 days. The modelled CH_4 mixing ratios are then adjusted at each timestep using the following equation:

$$[CH_4]_{new} = [CH_4]_{old} + [CH_4]_{old} \times (f-1) \times (1-e^{-dt/\tau}) \tag{4.1}$$

where $[CH_4]_{old}$ represents the modelled CH_4 mixing ratio, taking into account sources, sinks and transport, $[CH_4]_{new}$ is the adjusted CH_4 mixing ratio, and dt is the timestep. As will be described in Section 4.2.2, a combination of the two setups was used in this study.

Since TM5 does not include stratospheric O_3 chemistry, O_3 is nudged to the multi-sensor reanalysis data (van der A et al. 2010) above 45 hPa in the tropics and above 90 hPa in the extratropics. To constrain the stratospheric loss of CH_4 by OH, Cl and $O(^1D)$, CH_4 is also nudged above these pressure levels using climatological values from Grooß and Russell III (2005).

The aerosol module M7 simulates the following aerosol types: sulfate (SO_4), black carbon (BC) and organic carbon (OC), sea salt and mineral dust. In addition, TM5

simulates ammonium and nitrate using the Equilibrium Simplified Aerosol Model (EQSAM; Metzger et al. (2002)), and methyl sulfonic acid (MSA). The M7 module uses 7 modes to describe the size distribution of aerosols. Three modes are used for insoluble particles (aitken, accumulation, and coarse) and four modes for soluble particles (nucleation, aitken, accumulation, and coarse). Each mode is represented by a lognormal size distribution with a fixed width of σ=2.0 for coarse mode particles and σ=1.59 for the other modes.

For simulating the eruption, some adjustments were needed in this default representation of aerosols in M7. In Kokkola et al. (2009) the performance of the M7 scheme was tested for volcanic eruption conditions in a box model setup. They postulate that the coarse mode is representative for large sea salt and dust particles, and should not be used for modelling stratospheric sulfate, as this would lead to an overestimated particle size and to a short atmospheric lifetime of sulfate aerosol due to fast sedimentation. Furthermore, a decreased width of the particle distribution has been observed after large volcanic eruptions (Bauman et al. 2003). The findings of Kokkola et al. (2009) show that removing the soluble coarse mode, and reducing the width of the soluble accumulation mode to σ=1.2 significantly improves the model performance in such situations. Niemeier et al. (2009) and Toohey et al. (2011) used this setup to simulate the Pinatubo eruption within the global climate model MAECHAM5-HAM, showing realistic results. We therefore use the setup recommended in Kokkola et al. (2009) above 300 hPa, and the standard M7 setup below 300 hPa to model tropospheric aerosols. As a consequence, tropospheric coarse mode particles are restricted below 300 hPa. As stratospheric accumulation particles sediment below 300 hPa they are redistributed into the tropospheric accumulation and coarse modes. This redistribution might cause some unphysical changes in their radiative properties. However, particles have a short residence time in the troposphere of about one week. Therefore we expect the error on the radiative effect of volcanic sulfate particles due to this setup to be marginal. The nucleation scheme in M7 was also adapted to handle large sulfuric acid concentrations (H_2SO_4), according to Kokkola et al. (2009).

To model scattering and absorption of UV radiation by aerosols interactively, the TM5 photolysis scheme has been coupled to the M7 module. Aerosol optical properties are calculated using the lookup table generated by the Generic Aerosol Optics Toolbox (GAOT) (Aan de Brugh 2013). Note that unlike in global climate models, the radiative transfer scheme in our model is solely used for photolysis calculation. Modeled aerosol fields are therefore coupled to the chemistry, but not to the meteorological fields in our model. The perturbation in stratospheric temperature after Pinatubo is included in the reanalysis data used here through the assimilation of satellite observations.

Absorption by SO_2 between 280 and 340 nm has been implemented in order to infer the effect of SO_2 on tropospheric photolysis frequencies. SO_2 absorption cross

Table 4.1: Setup of the simulations

Simulation name	Pinatubo SO_2 emission	SO_2 absorption	Pinatubo aerosol extinction
PinS	Yes	Yes	Yes
PinS1	Yes	No	Yes
NoPinS	No	No	No

section values presented in Bogumil et al. (2003) are used. We find SO_2 absorption not to be significant on photolysis frequencies in volcanically quiescent conditions.

4.2.2 *Model simulations*

The simulations presented here (Table 4.1) were performed for the period June 1991 to May 1993, after a 1.5 year spin-up from the beginning of 1990. The spin-up was done starting from modelled concentrations of chemical species on 1 January 2007, and scaling CH_4 concentrations down by 1.5%, the ratio between observed CH_4 concentrations in 2007 and 1989. The 'NoPinS' simulation corresponds to a situation without a Pinatubo stratospheric injection of sulfur. To represent the Pinatubo eruption in the 'PinS' and 'PinS1' simulations, an emission of 18.5 Tg SO_2 was assumed at the location of the eruption on the 15th of June 1991 for three hours starting at 14.00 local time, as reported by (Wolfe and Hoblitt 1996). TM5 subsequently transports the SO_2 plume and the chemistry scheme accounts for the conversion of SO_2 to sulfate particles.

The aerosol plume was observed between 19 and 24 km at the end of June 1991 at Mauna Loa station (see Figure 4.2a). The Microwave Limb Sounder (MLS) found peak concentrations of SO_2 at 26 km in September 1991 (Read et al. 1993). In this study the SO_2 emission was distributed vertically between 15 and 23 km, with the bulk of the emission (80%) between 17 and 21 km. Other injection heights were tested and are presented in Appendix C.

While in the 'PinS1' simulation only aerosols were coupled to the photolysis, in the 'PinS' simulation both SO_2 and aerosols are allowed to interact with UV radiation. The main difference between 'PinS' and 'NoPinS' in the troposphere is due to the aerosol extinction of UV radiation. In the stratosphere, some additional differences in the chemistry are caused by the reaction of volcanic SO_2 with OH. The lifetime of SO_2 from Pinatubo is about one month, so absorption by stratospheric SO_2 becomes negligible in 1992. Therefore 'PinS1' was not continued in 1992. We find the difference between 'PinS1' and 'PinS' to be quite small at the end of 1991,

showing that nonlinear feedbacks, such as different aerosol fields or the feedback between CH_4 and its lifetime, cause only minor changes beyond 1992. Note that the meteorological fields and stratospheric O_3 values used in the three simulations have been taken from datasets that responded to the Pinatubo eruption (van der A et al. 2010). Therefore the effects of temperature and O_3 on OH and CH_4 are included in all simulations. However, differences between simulations represent only the direct effects of stratospheric sulfur.

Due to imbalances between uncertain CH_4 sources and sinks, modelled CH_4 concentrations tend to drift from observed values in free running models. In order to account for these uncertainties, we use a two-step setup. As a first step, the 'PinS' scenario was run with nudging to observed CH_4 concentrations, as described above. The monthly accumulated corrections introduced by the nudging to match CH_4 observations were stored. In the second step, the residual emissions (either positive or negative) obtained in the first step were used to scale the monthly CH_4 emission totals in each 10° latitude band, while maintaining the emission distribution from the original inventory. The three scenarios were run without further constraining CH_4 concentrations. This setup enables us to simulate realistic CH_4 concentrations, at the same time allowing them to respond interactively to photo-chemical perturbations. We verified that the modelled burdens and concentrations were almost identical in the two 'PinS' simulations. The results presented from here on are from the simulations of the second step.

4.3 RESULTS

The evolution of the global SO_2 burden after the eruption and a comparison with estimates based on satellite observations are shown in Figure 4.1. Although the initial SO_2 load corresponds to the one measured by TOVS (TIROS (Television Infrared Observation Satellite) Optical Vertical Sounder, Guo et al. (2004a)), our model generally overestimates the stratospheric SO_2 load by about 40%. We find an SO_2 lifetime of 35 days from August to November 1991, which compares well with the estimate of 33 days based on MLS data from September 1991 (Read et al. 1993). We do not find a significant difference in the SO_2 lifetime between the 'PinS' and 'PinS1' simulations. While an increase in SO_2 lifetime due to SO_2 absorption was found for the Toba mega-eruption (Bekki et al. 1996), we do not find this to occur for Pinatubo. The initial evolution of the burden is not well captured in the model. We find a reduced loss rate in the first few days after the eruption, which may be related to OH depletion within the plume. Contrarily, TOMS (Total Ozone Mapping Spectrometer) and TOVS data indicate a shorter lifetime of 23-25 days based on measurements during the first two weeks after the eruption. However, we expect that the initial overestimate of the SO_2 burden and the delay of about one month in its conversion to sulfate does not significantly affect our conclusions. The effect of the modelled SO_2 on tropospheric

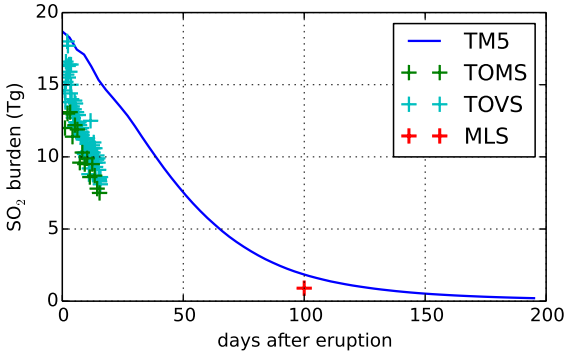

Figure 4.1: The modelled evolution of the stratospheric SO_2 burden, and comparison with TOMS, TOVS (Guo et al. 2004a), and MLS estimates (Read et al. 1993).

OH and CH_4 is found to be quite small on a global scale in comparison to the aerosol effect (see Sections 4.3.2 and 4.3.3).

4.3.1 *The modelled SO_2 and sulfate concentrations*

To investigate how the model simulates the evolution of the stratospheric aerosol field, Figure 4.2 presents the modelled and measured vertical profiles of aerosol backscatter at 694.3 nm at Mauna Loa station, using observations from a ruby lidar system (Barnes and Hofmann 1997). In the first few months after the eruption, our model captures well the backscatter values below 25 km, although it overestimates the backscatter between 25 and 35 km. This overestimate might be due to the lack of re-evaporation of aerosols, which becomes important near 30 km (Dhomse et al. 2014). Interestingly, periods of high backscatter occur about every 3 weeks in the first three months after the eruption, corresponding to the time needed for the plume to circle the globe before it is diffused in longitudinal and latitudinal directions. The agreement with observations suggests that the speed of the longitudinal transport and the latitudinal diffusion of the plume are well captured in our model. Starting from December 1991, the model agrees well with observations for both the backscatter values and the height at which the backscatter occurs.

Figure 4.3 shows the evolution of the zonal averaged aerosol optical depth (AOD) observed by SAGE II (Stratospheric Aerosol and Gas Experiment II; Thomason et al. (2008); Thomason and Peter (Eds)) at 525 nm above 10 km and by AVHRR (Ad-

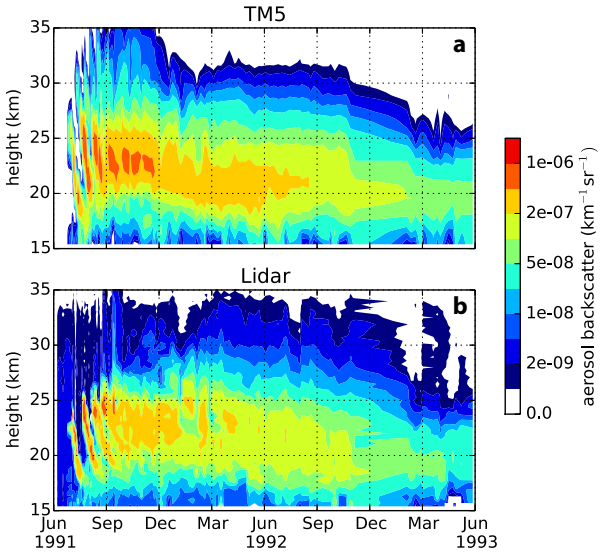

Figure 4.2: Evolution of a) simulated and b) lidar observed stratospheric aerosol backscatter profile at 694.3 nm at Mauna Loa station (Barnes and Hofmann 1997) in the first two years after the eruption.

vanced Very High Resolution Radiometer; data version 2.0; Zhao et al. (2013)) at 630 nm, and the corresponding modelled values. Since AVHRR measures the total column AOD including the troposphere, we removed the tropospheric signal by subtracting the AVHRR-measured AOD from the two years before the eruption (June 1989 to May 1991), as decribed in Long and Stowe (1994). The modelled AOD at 525 nm is generally lower than that at 630 nm. Since the simulated volcanic particles grow to 0.42 μm (Figure 4.4), they have a peak extinction efficiency around 0.6 μm. This wavelength dependence of the AOD was also captured by SAGE II, which showed highest extinction values for 525 nm among the four measured wavelengths (386, 452, 525 and 1020 nm) during 1992 and 1993 (Bauman et al. 2003). The AOD values in our model are generally higher than those measured by SAGE II and AVHRR in the tropics and northern mid-latitudes in the first year after the eruption. AOD reaches 0.45 in the tropics in autumn 1991, higher than the observed values of less than 0.35 by SAGE II and less than 0.4 by AVHRR. The transport of the volcanic cloud to both Northern and Southern Hemispheres is captured reasonably well by the model. However, the transport to the northern high-latitudes is more pronounced in the model compared to observations, while the transport to the southern high-latitudes is less pronounced than in the SAGE II data. In the second year after the eruption the modelled AOD compares well to SAGE II data and is about 0.05 lower than the AVHRR

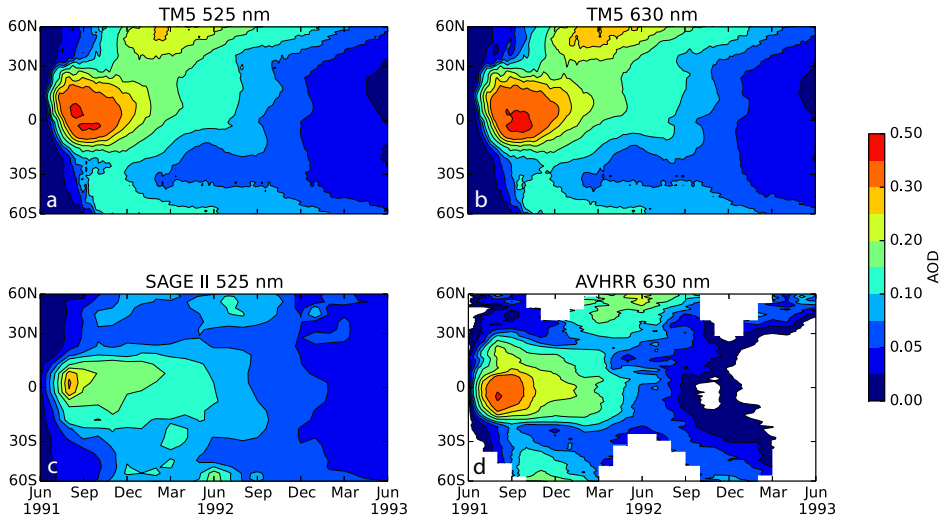

Figure 4.3: Evolution of the stratospheric aerosol optical depth after the eruption, modelled a) at 525 nm, and b) at 630 nm and measured c) by SAGE II at 525 nm (Thomason and Peter Eds) and d) by AVHRR at 630 nm (Zhao et al. 2013). The tropospheric signal was removed from AVHRR by subtracting the AOD from the two years prior to the eruption (June 1989 to May 1991), following the method described in Long and Stowe (1994). In some areas this procedure yields negative numbers, shown here in white.

data. In Appendix C we show that the AOD match with observations deteriorates when a different emission height is chosen. Concerning the lifetime of the Pinatubo aerosols, we find a value of 1.23 years, which is in the range of 1-1.37 years estimated based on lidar data at tropical and mid-latitude stations (Barnes and Hofmann 1997; Deshler 2008; Nagai et al. 2010).

The modelled aerosol effective radius between 10° and 20°N reaches a maximum of 0.42 μm, while the SAGE II estimate reaches 0.55 μm (Figure 4.4). The height of the aerosol layer is reasonably well estimated, with an upper bound around 27-30 km. The modelled effective radius is within the uncertainties of the measured effective radius from SAGE II, which give a lower estimate of 0.4 μm (Bauman et al. 2003). It also falls within the lower range of the lidar observations performed in northern Germany (Ansmann et al. 1996). Potential underestimations in aerosol size might be due to the use of parameterised water uptake on aerosols from Zeleznik (1991), as in the original M7 scheme, which underestimates the uptake under stratospheric conditions (Carslaw et al. 1995). Another possible reason is the model resolution, which dilutes areas with large concentrations of aerosols, decreasing aerosol coagulation in the first months after the eruption (see Appendix A). Our initial simulation on 34

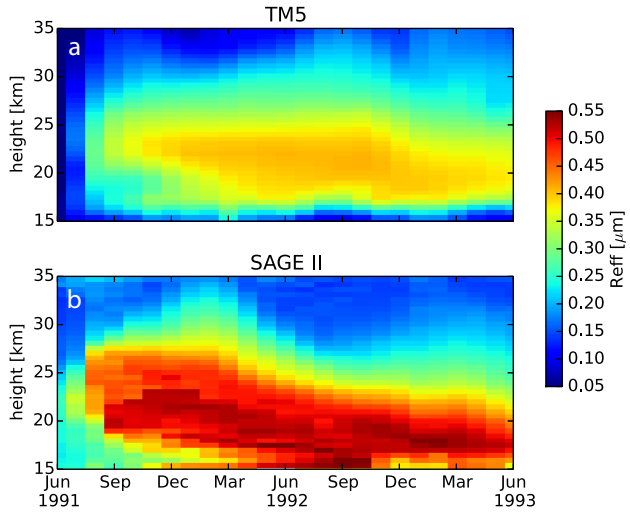

Figure 4.4: Evolution of the mean aerosol effective radius profile in the 10-20°N latitude band, a) modelled and b) measured by SAGE II (Thomason and Peter Eds).

vertical layers instead of 60 compared much poorer to the backscatter and AOD observations, with aerosol effective radius reaching only 0.28 μm. This indicates that the obtained results are quite sensitive to the model resolution.

4.3.2 *Changes in OH and J-values*

Figure 4.5 shows the time evolution of the zonal mean tropospheric J-values and OH concentrations, and differences between the three simulations. The tropopause was defined as a function of latitude as recommended in (Lawrence et al. 2001), and the vertical averaging was done by weighting with the air mass. The strongest reductions in J_{O_3} occur in the tropics (Figure 4.5d), where decreases of more than 10^{-6} s^{-1} between 'NoPinS' and 'PinS' are found from June to September 1991. The decrease in photolysis frequency of NO_2 (J_{NO_2}, Figure 4.5e) is weaker in the tropics, reaching 0.15×10^{-3} s^{-1} in autumn 1991, and more significant at mid-latitudes, with reductions of more than 0.25×10^{-3} s^{-1} in the northern mid-latitudes from November 1991 to April 1992. The stronger decrease in J_{NO_2} at mid-latitudes is related to a larger solar zenith angle. J_{NO_2} depends more strongly on direct radiation than J_{O_3}, which depends more strongly on diffuse radiation. With increasing solar zenith angle, the path of direct sunlight through the aerosol layer is longer, and therefore the

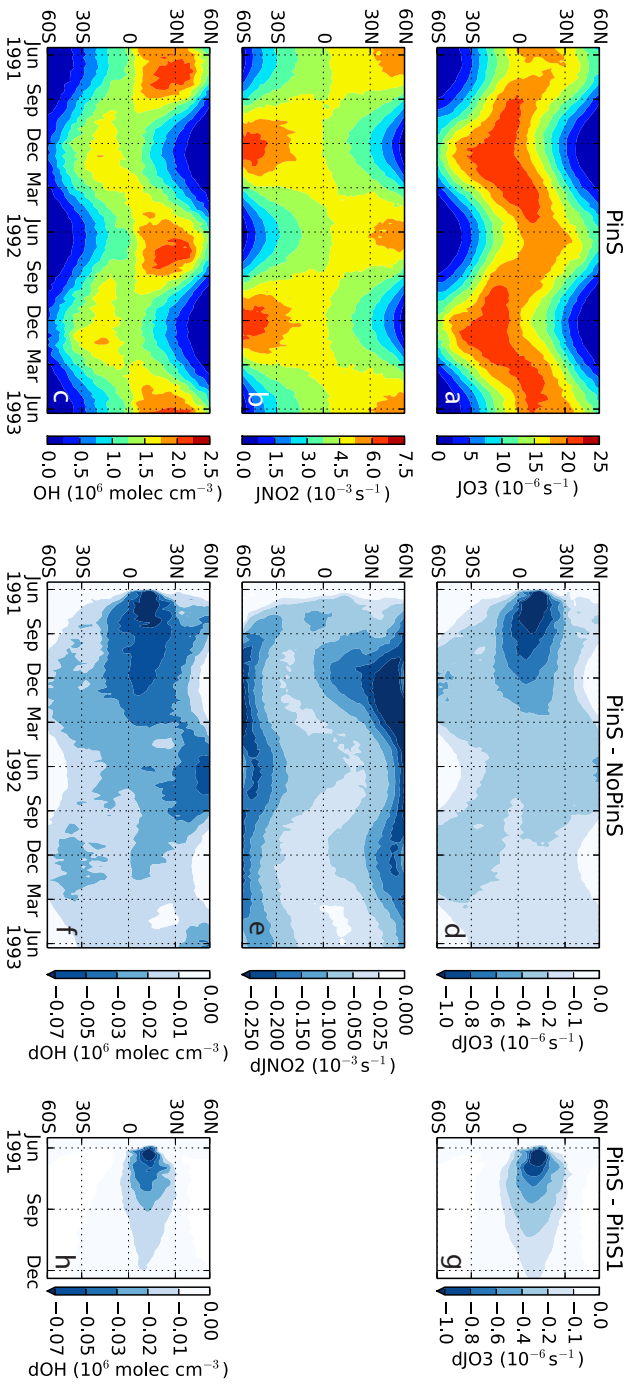

Figure 4.5: Evolution of the zonal mean tropospheric a) J_{O_3}, b) J_{NO_2} and c) OH, and differences between the 'PinS' and 'NoPinS' simulations (d-f), and between the 'PinS' and 'PinS1' simulations (g-h). For the difference 'PinS - PinS1' only the first six month are shown. The difference in J_{NO_2} between 'PinS' and 'PinS1' is omitted because it is found to be negligible.

amount of direct radiation is more strongly attenuated. The resulting change in OH, shown in Figure 4.5f, is a decrease of more than 3×10^4 molec cm^{-3} at 0-30°N from July 1991 to March 1992, and at 30-60°N during the summer of 1992.

By taking the difference between the results of the 'PinS' and the 'PinS1' simulation, we find the effect of the SO_2 absorption on UV radiation. In the first week after the eruption, the total column SO_2 amounts to more than 150 Dobson Units (DU) above eastern Africa and the Indian Ocean (not shown), leading to decreases of more than 50% in J_{O_3} and more than 35% in OH in the troposphere. This strong effect is quite localized, lasting for only a few weeks, and is less important on a global scale. This can be seen in Figure 4.5g and 4.5h, where the zonal mean effect of SO_2 absorption on tropospheric OH and J_{O_3} is plotted. Since SO_2 does not absorb at wavelengths larger than about 320 nm, at which NO_2 photolysis takes place predominantly, J_{NO_2} is mostly unaffected and therefore not shown here. The effect of SO_2 absorption is restricted to the northern tropical region, with maximum decreases in the zonally averaged J_{O_3} and OH of 0.8×10^{-6} s^{-1} and 4×10^4 molec cm^{-3}, respectively, during the first month after the eruption. With the SO_2 being converted almost entirely to aerosol within three months, its zonal mean effect on J_{O_3} and OH decreases to less than 0.3×10^{-6} s^{-1} and 2×10^4 molec cm^{-3}, respectively, by September 1991.

Figure 4.6 shows the evolution of the relative changes in the global mean vertical profiles of J_{O_3}, J_{NO_2} and OH between the three simulations. Extinction of UV radiation by sulfate aerosols and absorption by SO_2 lead to decreases in J_{O_3}, J_{NO_2} and OH below the volcanic plume between the 'NoPinS' and 'PinS' simulations (Figure 4.6 b-d). The photolysis frequencies and OH between 25-35 km increase by up to 2% due to an increase in UV radiation in the upper part of the aerosol plume and above. OH and J-values are affected by aerosol extinction throughout the atmosphere for 2 years after the eruption, with decreases of more than 2% in OH until the end of 1992. The decrease in J_{O_3} intensifies near the surface, while J_{NO_2} is affected more in the upper troposphere. As a result, OH decreases throughout the troposphere. At altitudes between 15 and 25 km, global mean OH decreases by 5-10% during the first two months after the eruption as a result of OH destruction within the plume by the reaction with SO_2. The SO_2 absorption affects O_3 photolysis throughout the column below the volcanic cloud, as can be seen in Figure 4.6f. The effect on tropospheric OH is a 1% decrease in the troposphere shortly after the eruption and gradually diminishes afterwards. This effect is about half of the relative effect of SO_2 absorption on J_{O_3}.

4.3.3 *CH_4 after Pinatubo*

Table 4.2 lists the chemical budget terms of CH_4 and O_3 and lifetimes of CH_4, O_3 and CO affected by the change in UV radiation due to volcanic SO_2 and aerosols.

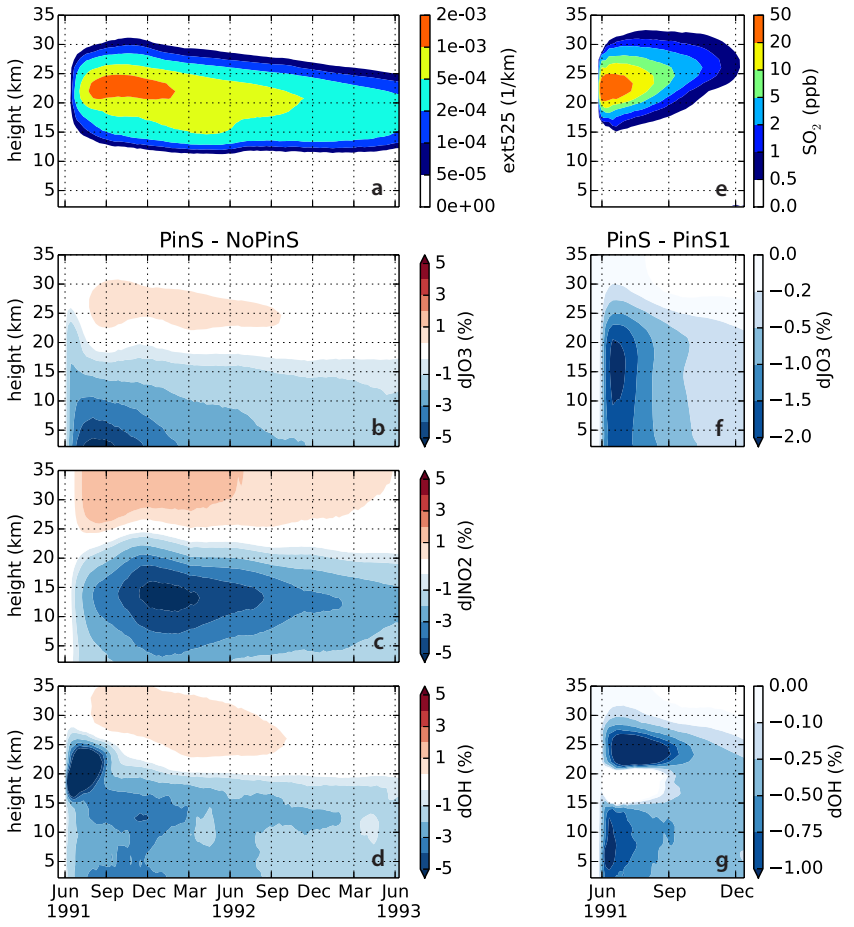

Figure 4.6: Evolution of the differences in the global mean profile of tropospheric J_{O_3}, J_{NO_2} and OH between the 'PinS' and 'NoPinS' simulations (b-d), and between the 'PinS' and 'PinS1' simulations (e-f). Pannels a) and e) show the global mean profiles of extinction at 525 nm and SO_2 concentrations, respectively.

Global budget values are shown for the 'PinS' simulation, as well as the absolute changes in the budget terms for the other two simulations. The loss of O_3 through photolysis decreases by 47.4 Tg (2.2%) in the first year and by 23.7 Tg (1.1%) in the second year after the eruption due to Pinatubo SO_2 and aerosols. Decreases are also found in the chemical production of O_3 from the reactions of NO with HO_2 and RO_2, and in the loss of O_3 through the reactions with OH and HO_2. These effects nearly cancel out, leading to changes in the O_3 burden of less than 1 Tg each year. The modelled CH_4 lifetime is 8.8 and 8.7 yrs in the first and second year after the eruption,

Table 4.2: Global yearly budgets and differences between budget terms between the three simulations.

	PinS 1st year	ΔPinS 1st year	ΔPinS1 1st year	PinS 2nd year	ΔPinS 2nd year
CH_4 emissions - soil sink	520.8	-	-	508.1	-
CH_4+OH troposphere	464.2	-11.2	-9.8	468.1	-6.6
CH_4 stratospheric loss	36.1	-0.2	-0.3	36.1	-0.9
CH_4 burden change	20.5	11.0	9.5	3.9	5.5
NOAA CH_4 burden change	27.2			2.9	
Tropospheric O_3 chemical production	4415.7	-57.2	-50.2	4489.7	-32.4
Tropospheric O_3+hν	2171.9	-47.4	-39.6	2198.4	-23.7
Tropospheric O_3 other chemical losses	1826.4	-11.9	-12.1	1853.4	-9.2
Tropospheric O_3 burden change	-2.0	1.0	1.2	-5.1	-0.2
CH_4 lifetime (yrs)	8.8	0.2	0.2	8.7	0.1
CO lifetime (days)	55.1	1.5	1.4	54.0	1.0
Tropospheric O_3 lifetime (days)	30.1	0.4	0.4	29.0	0.2

in good agreement with the observation-based present-day estimate of 9.1±0.9 yrs (Prather et al. 2012) and with the multi-model mean lifetime of 8.6±1.2 yrs from the Atmospheric Chemistry and Climate Model Intercomparison Project (ACCMIP, Voulgarakis et al. 2013). Since both CH_4 and CO are destroyed by OH, their lifetimes increase between the 'NoPinS' and 'PinS' simulations. We find increases in the CH_4 lifetime by 0.2 yr (2.2%) in the first year and 0.1 yr (1.4%) in the second year. The CO lifetime increases by 1.5 days (2.7%) in the first year and 1 day (1.9%) in the second year. A small part of this increase in the first year is related to the absorption of UV radiation by SO_2.

The CH_4 burden change during 1991 and 1992 can be estimated using global mean CH_4 mixing ratios from NOAA (GLOBALVIEW-CH4 2009). The ratio of 2.78 Tg/ppb reported by the IPCC (Denman et al. 2007) was used to convert from observed surface CH_4 mixing ratio to CH_4 burden. In 1991 the burden change obtained using this approach amounts to 27.2 Tg, while in 1992 an increase of only 2.9 Tg was observed. We model a CH_4 burden change of 20.5 Tg over the coarse of the first year after the eruption, when accounting for the radiative effects of stratospheric sulfur from Pinatubo ('PinS') and nudging the methane concentrations with surface observations. More than half of the modelled increase in CH_4 burden, 11 Tg, is related to the decrease in the OH sink of CH_4 due to stratospheric sulfur from the Pinatubo eruption. During the second year after the eruption, we find an increase of 3.9 Tg in the CH_4 burden in the 'PinS' simulation, while stratospheric sulfur leads to an increase of 5.5 Tg. Therefore we find a decrease of 1.6 Tg in the CH_4 burden in the

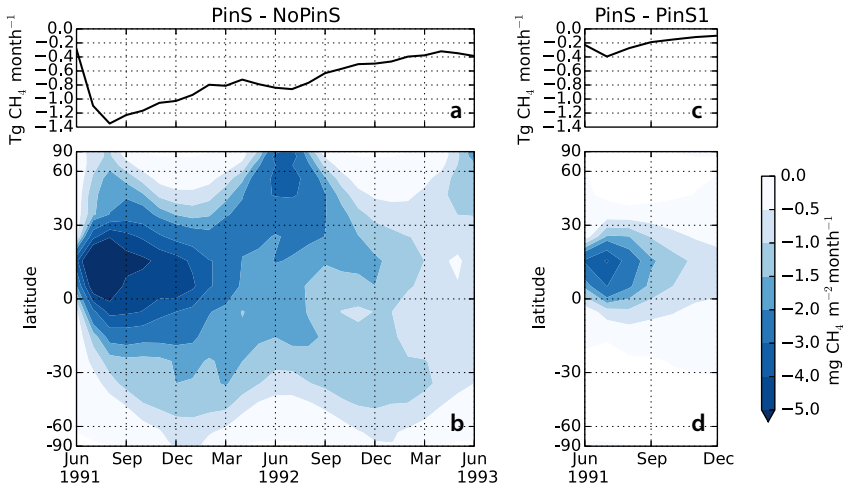

Figure 4.7: a) Differences in the global tropospheric OH sink of CH_4 and b) differences in the latitudinal average sink strength, integrated over the tropospheric column between the 'PinS' and 'NoPinS' simulations; c-d) corresponding differences between the 'PinS' and 'PinS1' simulations.

'NoPin' simulation. The differences of 6.7 Tg and 1.0 Tg between the NOAA-based and modelled burden changes in two years after the eruption may be due to the larger set of stations used in GLOBALVIEW compared to the set used to constrain our model (section 2.1). Furthermore, additional processing steps have been performed to homogenize the GLOBALVIEW data. By employing the ratio of 2.78 Tg/ppb CH_4, we find that stratospheric sulfur from Pinatubo leads to an increase in the methane growth rate of 4.0 and 2.0 ppb yr^{-1} in the first and second year after the eruption, respectively. In the first year, the SO_2 absorption accounts for 0.5 ppb yr^{-1} of this increase, contributing by 12.5% to the overall effect.

Differences in the CH_4 removal by OH in the global troposphere between the three simulations are presented in Figure 4.7a and 4.7c. The latitudinal distribution of these changes are shown in Figure 4.7b and 4.7d. SO_2 absorption leads to a small reduction of the CH_4 sink in the tropics during the first few months after the eruption, leading to an increase in the CH_4 burden of 1.4 Tg globally. The aerosol extinction determines more significant changes both in the tropics and during summer in the extratropics. Overall, we find global decreases in the tropospheric CH_4 sink due to volcanic stratospheric sulfur of 11.2 Tg and 6.6 Tg during the first and the second year after Pinatubo, respectively.

4.4 DISCUSSION

Several results presented above require additional analysis. First, the relative effect of SO_2 absorption on tropospheric OH is about half the relative effect on J_{O_3}. Fuglestvedt et al. (1994) find a ratio of 1.6, between the relative change in tropospheric J_{O_3} and the relative change in OH due to stratospheric O_3 changes, using a steady state assumption representative for the year 1990. Assuming an equilibrium between the production of OH from photolysis and the main losses of HO_X (HO_2+HO_2 and HO_2+OH) they derive the relation $P = \beta \times [\mathrm{OH}]^2$, with P the production rate of OH and β a factor that depends on the ratio $[\mathrm{OH}]/[HO_2]$. If β is constant, this implies a relation between a small change in OH production (ΔP) and a small change in OH ($\Delta[\mathrm{OH}]$) that satisfies $\Delta P = 2\beta \times \Delta[\mathrm{OH}] \times [\mathrm{OH}]$. The associated relative change in P is twice the relative change in OH ($\Delta P/P = 2\Delta[\mathrm{OH}]/[\mathrm{OH}]$). This relation is satisfied in our model, where the local and short-term changes in UV radiation only marginally affect concentrations of CO and NO_X, which drive the recycling between OH and HO_2 and determine β. In the case of Fuglestvedt et al. (1994), the effect is global and long-term, so the relationship is slightly changed. We find relative changes in J_{O_3}, J_{NO_2} and OH due to sulfate aerosols of similar magnitude, showing that in this case not only the primary production of OH is affected, but also the OH recycling and the ratio between OH and HO_2.

Another aspect that deserves attention is the vertical distribution of the effect on photolysis frequencies. We presented in Figure 4.6 the relative change in photolysis frequencies due to Pinatubo aerosols. While the effects on O_3 photolysis maximizes near the surface, the effect on J_{NO_2} maximizes in the upper troposphere. This can be explained by analysing the contributions of direct and diffuse radiation at different wavelengths and how they are affected by the aerosol layer. The primary response to a stratospheric aerosol layer is a decrease in the direct radiation and an increase in the diffuse radiation in the troposphere. While the effect on direct radiation is relatively constant with height, the aerosol layer increases more efficiently the diffuse radiation in the upper troposphere. This is because of the strong Rayleigh scattering in the lower troposphere, even in the absence of aerosols. By analysing the relative contributions to diffuse and direct radiation, we found that the net effect on radiation depends in a complex way on height, wavelength and solar zenith angle. Most O_3 photolysis in the troposphere occurs at small solar zenith angles, at a wavelength of about 300 nm, when direct and diffuse radiation contribute in similar amounts to the total radiation. In this case, the stratospheric aerosol layer causes a decrease in total radiation, due to a decrease in direct radiation, which is counteracted near the tropopause by an increase in diffuse radiation. At 400 nm, where NO_2 photolysis predominantly occurs, molecular scattering is less efficient. Therefore in the upper troposphere the total radiation is dominated by the direct radiation, while the diffuse radiation is more important near the surface. This causes the relative decrease in total radiation at 400 nm to be more pronounced near the tropopause.

Previous attempts to quantify the effect of volcanic SO_2 from Pinatubo on CH_4 have been made using column models. Although they are useful for illustrating the processes involved, an accurate regional or even global estimate of this effect using a column model is difficult due to the localized nature of the SO_2 plume. Dlugokencky et al. (1996) found a 12% decrease in J_{O_3} in the 9°S-9°N equatorial band, and in Chapter 3 we estimated a global 2.5% reduction in OH immediately after the eruption. In our current simulations, SO_2 absorption leads to a maximum decrease of 1% in the global tropospheric OH, and up to 3% in the northern tropical band. The above studies probably overestimate the effect of SO_2 by assuming an instant homogeneity of the SO_2 plume in the equatorial band or around the globe, due to the nonlinearity of the atmospheric photochemistry. In the present study we are able to take this into account more precisely by simulating the dispersion of the SO_2 plume. However, we might also overestimate this effect due to the large stratospheric SO_2 burden compared to observations.

The effect of aerosol extinction found by Dlugokencky et al. (1996), i.e. a maximum 6% reduction in J_{O_3} in the band 9°S-9°N, is similar to our findings. However, we also find significant effects on J_{NO_2}, and on J_{O_3} outside of this equatorial band, which are important for the global OH sink of CH_4. In Chapter 3 we found a maximum global increase in the CH_4 growth rate of 3.5 ppb yr^{-1} due to Pinatubo aerosols, while this study finds a maximum change of 1.35 Tg in August 1991 in the OH sink, equivalent to a growth rate increase of 5.8 ppb yr^{-1}. In their study, global mean AOD values were used, assuming aerosols to be evenly distributed around the globe. However, most CH_4 is destroyed in the tropical troposphere, where stratospheric AOD values exceed 0.4.

Using an inverse modelling approach, Bousquet et al. (2006) estimated a decrease in the tropospheric OH sink of CH_4 during 1991-1993 compared to the 1984-2003 mean of 26 Tg, or 8.7 Tg/yr. This is very similar to our estimate of 17.8 Tg in two years, or 8.9 Tg/yr on average. However, in our case we isolate the effect of aerosols and SO_2, while the OH fields used in Bousquet et al. (2006) were derived from inverse modelling of methyl chloroform. These fields also respond to other forcings after the eruption, such as changes in water vapour and stratospheric O_3, which might contribute to their estimated change in the tropospheric OH sink of CH_4. The good agreement between our result and Bousquet et al. (2006) suggests that other effects on OH in this period compensate each other, which was also shown to partly occur in Chapter 3.

There has been a debate on the magnitude of the global OH interannual variability (IAV). Previous studies estimated an IAV of 7-9% (Bousquet et al. 2005; Prinn et al. 2005). However, as argued by Montzka et al. (2011a), these estimates were likely affected by uncertainties in methyl chloroform emissions. Based on the decline of methyl chloroform since 1998, Montzka et al. (2011a) derived a lower IAV in OH of 2.3±1.5%. Our calculated response of tropospheric OH to the Pinatubo eruption (a reduction of about 2%) is in line with this finding.

Although our approach in quantifying the effects of stratospheric sulfur from Pinatubo on tropospheric chemistry is more sophisticated than previous attempts, our estimate still contains some uncertainty related to the modelled SO_2 and sulfate load. Our model overestimates by about 40% the stratospheric SO_2 burden due to an overestimate in the SO_2 lifetime in the first month after the eruption, in particular not capturing the reduced lifetime in the first few days after the eruption. Guo et al. (2004a) suggest that catalytic reactions on ice and ash particles enhanced the SO_2 removal in the first few days after the eruption, with about 3 Tg SO_2 being converted to sulfate within the eruption column. Such processes are not included in our model. Model resolution can also affect non-linear chemical processes in the early stage of the plume. Another possible reason for the initially enhanced SO_2 lifetime in the model compared to observations may be related to uncertainties in the modelled OH in the lower stratosphere due to missing stratospheric chemistry, or due to uncertainties in stratospheric water vapour fields (Oikonomou and O'Neill 2006). Enhanced OH concentrations were observed in the stratosphere after the eruption of El Chichon (Burnett and Burnett 1984) and were attributed to water vapour emission from the eruption. A large water vapour increase from the Pinatubo eruption would not be well captured in the ERA-Interim data used in our simulations.

The modelled aerosol distributions also show some discrepancies with satellite observations, with overestimated AOD in the tropics and at high-latitudes in the Northern Hemisphere in the first year after the eruption. These features are also found in other studies that simulate the Pinatubo aerosols using general circulation models (Aquila et al. 2012; Dhomse et al. 2014; English et al. 2013; Niemeier et al. 2009). Some differences between modelled and observed AOD might be related to measurement uncertainties. AVHRR measures the total AOD in nadir view, which makes it difficult to distinguish the stratospheric and the tropospheric contributions. SAGE II measures the vertical profile of aerosol extinction in limb view, and is generally taken as a reference for global climate studies. In the first year after the eruption, the SAGE II instrument was saturated, and the data used here has been gap-filled based on surface lidar data (Thomason and Peter Eds). The more reliable SAGE II data from the second year after the eruption are well represented by the model. Aerosol backscatter at the tropical station Mauna Loa is generally well captured, but also suggest an overestimate of the simulated stratospheric aerosol burden in the tropical band in the first months after the eruption.

The modelled transport of the aerosol plume to the Northern Hemisphere is more pronounced than to the Southern Hemisphere, while observations show an equally pronounced transport to the two hemispheres. The observed aerosol load in the Southern high-latitudes might be partly related to the eruption of Cerro Hudson in August 1991. This additional eruption, which injected 1.5 Tg SO_2 in the stratosphere at 45°S (Doiron et al. 1991), is not included in our model simulation. Other uncertainties in the latitudinal distribution of the plume might be related to uncertainties in transport. The cross-equatorial transport of the Pinatubo plume was shown to be

a result of dynamical changes caused by the absorption of longwave radiation by sulfate aerosols in the first two weeks after the eruption. The coupling between radiation and aerosols proved to be essential for simulating the southern transport of the Pinatubo plume in studies using global climate models (Aquila et al. 2012; Timmreck and Graf 2006; Young et al. 1994). Our model is driven by reanalysis winds, which are not coupled to the aerosol fields simulated by TM5. Furthermore, the aerosols from Pinatubo are not explicitly included in the ECMWF model. However, their effect on stratospheric temperatures is accounted for by assimilating satellite observations. Indeed, the long-term trend in stratospheric temperature after Pinatubo is well captured in ERA-Interim, with a 15% attenuation of the observed volcanic signal (Dee et al. 2011). However, more localized effects, such as the effect of aerosol absorption on stratospheric dynamics in the first two weeks after the eruption, are probably not well represented due to scarcity of observational data available for assimilation in the ECMWF model.

Based on the uncertainties in modelled SO_2 burden, aerosol load and aerosol size, we roughly estimate a 15% uncertainty in the modelled effect of stratospheric sulfur on the CH_4 burden in the first two years after the eruption.

4.5 CONCLUSIONS

We quantified for the first time the effect of SO_2 and sulfate aerosols from the Pinatubo eruption on tropospheric photochemistry using a three-dimensional global chemistry model. The overall impact of decreased UV radiation due to stratospheric sulfur on CH_4 during the first two years after the eruption was a decrease of 17.8 Tg in the CH_4 sink. This decrease was dominated by the effect of UV radiation scattering by volcanic aerosols. Stratospheric SO_2 absorption caused a reduction of 1.4 Tg in the CH_4 sink in the first few months after the eruption.

Due to the Pinatubo stratospheric sulfur, the global CH_4 growth rate was increased by 4.0 ppb yr^{-1} and 2.0 ppb yr^{-1} in the first and second year after the eruption, respectively. Based on the observed growth rate of CH_4 concentrations, the burden change of CH_4 in the first year after the eruption is estimated to be about +27 Tg. The calculated effect of sulfur from Pinatubo in our simulation amounts to a burden change of +11 Tg in the same period. Therefore the reduction in OH from the enhanced SO_2 and aerosol can explain about 40% of the observed CH_4 burden change in the period June 1991 - May 1992. In the second year after the eruption, the observed CH_4 burden change is +2.9 and the simulated sulfur effect is +5.5 Tg. This suggests that other processes counteracted this reduction of the chemical sink due to stratospheric sulfur in the second year, for example decreasing emissions or other factors affecting the sink.

This article investigates solely the direct effect of stratospheric sulfur on UV radiation and the related effects on the tropospheric OH sink of CH_4. Although we show

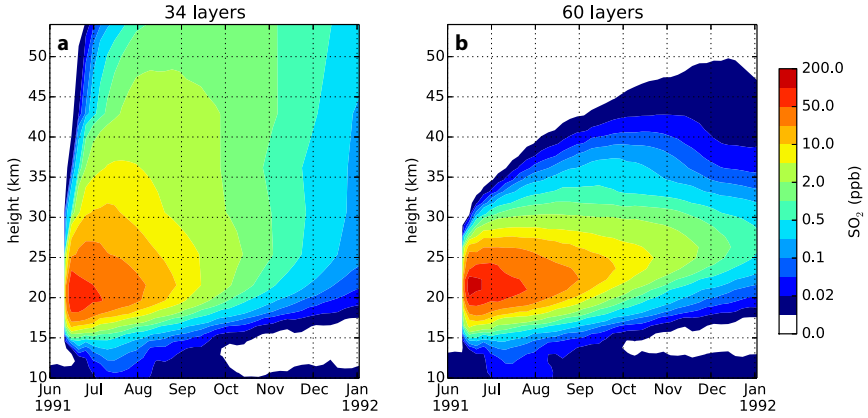

Figure 4.8: Mean SO_2 profile between 20°S and 20°N for a) 34-layer and b) 60-layer vertical resolution. Simulations with the 60-layer setup are discussed in the main text.

that the sulfur emissions from Pinatubo play a significant role in the methane budget, the exact reasons for the observed decrease in the CH_4 growth rate in 1992 remain unresolved. Several processes have been proposed to explain these observations, including an increase in the tropospheric OH sink due to stratospheric O_3 depletion on sulfate aerosols (Chapter 3; Bekki et al. 1994; Telford et al. 2009; Wang et al. 2004), decreased emissions from wetlands due to lower temperatures (Chapter 3; Bekki and Law 1997; Dutton and Christy 1992; Walter et al. 2001), and decreased anthropogenic emissions due to the collapse of the Soviet Union (Dlugokencky et al. 1994). These effects are included in our simulations, by imposing realistic year-to-year variations in meteorology, stratospheric O_3 and CH_4 emissions. Their impact on tropospheric chemistry will be assessed in Chapter 5.

Appendix A. Sensitivity to vertical resolution

The standard TM5 model setup uses 34 vertical layers out of the 60 sigma hybrid sigma-pressure vertical layers of ERA-Interim. This setup has a resolution of 4-5 km in the stratosphere above 23 km, while the full 60 layers of ERA-Interim have a resolution of 2 km or less up to 45 km altitude. Figure 4.8 shows a comparison between the mean SO_2 profile over the 20°S-20°N latitude band for two simulations performed using 34 and 60 layers, respectively. The 34-layer version of the model transports SO_2 to the top of the model domain at 55 km altitude within a couple of weeks. Concentrations of more than 1 ppb of SO_2 are found at this altitude between Au-

gust and November 1991. When using 60 layers, most of the SO_2 remains below 40 km throughout the simulation, with mean zonal concentrations over 1 ppb only between 15 and 33 km. We conclude that the slopes advection scheme (Russell and Lerner 1981), which is default in TM5, is not able to resolve the large SO_2 gradients in the stratosphere on a 5 km resolution. The resolution also affects the aerosol concentrations, with aerosols being formed in the 34-layer version up to 55 km. The aerosol plume is more diluted, leading to less coagulation and smaller aerosol size of 0.28 nm (not shown), much smaller than the observations (Figure 4.4). Therefore we chose to use the full 60-layer configuration for the simulations presented in this paper. To check whether the model continues to be diffusive on 60 layers, an additional simulation was performed using the second moment of the advection scheme (Prather 1986). However, this didn't lead to any significant further difference in the modelled stratospheric aerosol or SO_2.

Appendix B. Emissions setup

The emissions used in the model are as follows. Anthropogenic emissions of CH_4, CO, nitrogen oxides (NO_X), non-methane volatile organic compounds (NMVOC), sulfur dioxide (SO_2) and ammonia (NH_3) were taken from the EDGAR version 4.2 (European Commission and Joint Research Centre (JRC)/Netherlands Environmental Assessment Agency (PBL) 2011), except for transport sectors. EDGAR version 4.1 was used for the transport sectors because it provides aircraft NO_X emissions separately and allows us to implement a different vertical distribution of these emissions compared to other transport related emissions. Since the vertical distribution of aircraft NO_X emissions is not included in EDGAR 4.1, we used the monthly 3-dimensional historical aircraft emissions provided for the ACCMIP and the Coupled Model Intercomparison Project (CMIP5, Lamarque et al. 2010). These emissions were scaled with the global yearly aircraft NO_X emission total from EDGAR4.1 to include a realistic interannual variability. For the yearly anthropogenic NMVOC emissions from EDGAR, VOC speciation was applied on a grid-cell and sector basis according to the historical ACCMIP emissions for the year 2000. The anthropogenic EDGAR emissions for each species were scaled to match the total yearly anthropogenic emissions from the Regional Emission Inventory in Asia (REAS) version 1 (Ohara et al. 2007) over the south and east Asian region, between 50°N and 10°S latitude and 60°E and 150°E longitude. Seasonal cycles for the EDGAR emissions were implemented following the recommendations of Veldt (1992). Decadal anthropogenic and biomass burning emissions from the historical ACCMIP emission inventory were used for black carbon (BC) and organic carbon (OC), linearly interpolated to the simulation years.

Biomass burning emissions for gas-phase species were used from the Reanalysis of the Tropospheric chemical composition over the past 40 years project (RETRO) (Schultz et al. 2008). Production of NO_X by lightning and emissions of dimethyl

sulfide (DMS) and sea salt are calculated online (Huijnen et al. 2010; Vignati et al. 2010). Natural CH_4 monthly emissions were taken from the Hydrogen, Methane And Nitrous Oxide (HYMN) project (Spahni et al. 2011), including emissions and soil uptake from the LPJ-WhyMe vegetation model. Natural emissions of CO, NO_X, NH_3 and NMVOC were prescribed using a monthly dataset from the Monitoring Atmospheric Composition and Climate (MACC) project, as in van Noije et al. (2014). The emission heights of anthropogenic, biomass burning, and natural emissions have been revised, as described in van Noije et al. (2014).

Appendix C. Sensitivity to injection height

The injection height of the Pinatubo SO_2 is an important parameter for determining the plume evolution. The initial evolution of the erupted SO_2 is driven by reactions on volcanic ice and ash particles, and by dynamical changes due to absorption by sulfate and ash. Generally not all of these processes are included in studies of the Pinatubo eruption, and the assumed SO_2 injection needs to account for missing processes. Therefore the best injection height and the model sensitivity to this parameter might be dependent on the model setup. More studies are needed to quantify these parameters, preferably using climate models with radiatively interactive aerosols.

We test here two more injection height scenarios apart from the setup presented in the main text, where most SO_2 was injected between 17 and 21 km. In these additional simulations the SO_2 was injected between 15-27 km in scenario 'H1', and between 15-24 km in scenario 'H2'. The bulk of the material (80%) was injected in the highest 4 km (23-27 km and 20-24 km).

Figure 4.9 shows the AOD evolution for the three scenarios in the year after the eruption. The middle and high injection heights give larger AOD values in the northern tropical region, which would deteriorate the comparison with SAGE II observations in this region. The transport of the aerosols to high latitudes and the Southern Hemisphere is also less well captured in these simulations. For the high scenario 'H1' most of the material is transported within the tropical pipe. This leads to reduced transport to high latitudes in the first 5 months after the eruption, most aerosol remaining confined in the northern tropical region. For both 'H1' and 'H2', the plume is dominantly transported to the Northern Hemisphere, and the AOD values in the northern mid-latitudes are highly overestimated. Although the emission scenario in the main text also overestimates the AOD in the tropics and the high northern latitudes, the overestimate is smaller for this scenario, and the transport of the plume to both hemispheres is better captured. We chose the low injection scenario for the rest of the paper because it represents best the observed global aerosol distribution. In addition, the modelled peak aerosol backscatter values between 20 and 25 km altitude above Mauna Loa in July 1991 correspond best with lidar measurements (Figure 2).

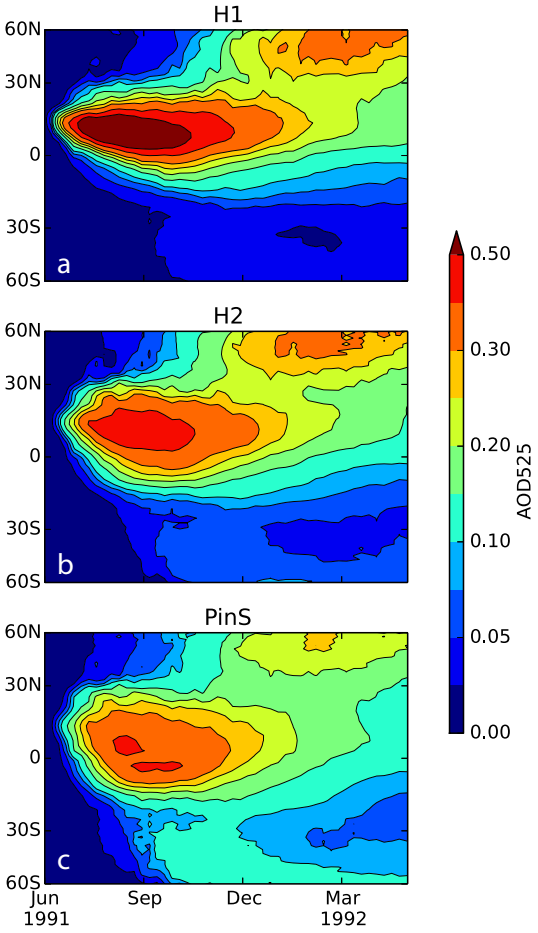

Figure 4.9: Zonal mean modelled AOD at 525 nm (AOD525) for three injection heights. The bulk of SO_2 emission was assumed between a) 23-27 km for 'H1', b) 20-24 km for 'H2' and c) 17-23 km for the 'PinS' simulation.

5

EXPLAINING THE OBSERVED METHANE VARIABILITY AFTER THE MOUNT PINATUBO ERUPTION

The CH_4 growth rate in the atmosphere showed large variations after the Pinatubo eruption in June 1991. A decrease of more than 10 ppb yr^{-1} in the growth rate over the course of 1992 was reported and a partial recovery in the following year. Several reasons have been proposed for the atmospheric CH_4 evolution after the eruption, however their contribution to the observed variations are not yet resolved. CH_4 is removed from the atmosphere by the reaction with tropospheric OH, which in turn is produced by O_3 photolysis under UV radiation. Therefore the CH_4 removal is sensitive to changes in tropospheric UV levels. Such changes occurred after the Pinatubo eruption, due to the presence of stratospheric SO_2 and sulfate aerosols, and due to enhanced ozone depletion on Pinatubo aerosols. The perturbed climate after the eruption also altered both sources and sinks of atmospheric CH_4. Furthermore, CH_4 concentrations were influenced by other factors of natural variability in that period, such as ENSO and biomass burning events. Emissions of CO, NO_X and NMVOCs also affected CH_4 concentrations indirectly by influencing tropospheric OH levels.

Potential drivers of CH_4 variability are investigated using the TM5 global chemistry model. The contribution that each driver had to the global CH_4 variability during the period 1990 to 1995 is quantified. We find that a decrease of 8-10 ppb yr^{-1} CH_4 is explained by a combination of the above processes. However, the timing of the minimum growth rate is found 6-9 months later than observed. The growth rate recovery is also not well represented by the model. Potential uncertainties include emissions of CH_4 from wetlands, biogenic NMVOC and the sensitivity of OH to NMVOC emission changes, and biomass burning emissions of CH_4 and other compounds. Two inventories were used for CH_4 emissions from wetlands, ORCHIDEE and LPJ, to investigate the role of uncertainties in these emissions. Although the ORCHIDEE improves the global balance between sources and sinks in TM5, none of the two inventories properly captures the observed CH_4 variability in this period.

This chapter is submitted to Atmopheric Chemistry and Physics:
Bândă, N., Krol, M., van Noije, T., van Weele, M., Le Sager, P., and Röckmann, T.: *Can we explain the observed methane variability after the Mount Pinatubo eruption?*

5.1 INTRODUCTION

Methane (CH_4) is the second most important anthropogenic greenhouse gas after carbon dioxide (CO_2). Its evolution in the atmosphere since the beginning of the record of continuous atmospheric CH_4 measurements in the 1980s is not fully understood (Kirschke et al. 2013). One of the events that affected CH_4 concentrations was the eruption of Mt. Pinatubo on 15 June 1991, the largest eruption in the last century. The eruption caused perturbations to climate and photochemistry for a few years afterwards. We investigate here the sensitivity of CH_4 concentrations to these perturbations, and our ability to explain the observed CH_4 variations in the atmosphere in the early 1990s.

After a stable CH_4 growth rate of 10 to 13 ppb yr^{-1} in the late 1980s, the growth rate showed large fluctuations in the early 1990s. An increased CH_4 growth rate of about 17 ppb yr^{-1} was registered by the NOAA network in 1991, followed by a strong decline in the growth rate during the next year, with values reaching nearly zero (Dlugokencky et al. 1994). The growth rate recovered to 6 ppb yr^{-1} in 1993. Processes driving these variations could be related to either the CH_4 sources or the CH_4 sinks.

CH_4 is emitted to the atmosphere from anthropogenic activities (fossil fuel production, agriculture and waste treatment), biomass burning, and from natural sources (wetlands, geological activity, termites). The main sink of atmospheric CH_4 is the reaction with the hydroxyl radical (OH) in the troposphere, which removes about 80% of the CH_4. Other removal processes are soil uptake and reactions with OH, chlorine (Cl) and excited oxygen ($O(^1D)$) atoms in the stratosphere. Tropospheric OH is produced by the photolysis of ozone (O_3) at wavelengths of 280-320 nm, followed by the reaction of $O(^1D)$ with water vapour. Therefore the abundance of OH in the troposphere is sensitive both to the amount of incoming UV radiation and to the water vapour abundance. Tropospheric OH also reacts with other atmospheric compounds such as carbon monoxide (CO) and non-methane volatile organic compounds (NMVOC), and is recycled in the presence of nitrogen oxides (NO_X). Thus, changes in the emissions of NO_X, CO and NMVOCs also affect the OH abundance (Lelieveld et al. 2002).

Interannual variations in both the sources and sinks of CH_4 occurred in the early 1990s. In part, these can be related to the Pinatubo eruption, which caused a decrease in tropospheric temperatures of about 0.5°C globally in the two following years (McCormick et al. 1995). The global cooling most likely resulted in decreases in both the CH_4 emission rates from wetlands and the removal of CH_4 by reaction with OH, both processes being temperature-dependent. OH production would have further responded to the decrease in water vapour associated with the temperature reduction (Soden et al. 2002).

The climate anomaly after Pinatubo might have affected natural emissions of other species as well, such as NMVOC emissions from vegetation, which may in turn have

caused changes in OH and thus the CH_4 sink. Changes in UV radiation due to stratospheric aerosols and stratospheric O_3 anomalies might have also affected the removal of CH_4 by OH in the post-Pinatubo years (Chapter 4; Bekki et al. 1994; Dlugokencky et al. 1996). Stratospheric O_3 changes in this period were partly caused by heterogeneous removal on volcanic aerosol particles, and partly by other factors of natural variability (Bekki and Pyle 1994; Telford et al. 2009). Other potential effects of the eruption on the CH_4 budget included changes in the transport between the troposphere and the stratosphere (Schauffler and Daniel 1994) and inhibition of wetland emissions due to sulfur deposition (Gauci et al. 2008). CH_4 concentrations in this period were also affected by natural variability not related to Pinatubo, such as the 11-year solar cycle, the El-Niño Southern Oscillation (ENSO) cycle and biomass burning events. Significant reductions in the anthropogenic emissions from gas production and distribution in the Former Soviet Union (FSU) might also have occurred in this period (Law and Nisbet 1996). However, gaps in reporting make the magnitude and timing of these reductions quite uncertain.

Previous bottom-up studies quantified the impact of individual processes on the CH_4 abundance, without attempting to solve the whole CH_4 budget. Bekki and Law (1997) found compensating effects of temperature on the CH_4 emissions and the CH_4 removal by OH on a global scale. Dlugokencky et al. (1996) showed that the increase in both CH_4 and CO mixing ratios in late 1991 and early 1992 could be related to a decrease in OH due to UV scattering by stratospheric aerosols and UV absorption by sulfur dioxide (SO_2) from the eruption. In Chapter 4 we found a decrease of 11.2 and 6.6 Tg, respectively, in the CH_4 removal in the first and second years following the eruption due to stratospheric sulfur. The above decreases in CH_4 removal translate into corresponding increases of 4 and 2 ppb yr^{-1}, respectively, in the CH_4 growth rate. Here and in the remainder of the paper, we use the ratio of 2.78 Tg/ppb reported by the IPCC (Denman et al. 2007) to convert from CH_4 burden changes to growth rate variations. Using a two-dimensional model, Bekki et al. (1994) attributed half of the decrease in CH_4 and CO growth rates in 1992 to stratospheric O_3 depletion. Additionally, Dlugokencky et al. (1994) and Law and Nisbet (1996) estimated that a decrease in the gas leak emissions from the FSU could be in the order of 15 Tg yr^{-1}, and would also explain part of the observed decrease in the CH_4 growth rate in 1992. Using a 4-box model, Schauffler and Daniel (1994) found that an increase in the exchange rate between stratosphere and troposphere due to volcanic aerosol heating can cause lower CH_4 concentrations in the troposphere.

Prior attempts to explain the CH_4 variability in this period include inverse modelling studies and a column model study. The inverse modelling studies of Bousquet et al. (2006) and Wang et al. (2004) (B06 and W04 from here on, respectively) find a positive anomaly in the CH_4 flux to the atmosphere in 1991, and a negative anomaly in 1992, with a difference of about 30 Tg between the two years. Both studies find a significant contribution from wetland emissions to this anomaly and a small contribution from biomass burning. However, the two studies use OH variations of

opposite sign. The OH fields in B06 are determined by methyl chloroform inversions, showing a reduced OH sink of CH_4 of about 30 Tg yr^{-1} over the period 1991 to 1993 compared to 1990. To close the CH_4 budget, their anthropogenic and wetland CH_4 emissions also show pronounced decreases. When using both CH_4 and methyl chloroform to constrain OH, Pison et al. (2013) found a more moderate OH variability. In W04, OH is parameterised based on chemical and meteorological parameters with coefficients determined from 3D model simulations. W04 find an increase of about 5% in OH from 1991 to 1993 due to stratospheric O_3 depletion. Stratospheric aerosols from the eruption are, however, not included as a parameter in their calculation. Our previous column model study Chapter 3 supports a decrease in OH in the first year after the eruption due to aerosols, temperature and water vapour changes, and a subsequent decrease due to stratospheric O_3 depletion. In that study we found that the stratospheric O_3 depletion together with changes in anthropogenic emissions could explain a 12 ppb yr^{-1} decrease in 1993 compared to 1991. However, the one-dimensional model was unable to capture the strong CH_4 decrease in 1992. In the present study, we quantify the combined impact of the drivers of CH_4 variability described above in the early 1990s using the global chemistry and transport model TM5 and we identify the potential gaps in our understanding of the CH_4 budget. For the first time, all the known processes that could have significantly contributed to the CH_4 variations in the early 1990s are included in a modelling study.

The chapter is structured as follows. A description of the TM5 model is presented in Section 5.2.1 and of the simulation setup in Section 5.2.2. Section 5.2.3 describ the drivers that have been considered to explain the observed CH_4 variability, and Section 5.3.1 presents their impact on the simulated CH_4 budget. The unexplained CH_4 variability is shown in Section 5.3.2, and possible reasons for mismatch between the model and observations are discussed in Section 5.4. Conclusions are drawn in Section 5.5.

5.2 METHOD

5.2.1 *Model description*

The TM5 global chemistry and transport model (Huijnen et al. 2010; van Noije et al. 2014; Williams et al. 2012) was used to simulate the chemical composition of the atmosphere during the period 1990 to 1995. The model was run on 60 hybrid sigma-pressure vertical levels and at a horizontal resolution of 3° x 2° (longitude x latitude) globally, except for the polar region, where a reduced grid was used for advection in the zonal direction. The model was driven by meteorological fields from the ECMWF ERA-Interim reanalysis (Dee et al. 2011). The gas-phase chemistry scheme is based on a modified version of the carbon bond mechanism 4 (Houweling et al. 1998). Photolysis frequencies are calculated by the on-line parameterisation scheme based

on Williams et al. (2006). To account for missing O_3 chemistry in the stratosphere, O_3 is nudged to the multi sensor reanalysis data (MSR; van der A et al. 2010) above the 45 hPa level in the tropics (30°S-30°N) and above the 90 hPa level in the extra-tropics. CH_4 is also nudged above these pressure levels to climatological values from Grooß and Russell III (2005) to compensate for possible errors in stratospheric chemistry, specifically the loss of CH_4 by OH, Cl and $O(^1D)$.

The modal scheme M7 (Aan de Brugh et al. 2011; Vignati et al. 2004) is used to simulate aerosol microphysics. M7 simulates the following aerosol types: sulfate (SO_4), black carbon (BC), organic carbon (OC), sea salt and mineral dust. In addition, TM5 calculates ammonium and nitrate partitioning between gas phase and aerosols using the Equilibrium Simplified Aerosol Model (EQSAM; Metzger et al. 2002), and accounts for methyl sulfonic acid (MSA). The aerosols are coupled to the radiative transfer scheme that is used to calculate photolysis frequencies. Some adjustments to the M7 default setup have been applied in order to realistically simulate stratospheric volcanic aerosols, as described in Chapter 4. This setup has been used in the aforementioned paper to model SO_2 and sulfate aerosols from the Pinatubo eruption, and to infer their effect on photolysis frequencies.

Here we use the new massively parallel model version TM5-mp. The new MPI parallelisation does not influence the model results, but brings a significant speedup of the model runs by allowing us to use more computing cores more efficiently. A few additional updates have been incorporated in the model compared to the version used in Chapter 4. Convective fluxes used for tracer transport are now read from the ERA-Interim input data, instead of calculating them with the Tiedtke scheme (Tiedtke 1989). Heterogeneous removal of N_2O_5 on aerosol and cloud particles was updated according to Huijnen et al. (2014). The CH_4 surface nudging timescale has also been adjusted. We now use a nudging timescale of 10 days instead of 3 days in Chapter 4. By comparing the budget terms and concentrations of simulations with the different nudging timescales, we find that both nudging timescales give a similar performance in simulating the CH_4 concentrations and inter-annual variability (IAV). Although similar global nudging values are found for the two simulations, the local nudging amount is 2 to 3 times larger using a 3-day nudging. Therefore we find that a 10-days nudging timescale is more appropriate for inferring CH_4 budget mismatches based on monthly observations, allowing for synoptic-scale variability in CH_4 concentrations (Dentener et al. 2003). Finally, some of the emission inventories used here differ from the ones used in Chapter 4, and are described below. We verified that the model updates did not cause any significant differences in modelled SO_2 and stratospheric aerosols compared to the results presented in Chapter 4.

Table 5.1 lists the CH_4 source and sink categories, the inventories used, and their yearly global mean and variability over the period 1990 to 1995. Two inventories for CH_4 emissions from wetlands are employed to investigate the uncertainty in these emissions. We use the ORCHIDEE emissions from the WETCHIMP intercomparison project (Wania et al. 2013) and LPJ emissions from the Hydrogen, Methane and Ni-

Table 5.1: Annual mean CH_4 sources and sinks, and their interannual variability (IAV). All values are in $Tg\,yr^{-1}$.

Category	Inventory or simulation	1990	1991	1992	1993	1994	1995	Mean	IAV
Natural wetlands	ORCHIDEE	273.9	276.6	251.7	262.1	272.1	260.8	266.2	11.9
	LPJ	167.4	163.9	161.9	165.6	167.7	169.3	166.1	2.6
Natural other	HYMN	41.4	41.4	41.4	41.4	41.4	41.4	41.4	-
Anthropogenic	EDGAR	256.7	256.2	257.2	256.4	257.3	260.0	257.3	1.2
Biomass burning	RETRO	19.5	21.2	23.0	17.8	20.4	16.5	19.7	3.0
Trop CH_4+OH	Base1	489.7	489.2	483.6	505.3	511.9	517.7	499.6	8.1
	Base2	487.8	487.4	482.8	504.5	511.1	517.0	498.4	7.9
Stratospheric sink	Base1	35.0	39.1	39.7	40.2	41.9	41.5	39.5	1.5
	Base2	33.	37.1	38.6	39.3	41.2	40.7	38.3	1.8
Soil sink	Base1	29.2	30.4	26.3	28.5	26.4	25.5	27.7	2.1
	Base2	27.1	26.8	27.0	27.2	26.9	27.5	27.1	0.3
Nudging	Base1	-11.1	-13.7	-17.5	5.0	24.4	13.4	0.1	11.8
	Base2	89.	92.1	70.9	101.5	122.5	103.	96.5	19.1

trous oxide (HYMN) project (Spahni et al. 2011). Other natural CH_4 monthly emissions from wild animals and termites were also used as compiled in HYMN. Anthropogenic emissions of CH_4, CO, NO_X, NMVOC, SO_2 and ammonia (NH_3) were taken from the EDGAR4.2 inventory, except for transport sector, for which EDGAR4.1 was used. Decadal anthropogenic emissions of BC and OC were taken from the historical AR5 emission inventory (Lamarque et al. 2010). Biomass burning emissions of CH_4, CO, NMVOC, NO_X, SO_2 and NH_3 are used from the RETRO inventory (Schultz et al. 2008). Production of NO_X by lightning and emissions of dimethyl sulfide (DMS), sea salt and dust are calculated online (Huijnen et al. 2010; van Noije et al. 2014; Vignati et al. 2010). Monthly biogenic emissions of CO, NH_3 and NMVOC were taken from the MEGAN inventory (Sindelarova et al. 2014). Climatological emissions from the MACC inventory are used for continuous volcanic SO_2 (Andres and Kasgnoc 1998) and biogenic NO_X emissions.

5.2.2 *Simulation setup*

We designed a series of simulations with the aim to quantify the impact of specific processes on the tropospheric CH_4 concentrations. The difference between two sim-

ulations, one including, and one excluding a specific driver, is used to quantify the effect of that driver. For instance, we calculate the effect of IAV in meteorology on tropospheric CH_4 as the difference of a simulation that includes varying meteorological fields and a simulation that fixes meteorological fields to 1990 values. Two sets of simulations were performed for seven drivers of CH_4 variability for the period 1990 to 1995, as outlined in Table 5.2.

As described in Chapter 4, we use a two-step setup to simulate realistic CH_4 concentrations. In a first simulation of the 'Base1' and 'Base2' scenarios, in which all drivers of CH_4 variability are included, we nudge CH_4 mixing ratios in the lowest 2 km of the model towards measured mixing ratios from background sites. This allows us to account for uncertainties in sources and sinks of CH_4 and to avoid a long-term drift of mixing ratios compared to observations. This setup is particularly important for the second simulation set using the lower LPJ wetland emissions, where nearly 100 Tg yr^{-1} additional source or reduced sink is needed to close the CH_4 budget. The nudging is performed as follows. The North-South gradient in CH_4 mixing ratio is reconstructed by interpolating the measured CH_4 monthly mean mixing ratios at the background stations South Pole, Cape Grim, Mauna Loa, Niwot Ridge, Barrow, and Alert. In this way a realistic zonal mean CH_4 distribution is obtained from the observations, which is then compared to the modelled concentrations at the dateline. The concentrations in the whole zonal band are then adjusted based on this comparison. The amount of CH_4 needed to compensate for the difference between the model and observation-based North-South gradient in CH_4 is stored on a monthly basis for each 10-degree latitude band. In the second step, CH_4 is no longer constrained by observations, but instead the nudging amount calculated in the first step is applied as an emission in all scenarios. In Chapter 4 we used this nudging to scale the CH_4 emissions in each 10-degree latitude band. In these simulations, we observed slight time shifts in the derived CH_4 growth rates in the second step compared to the first step. To obtain an almost perfect match between the simulated CH_4 concentrations of the two steps, in the present study we apply the nudging homogeneously over the latitude band and in the lowest 2 km from the surface. This two-step setup enables us to model realistic CH_4 concentrations, and at the same time allowing them to respond to changes in emissions or photochemistry. The nudging term that is needed to force the 'Base1' and 'Base2' simulations to background atmospheric observations indicates in which latitude bands sources and sinks are unbalanced when all drivers of CH_4 variability are included. These mismatches will be further analysed in Section 5.3.2. Validation results for this two-step setup are shown in Appendix A.

The first simulation set (Set I in Table 5.2) uses the ORCHIDEE inventory for natural CH_4 emissions from wetlands, while the second set of simulations uses the LPJ inventory. The 'Base1' simulation from the first simulation set accounts for all drivers of CH_4 IAV in the model, including modelled stratospheric sulfur, varying amounts of stratospheric O_3, ERA-Interim fields for temperature and humidity, and emission vari-

Table 5.2: Setup of the simulations, including CH_4 wetland inventory used and drivers of CH_4 included in each simulation. The crosses indicate that the variability of a certain driver is included in the simulation. Otherwise the driver is not included (in the case of Pinatubo SO_2 and aerosol) or 1990 values are used throughout the simulation.

Simulation name	Inventory for CH_4 emissions from wetlands	Drivers of CH_4 variability included						
		Pinatubo SO_2 and aerosol and aerosol	Stratospheric O_3	Meteorology	CH_4 wetland emissions	Natural emissions of CO, NMVOC and NH_3	Anthropogenic emissions of CH_4 and other compounds	Biomass burning emissions of CH_4 and other compounds
Set I								
Base1	ORCHIDEE	X	X	X	X	X	X	X
NoPinS1	ORCHIDEE		X	X	X	X	X	X
FixOzone1	ORCHIDEE			X	X	X	X	X
FixMet1	ORCHIDEE		X		X	X	X	X
FixWetl1	ORCHIDEE		X	X		X	X	X
FixEmis1	ORCHIDEE		X	X	X			
FixAll1	ORCHIDEE							
Set II								
Base2	LPJ	X	X	X	X	X	X	X
NoPinS2	LPJ		X	X	X	X	X	X
FixWetl2	LPJ		X	X	X		X	X

ations of CH_4 and other species. Emission of SO_2 in the stratosphere by the Pinatubo eruption of 18.5 Tg SO_2 were considered, and the SO_2 subsequently reacts with OH to form aerosols. In the other simulations, we fix different variables in the model to investigate their effect on CH_4 concentrations. In all simulations except for the 'Base1' simulation, we removed the effects of Pinatubo SO_2 and sulfate, because using different meteorology or O_3 column might lead to different SO_2 and aerosol fields. By using this setup we minimise the nonlinearities between drivers of CH_4 variability. In 'FixMeteo1' and 'FixOzone1', we additionally used the meteorology and, respectively, the stratospheric O_3 of the year 1990 for the whole length of the simulation. In the 'FixWetl1' simulation we used constant CH_4 emissions from wetlands from the year 1990. Simulation 'FixEmis' used anthropogenic and biomass burning emissions of CH_4 and other species from the year 1990. Biogenic emissions of CO, NMVOC and NO_X are also fixed to 1990 in 'FixEmis'. Finally, to infer the combined effect of all seven drivers of CH_4 variability, the simulation 'FixAll1' is performed, where all drivers of variability are fixed to 1990 values. This allows us to quantify the possible effect of nonlinearities, as discussed in Appendix B.

To test the impact of using a different inventory for CH_4 emissions from wetlands, a second set of simulations (Set II in Table 5.2) is performed using LPJ emissions. The second set of simulations consists of simulations 'Base2', 'NoPinS2' and 'FixWetl2', which are equivalent to the 'Base1', 'NoPinS1' and 'FixWetl1', respectively, of the first set. The 'Base2' simulation is similar to the 'PinS' simulation in Chapter 4, extended for three more years. The LPJ emissions from the year 1990 are used in 'FixWetl2' throughout the simulation.

5.2.3 *Drivers of CH_4 variability*

In this section we present the drivers of CH_4 variability in our model. The factors that affect the CH_4 sinks are stratospheric sulfur, stratospheric O_3, changes in meteorology, and emissions of CO and NMVOC. The CH_4 emissions for different sectors are also presented. We show model results for sulfate aerosol, while for other drivers of CH_4 variability we give a quantitative description of the input data. Their impact on the CH_4 concentration is analysed in Section 5.3.1.

The main drivers of CH_4 variability in our model for the period 1990 to 1995 are shown in Figure 5.1. All variables have been averaged with a 12-month running mean to remove the seasonal cycle. The globally averaged stratospheric aerosol optical depth (AOD) is shown in Figure 5.1a. The simulated AOD values were validated against measurements in Chapter 4. A global maximum AOD of 0.16 is simulated in early 1992. The aerosols remained in the stratosphere for a few years, with the AOD returning to pre-eruption levels towards the end of 1994.

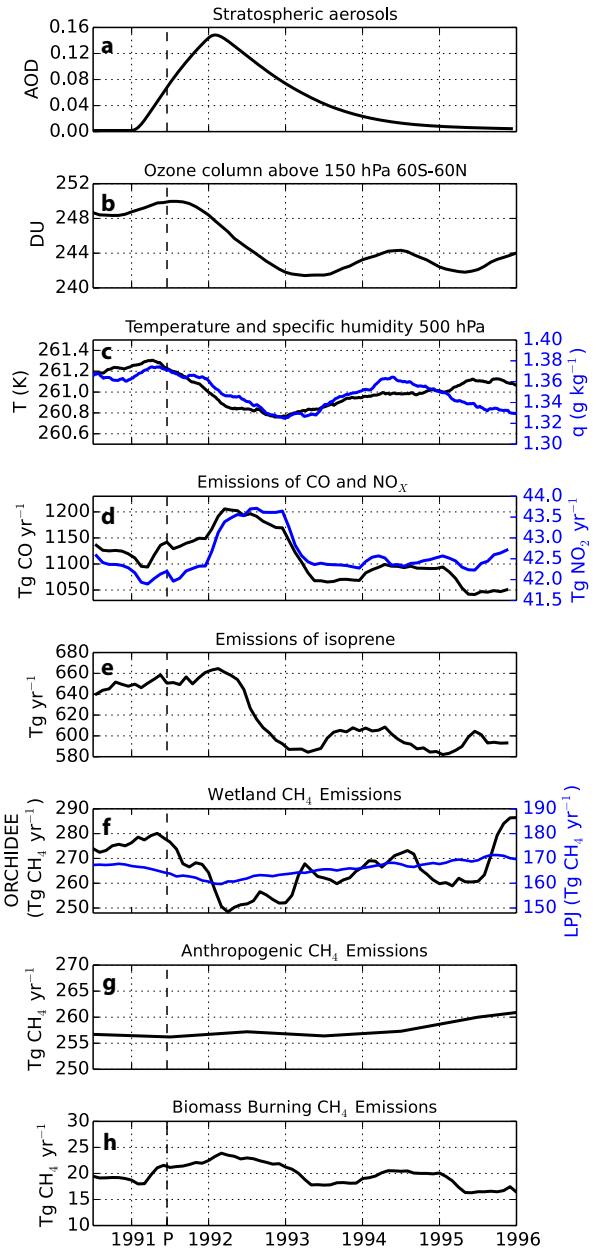

Figure 5.1: The drivers of CH_4 IAV in the early 1990s considered in this study. The black dashed line denotes the timing of the Pinatubo eruption.

Figure 5.1b presents the average stratospheric O_3 above 150 hPa between 60°S-60°N from the MSR data set (van der A et al. 2010). High-latitude O_3 anomalies are not taken into account here because the CH_4 is mainly oxidised in the tropics and at mid-latitudes during summer. A number of processes caused variations in stratospheric O_3 in the period 1990 to 1995. The 11-year cycle in solar radiation determined an overall decrease of 2.5% (6 Dobson Units) in the O_3 column over this period. The quasi-biennial oscillation (QBO) in stratospheric winds caused an additional IAV of about 1% (2 DU). In addition to these natural cycles, enhanced O_3 depletion occurred in 1992 to 1994 due to dynamical changes and heterogeneous chemistry associated with the presence of Pinatubo sulfate particles in the stratosphere (Aquila et al. 2013; Telford et al. 2009). This caused a 3.5% (8 DU) decrease in stratospheric O_3 from 1991 to early 1993, with largest perturbations observed at northern mid-latitudes. A smaller decrease of about 4 DU is found in the tropics (Shepherd et al. 2014). The effect of observed O_3 variations on CH_4 concentrations is investigated in Section 5.3.1. We do not separate in this study the effect of Pinatubo on stratospheric O_3 from other factors of O_3 variability.

A global-scale decrease in surface temperature was registered in 1992 caused by the decrease in surface shortwave radiation due to the volcanic aerosols. The effect of the eruption was partly counteracted by the 1992-1993 El-Niño (McCormick et al. 1995). In our ERA-Interim input data we find a global mean temperature decrease of 0.5°C in the free troposphere and of 0.3°C at the surface between 1990 and 1992, followed by a temperature recovery in 1994 (Figure 5.1c). The temperature decrease was associated with a 3% decrease in tropospheric water vapour. Other meteorological changes in this period, such as dynamics or cloudiness, might have also affected the stratosphere-troposphere exchange of CH_4 and the CH_4 removal by OH. Although these other meteorological parameters are not presented in this section, their potential effects on CH_4 are included when comparing the 'NoPinS' and 'FixMeteo' simulations.

Variability in emissions of chemical species might have determined changes in OH concentrations. Global CO and NO_X emissions have a similar evolution over the period 1990 to 1996, mainly driven by variations in biomass burning (Figure 5.1d). A large biomass burning event in 1992 leads to an increase of 100 Tg CO yr^{-1} in CO emissions and of 1.5 Tg NO_X yr^{-1} in 1992, and a decrease of similar magnitude one year afterwards. The NO_X emissions remain relatively constant throughout the rest of the period, while CO emissions decrease by about 50 Tg between 1990 and 1996. Biogenic emissions of NMVOC can also influence CH_4 concentrations indirectly through their reaction with OH. Isoprene, the NMVOC species with the largest emission rate in the atmosphere, is mainly produced by plants. Biogenic isoprene emissions are sensitive to changes in temperature, precipitation and radiation, and were likely affected by the Pinatubo eruption (Telford et al. 2010; Wilton et al. 2011). Global emissions of isoprene, shown in Figure 5.1e, given by the MEGAN inventory are 640-660 Tg yr^{-1} during 1990 and 1991. Over the coarse of 1992, the isoprene emissions

decrease by about 70 Tg yr^{-1}, remaining at about 580-600 Tg yr^{-1} throughout the simulations period.

Changes in the main CH_4 emission categories are presented in Figure 5.1f-h. Interannual variability in total CH_4 emissions is dominated by emissions from wetlands and biomass burning. Both the LPJ and ORCHIDEE inventories show decreased CH_4 emissions from wetlands in 1991-1993. However, the exact timing and magnitude varies considerably between the two inventories, as well as the global emission amount and IAV. The ORCHIDEE inventory finds on average 266 Tg yr^{-1} CH_4 global emissions from wetlands, with interannual variability of 11.9 Tg yr^{-1} (see Table 5.1). The largest anomaly in this period is found after the Pinatubo eruption, with a decrease of 30 Tg yr^{-1} between the time of the eruption and one year afterwards. The LPJ inventory shows global wetland emissions of 166 Tg yr^{-1} with IAV of 2.6 Tg yr^{-1}. A decrease of 8 Tg yr^{-1} in CH_4 emissions from wetlands is found by LPJ during the year of the eruption, and a recovery starting from early 1992. Wetland extent has been shown to be important for simulating the IAV in wetland emissions, and might be a reason for the large differences between the two models (Ringeval et al. 2010; Spahni et al. 2011). ORCHIDEE simulates wetland extent interactively through the coupling to the TOPMODEL hydrology, while LPJ uses fixed wetland extent. The ORCHIDEE global emissions have been shown to be larger than those of other models from the WETCHIMP intercomparison study, having a high sensitivity to changes in CO_2, temperature and precipitation (Melton et al. 2013).

We used in our simulations the biomass burning emissions of CH_4 reported by the RETRO inventory, which amount to a global mean of 19.7 Tg yr^{-1} over this period, with an IAV of 2.6 Tg yr^{-1} and higher emissions in the years 1991, 1992 and 1994. The IAV in RETRO is determined from national fire reports, and from climate, soil moisture and carbon pool data used in the regional fire model Reg-FIRM (Schultz et al. 2008). Global anthropogenic emissions were quite stable at 256 to 261 Tg yr^{-1} during 1990 to 1995, according our input date based on EDGAR 4.2 and REAS 1 emission inventories, with an IAV of 1.2 Tg yr^{-1} and an increase towards the end of the period. More significant changes occurred at a regional level, with an overall increase in emissions in South-East Asia, and a decrease in Europe, North America and the FSU in this time period. Note, however, that inverse modelling studies report significantly higher total anthropogenic CH_4 emissions for this time period than the bottom-up inventories, exceeding 350 Tg yr^{-1} (Kirschke et al. 2013; Pison et al. 2013).

5.3 RESULTS

5.3.1 *Explained CH_4 variability*

By taking differences between the budget terms of the simulations in Table 5.2 we are able to infer the effect of each driver of CH_4 variability described above. Figure 5.2 shows zonally averaged differences in CH_4 sources and sinks between the different simulations, vertically integrated over the troposphere. The tropopause level is defined here as a function of latitude, as recommended in Lawrence et al. (2001).

Absorption of UV radiation by volcanic SO_2 and UV scattering by sulfate aerosol are both included in the 'Base1' simulation, and lead to a decrease of UV radiation entering the troposphere. As shown in Chapter 4, the effect of stratospheric aerosols on global CH_4 is dominating and longer lived in comparison to the effect of SO_2 absorption. A decrease in the CH_4 sink is depicted in Figure 5.2a due to stratospheric sulfur, calculated as the difference between the 'Base1' and 'NoPinS1' simulations. The impact of stratospheric sulfur is strongest in the months after the eruption in the tropical region, with decreases in the zonal mean CH_4 sink of 2 to 5 mg m^{-2} month^{-1}. Starting from 1993, the difference in the CH_4 sink due to stratospheric sulfur decreases below 1 mg m^{-2} month^{-1} globally.

Stratospheric O_3 decreased in the tropical region in 1991 to 1995 compared to 1990. A slight increase in stratospheric O_3 was observed in 1991 in the southern mid-latitudes because of an increase in the strength of the Brewer-Dobson circulation due to stratospheric heating by Pinatubo aerosols (Aquila et al. 2013). Figure 5.2b shows that these stratospheric O_3 changes led to variations in the OH sink of CH_4 between -5 and +10 mg m^{-2} month^{-1} in the period 1991 to 1996. Decreases in the CH_4 sink of up to 5 mg m^{-2} month^{-1} are modelled in 1991 in the extra-tropics, compensated by increases of similar magnitude in the equatorial region. From 1992 to 1996, reduced stratospheric O_3 levels caused increases in the CH_4 sink in the equatorial band, the northern tropics and part of the northern mid-latitudes. An increase in the CH_4 sink of more than 5 mg m^{-2} month^{-1} is modelled in the northern tropics in the summers of 1993, 1994 and 1995.

The decrease in temperature and water vapour following the eruption led to a decrease in both OH production and the rate of reaction between OH and CH_4. Our model results show that variations in meteorology caused decreases in the CH_4 sink of 2 to 10 mg m^{-2} month^{-1} in the northern tropical region during September 1991 to March 1993, and in the northern mid-latitudes during the summers of 1992 and 1993 (Figure 5.2c).

Variations in emissions of other species indirectly affect CH_4 concentrations through the CH_4 sink. On the one hand, CO and NMVOC emissions decrease OH concentrations because of their reaction with OH. Recycling of OH, on the other hand, increases due to NO_X emissions. Anthropogenic activity and biomass burning events lead to

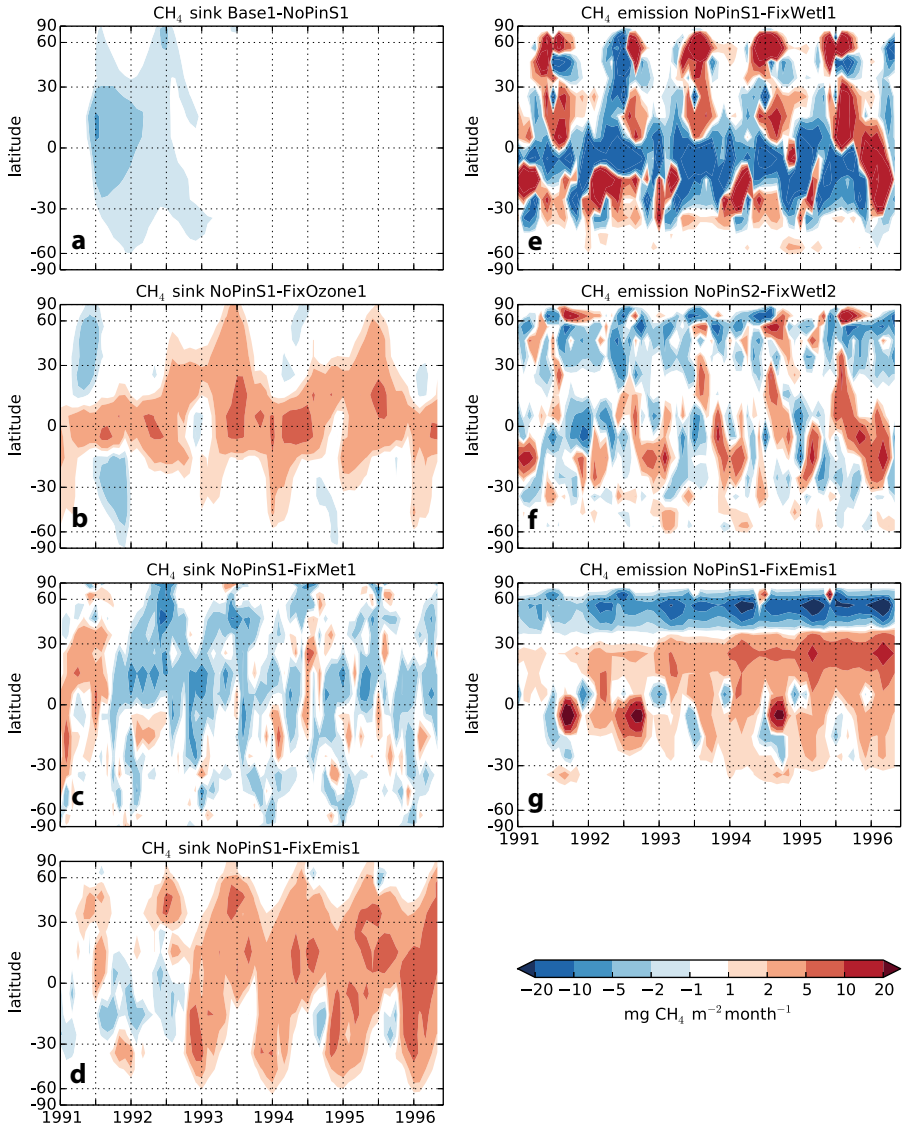

Figure 5.2: Zonal mean differences in the CH_4 budget terms caused by the different drivers of CH_4 variability, vertically integrated over the troposphere. Changes in the CH_4 sink by the reaction with OH are shown for the effects of a) stratospheric sulfur, b) stratospheric ozone, c) meteorology and d) emissions of CO, NO_X and NMVOC. CH_4 emission changes are shown for wetlands from e) ORCHIDEE and f) LPJ, g) for biomass burning and anthropogenic sectors. The years on the x-axis in this and later figures refer to the start of the year.

emissions of all these compounds. In addition, the difference between 'NoPinS' and 'FixEmis' also includes changes in biogenic emissions of CO and NMVOC that are sensitive to climate variations (Sindelarova et al. 2014). The overall effect on OH is determined by the relative increases in total emissions of CO and NMVOC compared to total NO_X emissions (Dalsøren and Isaksen 2006). The OH variability due to changes in emissions is shown in Figure 5.2d. Particularly large decreases in emissions of CO from biomass burning and in biogenic NMVOC emissions in our input data occurred between 1992 and 1993, leading to an increase of 3 to 5 mg m^{-2} $month^{-1}$ in the CH_4 sink.

Figure 5.2e and 5.2f show differences in wetland emission strength with respect to the year 1990 for the ORCHIDEE and LPJ emission inventories. These emission differences are often larger that those found for the CH_4 sink, but they are of shorter duration and more localised. The most striking difference between the CH_4 emission variations in the LPJ and in the ORCHIDEE inventories is their magnitude. While the magnitude of LPJ differences compared to 1990 have values mostly between -10 and 10 mg m^{-2} $month^{-1}$, the ORCHIDEE differences often exceed 20 mg m^{-2} $month^{-1}$. Both inventories show a decrease in emissions in the tropics and in the Northern Hemisphere in late 1991 and early 1992. The strength and the duration of the decrease differs between the two inventories. In the equatorial region, ORCHIDEE gives decreases that often surpass 20 mg m^{-2} $month^{-1}$ from 1992 to 1995. LPJ reports decreased emissions in the equatorial region in the second half of 1991 and first half of 1992. This period is followed by alternating short periods of increased and decreased emissions near the equator until 1995. Both inventories give some increases in emissions in the subtropics throughout the period and a strong increase in emissions throughout the tropics in the second half of 1995 and beginning of 1996. In the northern mid- and high-latitudes, decreases of 2 to 5 mg m^{-2} $month^{-1}$ are maintained from the second half of 1991 to mid-1993 in LPJ. In ORCHIDEE, CH_4 emission decrease by up to 20 mg m^{-2} $month^{-1}$ in the first half of 1992, but are compensated by increases of similar magnitude in the second half of 1992. Increased emissions are reported by ORCHIDEE in this region every summer from 1993 to 1995.

Variations in emissions other than wetlands also cause significant changes in the CH_4 budget. The CH_4 emissions are affected by variations in biomass burning and anthropogenic activity (Figure 5.2g). Anthropogenic emissions in the northern mid-latitudes show a gradual decrease of up to 20 mg m^{-2} $month^{-1}$ from 1990 to 1996. This decrease is compensated by an increase in anthropogenic emissions in the tropical region, with values reaching 5 to 10 mg m^{-2} $month^{-1}$ between 15-30°N. Enhanced biomass burning emissions are also found close to the equator in the autumn of the years 1991, 1992, and 1994.

The modelled growth rate variations caused by the changes in CH_4 sources and sinks described above are depicted in Figure 5.3. A 12-month running mean was applied to all the growth rate variations, to remove seasonal effects. The black line

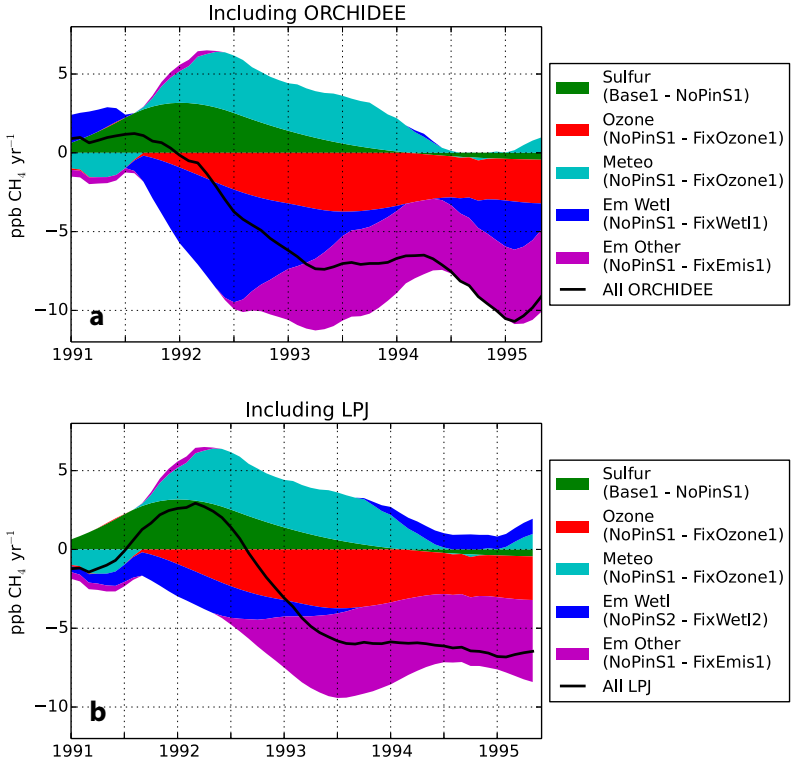

Figure 5.3: Global CH_4 growth rate variations induced by the different drivers, using a) ORCHIDEE and b) LPJ to represent variability in CH_4 emissions from wetlands. Simulations from Set I are used in both plots to infer the effect of stratospheric sulfur, stratospheric ozone, meteorology and emissions other than wetlands. Simulations from Set II are used only to infer the effect of LPJ emission variability. The overall variability ('All') is calculated as the sum of the individual variations.

shows the cumulative effect of these processes on the CH_4 growth rate, representing the combined effect of all considered drivers of variability on the global CH_4 growth rate, which we will refer to as the 'explained' CH_4 growth rate. We assume here additivity between the changes in CH_4 growth rate caused by the different drivers. The effect of nonlinearities is discussed in Appendix B. Figures 5.3a and 5.3b show the two cases in which the ORCHIDEE and the LPJ inventory, respectively, are used to represent the effect of IAV in wetland CH_4 emissions. In early 1991 the growth rate the CH_4 growth rate remains within 2 ppb yr^{-1} of that in 1990. Values of more than 10 ppb yr^{-1} are found in 1990-1991 (see Figure 5.7) due to relatively high emissions

from all source categories of CH_4. The relatively large ozone column values in these years, together with large emissions of CO and NMVOC, lead to a reduced CH_4 sink in 1990 and 1991. When using ORCHIDEE emissions, the further decrease in the CH_4 sink due to stratospheric aerosols and meteorological changes during the year 1991 is compensated by a decrease in natural emissions from wetlands. The decrease in LPJ emissions in 1991 is much smaller, resulting in a 3.5 ppb yr^{-1} increase in CH_4 growth rate in the second half of 1991. The explained CH_4 growth rate decreases afterwards by 9-10 ppb yr^{-1} in both cases, though the timing of the decrease is about half a year later when using LPJ emissions than when using ORCHIDEE. The 8 ppb yr^{-1} decrease in the growth rate obtained with ORCHIDEE wetland emissions in late 1991 and early 1992 causes an earlier decrease in the overall growth rate. While CH_4 emissions from wetlands gradually recover, a combination of other processes leads to a continued decrease in CH_4 growth rate until spring 1993 with ORCHIDEE, or summer 1993 with LPJ. The processes contributing to the decrease in the explained CH_4 growth rate in the second half of 1992 and early 1993 are stratospheric O_3 depletion, a recovery of stratospheric aerosols towards background levels, and changes in other emissions than CH_4 emissions from wetlands. The former effect includes a decrease in CH_4 emissions from biomass burning of 4-5 Tg yr^{-1} between 1992 and 1993, and a 2 Tg yr^{-1} decrease in anthropogenic emissions. This would lead to a combined decrease of 6-7 Tg yr^{-1}, or 2 ppb yr^{-1}. A decrease in isoprene emissions of 60 Tg yr^{-1} and a decrease of 50 Tg yr^{-1} in CO emissions also occur over this period. They cause an increase in the CH_4 removal and lead to a decrease of 6 ppb yr^{-1} in 'FixEmis1' compared to 'NoPinS1'. The overall effect remains stable at -6 to -7 ppb yr^{-1} from mid 1993 to spring 1994. An additional 3 ppb yr^{-1} growth rate decrease occurs by the end of 1994 with ORCHIDEE due to a decrease in CH_4 emissions from wetlands.

Our explained CH_4 growth rates are compared to observations in Figure 5.4. Two estimates for the observed global mean growth rate are shown. The first estimate is calculated from the NOAA GLOBALVIEW-CH4 (2009) marine boundary layer zonal mean CH_4 concentrations. The second estimate, 'Background5', is taken from the CH_4 background data used for nudging the model, based on measurements from five stations (see Section 5.2.2). The other CH_4 growth rate curves in Figure 5.4 are the same as the black lines in Figure 5.3, representing the explained growth rate differences with respect to 1990. In order to obtain the variability with respect to the year 1990 from the observations, the 1990 CH_4 concentrations have been subtracted from both observation timeseries (see absolute growth rate values in Figure 5.7). A running mean of 12 months was further applied to remove seasonal effects. The explained CH_4 growth rate variability shows differences of -1.0 to 2.5 ppb yr^{-1} in 1991 with respect to 1990, which falls in between the two observational estimates of 3 ppb yr^{-1} for GLOBALVIEW-CH4, and -1.5 ppb yr^{-1} for 'Background5'. The model gives an increase of 3.5 ppb yr^{-1} over the course of 1991 when using LPJ, while using ORCHIDEE we find a decrease of 1 ppb yr^{-1}. The observations from GLOBALVIEW show an increase in the CH_4 growth rate in the first half of 1991 and a decrease in

the second half, while the 'Background5' growth rate decreases throughout the year 1991. A continued decrease in the CH_4 growth rate is found in observations in 1992, reaching -10 ppb yr^{-1} in autumn 1992. The explained growth rate also decreases compared to 1990 when using ORCHIDEE emissions, reaching -8 ppb yr^{-1} about half a year later than the observations. With LPJ emissions, the decrease in the CH_4 growth rate occurs between spring 1992 and summer 1993, reaching -6 ppb yr^{-1}. The observations show a further recovery at the end of 1992 and the first half of 1993 to -5 ppb yr^{-1}, remaining relatively constant for the rest of the period. The recovery is not captured in the model, irrespective of the wetland emissions used. The explained growth rate in the model remains stable in the second half of 1993 and first half of 1994 and, in the case of ORCHIDEE emissions, decreases again in the second half of 1994.

5.3.2 *Unexplained CH_4 variability*

As explained in Section 5.2.2, CH_4 observations are used in a first step to quantify the mismatch between the model and observations. This nudging amount is analysed further to better understand the possible reasons for this mismatch.

The global deseasonalised nudging amounts for 'Base1' and 'Base2' are shown in Figure 5.5. Due to the difference of about 100 Tg yr^{-1} in the global emissions from the two wetland inventories, the global nudging amount also shows an offset of similar magnitude. The global nudging over the period 1990 to 1995 is close to 0 with ORCHIDEE, and about 100 Tg yr^{-1} with LPJ. However, there is quite some variability for both simulations within a range of about 50 Tg yr^{-1}. In the first period of the simulation, the nudging term for the ORCHIDEE simulations varies between 0 and -20 Tg yr^{-1}, and between 75 and 105 Tg yr^{-1} for LPJ. The nudging increases by 25-30 Tg yr^{-1} during the first half of 1993 for both the 'Base1' and 'Base2' because the increase in the observed CH_4 growth rate in this period is not reproduced by the explained growth rate. Between the second half of 1993 and the end of 1995, the nudging term for the two simulations shows similar variations, between 5 and 30 Tg yr^{-1} for ORCHIDEE, and between 100 and 125 Tg yr^{-1} for LPJ.

To better quantify the nudging term, the zonal mean nudging amounts for the two simulations as a function of time are given in Figure 5.6c and 5.6d. The zonal mean emission and sink strengths for the 'Base1' simulation are also shown in Figure 5.6c and 5.6d. In both simulations, nudging is predominantly needed in the Northern Hemisphere, where most CH_4 is emitted. This suggests that the uncertainties related to the CH_4 sources dominate the ones related to the sink or to transport, which occur in both hemispheres. Positive nudging is needed in the tropics in both hemispheres during summer, following the position of the inter-tropical convergence zone (ITCZ).

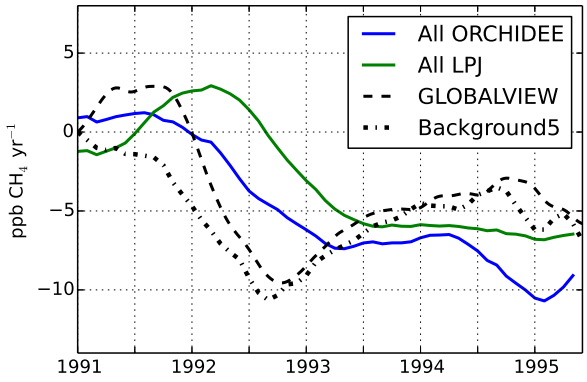

Figure 5.4: The explained CH_4 growth rate variability in the model using two wetland CH_4 emission inventories, and global deseasonalised CH_4 growth rate differences with respect to 1990 from the GLOBALVIEW observations, and from observations at 5 background stations.

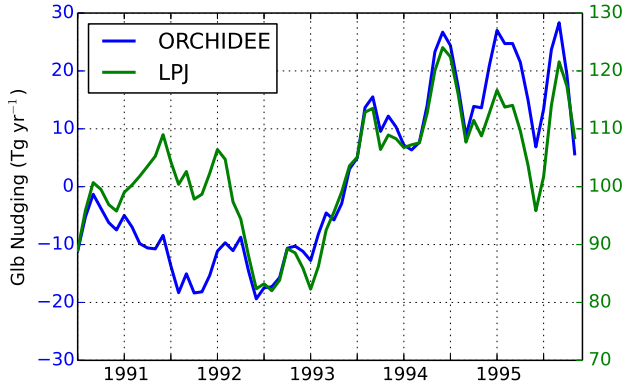

Figure 5.5: Global deseasonalised CH_4 nudging term for the 'Base1' (left y-axis) and 'Base2' (right y-axis) simulations, using CH_4 wetland emissions from ORCHIDEE and LPJ, respectively.

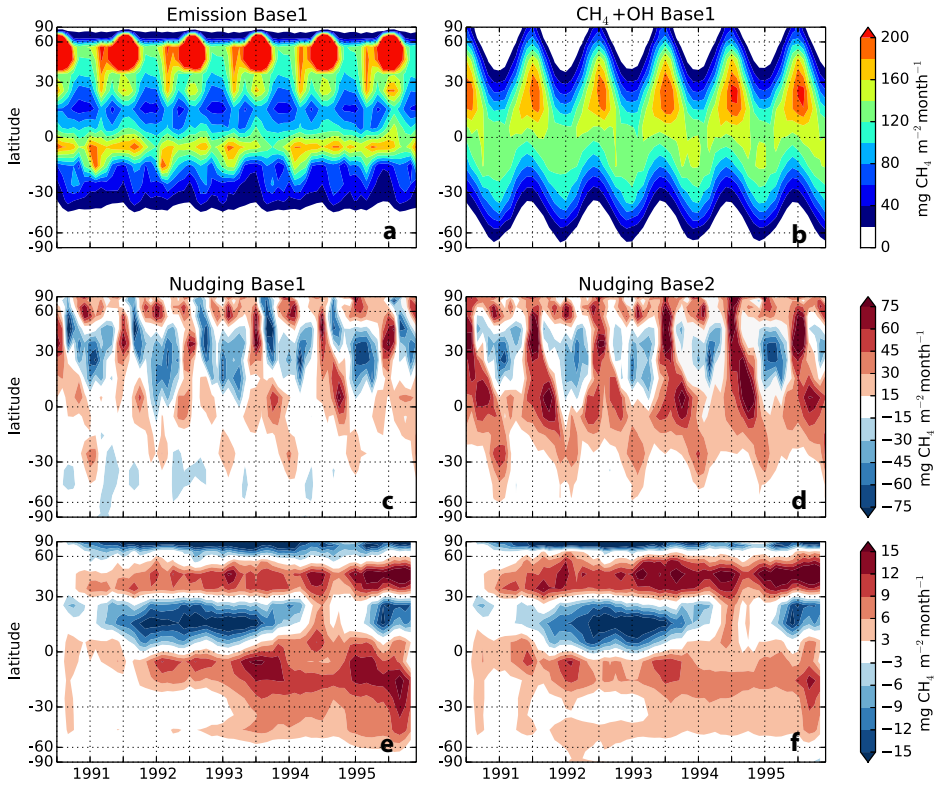

Figure 5.6: Zonal mean CH_4 a) emission and b) sink by reaction with OH in the 'Base1' simulation, zonal mean CH_4 nudging term when using CH_4 wetland emissions from c) ORCHIDEE ('Base1' simulation) and d) LPJ ('Base2' simulation), e and f) the deseasonalised nudging anomaly compared to 1990.

This suggests either missing emissions from tropical wetlands or biomass burning, or an overestimated strength of the tropical OH sink. In the northern mid-latitudes, the model overestimates CH_4 concentrations in the winter, and underestimates concentrations in the summer. This suggests a missing seasonality in one of the CH_4 budget terms. Positive nudging amounts at northern high-latitudes are needed throughout the two simulations, especially during winter. These might be related to underestimated anthropogenic emissions, as well as to errors in transport or vertical mixing, since both natural emissions and the CH_4 sink are almost negligible at high-latitudes during winter.

In Figure 5.6e and 5.6f the nudging for the year 1990 was subtracted from the whole time series, and a 12-month running mean was applied. These plots thus highlight the potential missing IAV in the model compared to observations. For both simulations we find a missing decrease in the CH_4 burden in the northern tropics during 1991 to 1993. This points to either a missing decrease in both wetland emission inventories in this region, or to potential uncertainties in tropical biomass burning. At northern mid-latitudes the CH_4 emissions are dominated by anthropogenic emissions, therefore the missing CH_4 increase revealed in this region suggests that the decrease in anthropogenic emissions over Europe, North America and the FSU in this time period might be overestimated. When using ORCHIDEE emissions we find an additional missing increase in the southern tropics from 1992 onwards, in particular in 1993 and 1995.

5.3.3 *Comparison to inverse modelling studies*

The CH_4 inverse modelling studies of W04 and B06 included the post-Pinatubo period. The OH fields used were derived by different methods. W04 used parameterised OH fields based on chemistry model results. Changes in meteorology, O_3 column, concentrations of CO and NMVOC were included in their parameterisation. However, stratospheric aerosols from the Pinatubo eruption were not included. The OH fields in B06 were determined from an inversion of methyl-chloroform observations, and might be affected by uncertainties in emissions of methyl chloroform.

With regard to the either applied or inferred OH sink variations, the inversion studies for this time period are only partly in line with our simulated variations in the OH sink, including the combined effect of stratospheric aerosols, stratospheric O_3 depletion and tropospheric emissions of CO and NMVOCs. We will now discuss the comparison between our results with these earlier studies for the different time periods: (i) the sharp decrease in the CH_4 growth rate in the second half of 1991 throughout 1992, (ii) the subsequent increase in the CH_4 growth rate in 1993, (iii) the moderate growth rates over the years 1994 and 1995, and the decrease in CH_4 growth rate over the period 1990 to 1995.

1991-1992

W04 inferred a slight decrease in the OH sink of CH_4 in 1991 compared to 1990, and an increase of about 10 Tg yr^{-1} in 1992. In B06, a decrease of about 25 Tg yr^{-1} in the OH sink was found during 1990 to 1992. In our study we find smaller OH variations than both studies, with a decrease in the OH sink of CH_4 of about 5 Tg yr^{-1} in 1992 compared to 1990 and 1991. This reduction in OH is due to sulfate aerosols and atmospheric cooling, compensated by the OH increase caused by ozone depletion (see Table 5.1, Figure 5.3).

Based on their assumed OH concentrations, W04 obtained a 20-25 Tg decrease in wetland emissions in 1992 compared to 1991 and 1990. To explain the de-

crease in the CH_4 growth rate in 1992, B06 found a 35-40 Tg yr^{-1} decrease in wetland emissions in the first half of 1992. To compensate for their simultaneous decrease in OH sink, they found 5-10 Tg lower biomass burning emissions in 1992 than 1991 and 1993, and a 20 Tg decrease in anthropogenic emissions, which is sustained for the rest of the 1990s. With ORCHIDEE we applied a 25 Tg yr^{-1} emission decrease in 1992. Our nudging suggests that this decrease could reach 29 Tg yr^{-1}, which is similar in magnitude to the other studies.

1993

The observed CH_4 growth rate partially recovers during 1993 from the strong decrease in the year 1992. In our study we capture the decrease in CH_4 growth rate in 1993 rather than 1992 due to a 22 Tg increase in the OH sink of CH_4 because of reduced ozone columns, biomass burning emissions and a recovery of sulfate aerosols. A partial recovery in wetland emissions is found in both inventories. This recovery might be underestimated, since an increase in the nudging term is needed to explain the observed growth rate. Both W04 and B06 found increases in the CH_4 sink of about 10 Tg yr^{-1} during 1993. Similarly to our study, W06 simulate a continued decrease in CH_4 growth rate rather than a recovery. In B06, increases in wetland and biomass burning emissions in 1993 are found to overwhelm the increase in the CH_4 sink, leading to an increase in the CH_4 growth rate.

1994-1995

The OH sink of CH_4 showed variations of 3 to 5 Tg yr^{-1} in W06 in the years 1993 to 1995, while an increase of about 15 Tg yr^{-1} in the years 1993 to 1995 was obtained in B06. In agreement to B06, we find a 12 Tg yr^{-1} increase in the OH sink of CH_4 between 1993 and 1995 due to the recovery of the anomaly in temperature, water vapour and stratospheric aerosols caused by the eruption.

Similar to the study of W06, we find that the decrease in the CH_4 growth rate over the period 1990 to 1995 can be entirely explained by an increase in the OH sink of CH_4, rather than by changes in emissions. In B06, however, this decrease in CH_4 growth rate is explained by a decrease in anthropogenic emissions.

The more recent study of Pison et al. (2013) extended the study of B06 by using both methyl chloroform and CH_4 observations to constrain OH concentrations in their INVARR inversion. Smaller OH variability is found in this case compared to B06, and their derived global emission changes are more in line with W04 and with the emissions applied in our first simulation set.

5.3.4 *Comparison to previous bottom-up studies*

In Chapter 3, we analysed the CH_4 growth rate variability after the Pinatubo eruption using a column chemistry model. The timing of the minimum CH_4 growth rate reported in that study is similar to the one found in this three-dimensional study, implying that the delay compared to observations is a result of uncertainties in model input rather than model setup. However, some differences between the two studies occur in the magnitude and contribution of the different processes to the CH_4 growth rate decrease in 1991 to 1993. In Chapter 3, the overall explained growth rate decrease was found to be 12 ppb yr^{-1}, while here we find only 8 to 10 ppb yr^{-1}. A 5 ppb yr^{-1} decrease was found due to CH_4, NO_X and CO anthropogenic emission changes. This is similar to the decrease of 6 ppb yr^{-1} due to changes in non-wetland emissions obtained in this study. However, our current estimate also includes variations of emissions from biomass burning, natural emissions of CO and NMVOC. The sulfate aerosol and O_3 column effects also differ by 2 to 3 ppb yr^{-1} from the estimates presented in Chapter 3, probably because the regional distribution of these effects could not be taken into account in the simplified column model approach. Furthermore, our previous study showed that CH_4 concentrations are affected for a long time period after a perturbation is applied due to the CH_4 lifetime of about 10 years. This delayed effect can be seen here for stratospheric sulfur, where a small negative difference in the CH_4 growth rate is found towards the end of the simulation period (Figure 5.3). The delayed effect that a perturbation in a driver of CH_4 variability has on the CH_4 growth rate also occurs in our other simulations. However, it is in general overwhelmed by the instantaneous effect of variability in the CH_4 driver.

Other studies have focused on only one of the drivers of CH_4 variability after the Pinatubo eruption. Bekki and Pyle (1994) found a decrease in CH_4 growth rate of 7 ppb yr^{-1} globally due to stratospheric O_3 using a two dimensional model between spring 1991 and autumn 1992. Here we obtain a comparable estimate of 5 ppb yr^{-1} decrease over the period 1991 to autumn 1993 due to the pronounced stratospheric O_3 depletion in the tropics and northern mid-latitudes in 1993.

Using a two-dimensional chemistry and transport model, Bekki and Law (1997) investigated the effect of temperature on both chemistry and wetland emissions in 1991-1992. They found that the temperature decrease after Pinatubo led to a 4 ppb yr^{-1} increase in the global CH_4 growth rate between mid-1991 and mid-1992, similar to our meteorological effect of 5 ppb yr^{-1}. By applying a $Q_{10} = 2$ temperature sensitivity of CH_4 emissions (Dunfield et al. 1993), they found that CH_4 emissions from wetlands would decrease the CH_4 growth rate by 2 ppb yr^{-1} in the same period. This is similar to our result using LPJ wetland emissions. The ORCHIDEE inventory gives a much larger decrease in the CH_4 growth rate of 9 ppb yr^{-1}, which overwhelms the meteorological effect on the CH_4 sink. This shows that the climate sensitivity of wetland emissions is larger in ORCHIDEE, where changes in wetland extent are taken into account.

Stratospheric aerosols were found to enhance the Brewer-Dobson circulation after the Pinatubo eruption (Aquila et al. 2013). This change in the dynamics of the atmosphere might also affect CH_4 concentrations. Schauffler and Daniel (1994) hypothesized that increased exchange between the stratosphere and troposphere might be responsible for the decrease in CH_4 growth rate observed in 1992. By performing an additional simulation where only temperature and humidity were fixed to 1990 values, we found that the meteorological effect is dominated by the effect of these two variables (results not shown). The global impact of changes in ERA-Interim wind fields is marginal. The wind fields in ERA-Interim have some uncertainty for the first weeks after the eruption related to the fact that Pinatubo aerosols are not explicitly accounted for. However, the longer-term effect on temperature and the corresponding dynamical effect are included in ERA-Interim through the assimilation of satellite radiances.

Dlugokencky et al. (1994) and Law and Nisbet (1996) hypothesized that the emission decline in the FSU could have had a significant contribution to the decrease in CH_4 concentrations during 1992, because the decrease is primarily found in the Northern Hemisphere. However, our results indicate a missing CH_4 burden decrease in 1992 which originates in the northern tropics (Figure 5.6). Furthermore, a missing increase in CH_4 concentrations is found in the Northern Hemisphere extratropics, pointing to a potential missing source in this region rather than reduced emissions due to gas leak fixes. Furthermore, the overall decrease in growth rate between 1990 and 1996 is captured by our model, and can be attributed to stratospheric O_3 decrease over this period, and decreases in biomass burning and biogenic emissions of NMVOC and CO. We acknowledge, however, that the nudging procedure used here introduces some uncertainty in providing the location of missing emissions. The procedure attributes the source-sink mismatch at the dateline to sources or sinks in the same 10-degree latitude band. Potential sub-monthly transport of emissions from other latitudes is not taken into account. To further constrain the sources of model-measurement mismatch, an inverse modelling study should be performed to estimate the variability of the CH_4 sources using modelled OH variability.

5.3.5 *Potential sources of uncertainty*

In this study all known major drivers of CH_4 variability have been included. We estimate that potential missing processes had a minor effect on CH_4 concentrations, and would therefore not significantly affect our results. Such processes are the radiative effects of ash and water vapour injected in the stratosphere by the eruption, and the effect of sulfur deposition on CH_4 emissions from wetlands. Ash particles emitted by the eruption have a short lifetime of a few days (Guo et al. 2004a; Niemeier et al. 2009), and were found to have a negligible effect on global radiation. Changes in water vapour are included through ERA-Interim reanalysis, and might contain some

uncertainties (Dessler et al. 2014). Sulfur deposition has also been proposed to affect CH_4 emissions from wetlands (Gauci and Chapman 2006). This effect is not included in our input data. In Chapter 3 we made a rough estimate of this effect, and found it to be of the order of 1 Tg CH_4 yr^{-1} for the Pinatubo eruption.

The zonal mean nudging term in our model points to either underestimated emissions or overestimated sinks in the tropics and during summer at mid-latitudes. An overestimated source is identified at mid-latitude during winter. Uncertainties in the OH sink of CH_4 might relate to uncertainties in the chemistry. CO concentrations in TM5 are underestimated at the northern mid-latitudes (Huijnen et al. 2010; van Noije et al. 2014), which might lead to overestimated OH concentrations in this region. An overestimate in OH concentrations at northern mid-latitudes and an overestimated north-south gradient in global chemistry models is also found from methyl chloroform observations in Patra et al. (2014). In the tropics, OH uncertainties might arise due to NMVOC chemistry, and are discussed in more detail below. Other uncertainties in tropical OH might relate to NO_X and CO emission factors from biomass burning. CO decreases OH concentrations, while NO_X increases OH recycling, therefore the overall effect of biomass burning emissions on OH are strongly dependent on the emission factors of these species, which are uncertain in tropical region in the early 1990s (Schultz et al. 2008).

Our results show that the decrease in CH_4 growth rate observed in 1992 is reasonably well explained by the processes considered here. However, the exact timing of the minimum growth rate is captured 6 to 9 months later than in the observations. Since missing processes are estimated to have a small impact on CH_4 variability in the early 1990s, the mismatch between modelled and measured CH_4 concentrations can only be related to uncertainties in either input data or modelled CH_4 processes. Measurement uncertainty might also contribute to the mismatch. The differences given by the two measurement-based estimates of the global CH_4 growth rate in Figure 5.4 show that uncertainties can be of the order of 2-3 ppb yr^{-1}. Our input data and chemical processes related to aerosols, O_3 and meteorological effects are fairly well studied and understood. The uncertainty related to these processes is in the order of 10-20%, and cannot explain the different timing of the decrease in CH_4 growth rate between the model and observations.

Larger uncertainties are related to the CH_4 emissions. The differences between the CH_4 emissions from the ORCHIDEE and LPJ inventories, both in terms of magnitude and IAV (Table 5.1), show that there are still many unknowns in the processes governing emissions from wetlands. One of the most important differences between the two models is the fact that ORCHIDEE simulates changes in wetland extent, while LPJ uses fixed wetland extent. This might be the cause for the larger IAV in ORCHIDEE, and for the higher climate sensitivity. Large differences in the response of ten wetland emission models to a temperature perturbation were also found in the WETCHIMP model intercomparison project, showing that a better understanding of wetland processes is needed (Melton et al. 2013).

Biomass burning emission uncertainties could also contribute to the mismatch between model and observations. However, given the IAV in biomass burning emissions in both the RETRO and the more recent GFED emission inventory of about 3 Tg CH_4 yr^{-1}, it is unlikely that uncertainties in biomass burning CH_4 emissions could be the sole reason for the mismatch. As explained above, it is also unlikely that anthropogenic emission changes due to gas leak fixes within the FSU contributed to the mismatch.

We find a significant impact of CO and NMVOC emission changes on the CH_4 removal by OH. Some uncertainty is associated with NMVOC emission changes and their effect on CH_4 chemistry in the period after Pinatubo. Natural emissions of isoprene respond to both changes in climate and in solar radiation (Telford et al. 2010; Wilton et al. 2011). A decrease in surface temperatures would lead to a reduction in isoprene emissions. Concerning the effects of radiation, the increase in diffuse radiation after the eruption, leading to deeper penetration into canopies, has been shown to have overwhelmed the effect of decreased direct radiation in terms of plant growth (Mercado et al. 2009). Therefore the increase in diffuse radiation would have increased isoprene emissions. However, in this study only the effect of climate change and the effect of decrease in total shortwave radiation after the eruption are included through the MEGAN inventory. The isoprene emissions in MEGAN show a decline of 50 Tg yr^{-1} globally during 1992, likely due to the decrease in surface temperature and global shortwave radiation. The CH_4 growth rate decreases by about 4 ppb yr^{-1}, or 11 Tg yr^{-1} due to changes in emissions of other species than CH_4 including isoprene. These changes are of similar magnitude as found in Telford et al. (2010), where a 40 Tg decrease in isoprene emissions between 1990 and 1992 resulted in a 5 Tg increase in CH_4 removal by OH. The estimated effect of NMVOC emissions on CH_4 concentrations has several sources of uncertainty. Firstly, including the effect of Pinatubo on diffuse radiation might have led to increased NMVOC emissions in 1991-1992, and an even stronger decrease in 1993, when the aerosols were removed from the atmosphere. Secondly, recent studies have shown that the sensitivity of OH concentrations to NMVOC is smaller than previously thought (Rohrer et al. 2014; Stone et al. 2011). The CBM4 chemistry scheme used here does not include an updated isoprene chemistry mechanism, and might exhibit a too high OH sensitivity to isoprene. Telford et al. (2010) used a chemistry scheme that includes the Mainz isoprene mechanism, a parameterisation based on the Master Chemical Mechanism (MCM), which was also shown to misrepresent OH recycling in VOC-rich environments (Pöschl et al. 2000; Stone et al. 2011). Nevertheless, it is important to take NMVOC emission changes into account for evaluating CH_4 variability. Due to the potentially overestimated OH sensitivity, our calculated effect on CH_4 can be seen as an upper estimate.

5.4 CONCLUSION

The processes responsible for CH_4 variability in the early 1990s have been investigated in the global chemistry and transport model TM5. Known drivers of CH_4 variations include: (i) photochemical effects of stratospheric sulfur from Pinatubo and (ii) of stratospheric O_3 changes, (iii) temperature and humidity perturbations, and their effect on CH_4 chemistry, (iv) variations in CH_4 emissions from wetlands, (v) biomass burning and (vi) anthropogenic sources, and (vii) changes in emissions of other compounds and their effect on OH. We find that all these processes contributed in a significant way to the CH_4 growth rate variations in the early 1990s.

The 'explained' growth rate evolution falls within the observational range during 1991. However, the increase in growth rate modelled at the end of 1991 using wetlands CH_4 emissions from LPJ is not found in the observations. The observed decrease of about 10 ppb yr^{-1} in CH_4 growth rate during the year 1992 is captured by the model with a delay of half a year to one year. We have used two inventories for CH_4 emission from wetlands to explore the potential role of uncertainties in this emission sector. Although they have a significantly different variability, the two inventories give a similar performance in capturing the global CH_4 variations. When using ORCHIDEE, the global CH_4 growth rate is better captured in 1990 to 1993, while using LPJ we are able to reproduce better the CH_4 growth rate at the end of the analysed period. The increase in CH_4 in 1993 is not captured by either of the two scenarios. According to our breakdown in individual causes for CH_4 growth rate changes, the overall decrease in the CH_4 growth rate of 5 ppb yr^{-1} during 1990 to 1995 is explained by the observed decrease in O_3 column due to the 11-year cycle in solar activity, and by the estimated decrease in CO and NMVOC emissions in this period.

By analysing the nudging term, we find that the mismatch most likely originates in the northern tropical region. Since the effects of UV changes and temperature changes on OH are considered to be robust, the most likely source of missing variability is natural CH_4 emissions from wetlands. Uncertainties in tropical biomass burning emissions, and in biogenic NMVOC emissions and their effect on OH might have also contributed to the mismatch between the modelled and observed CH_4 concentrations. Modelling CH_4 emissions from wetlands is a challenging topic, due to the large spatial and temporal variability of these ecosystems. The large differences between the two emission datasets used here in terms of CH_4 emission amount and variability show that further research is needed to understand the factors driving emissions from wetlands and their response to environmental factors. Furthermore, the effect of changes in diffuse radiation and sulfur deposition after the eruption are not taken into account in the inventories used in this study. Another source of uncertainty are changes in NMVOC emissions, as well as the impact of NMVOC changes on OH. Further study is recommended using an updated isoprene chemistry scheme that considers the OH recycling by NMVOC, and using NMVOC emission models that

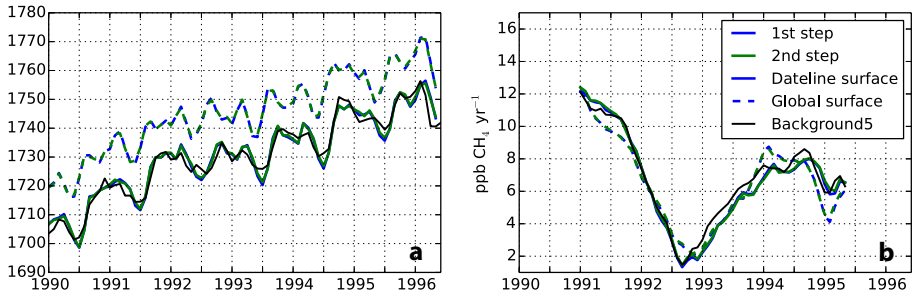

Figure 5.7: Surface mean CH_4 a) concentrations and b) growth rate for the two runs of 'Base1' simulation at the dateline (solid lines) and global mean (dashed lines). The black line shows the background mean concentrations based on 5 background stations.

take into account the effect of both direct and diffuse radiation. Finally, some uncertainty exists in the timing and location of the missing emission variations given by the nudging term. Our nudging procedure is able to capture the global growth rate variations. However, because the nudging corrects the amount of CH_4 in the zonal band where the mismatch occurs, it does not account for sub-monthly transport between zonal bands. An inverse modelling approach using OH fields from this study could better resolve the sources and timing of model-measurement mismatch. This might, almost 25 years after the Pinatubo eruption, further improve our knowledge on the drivers of CH_4 growth rate variations.

Appendix A. Validation of the two-step nudging setup

We use a two-step method to simulate realistic CH_4 concentrations. In a first step, 'Base1' and 'Base2' scenarios are run with near-surface CH_4 mixing ratios nudged towards the zonal mean background mixing ratios inferred from measurements at the five stations of South Pole, Cape Grim, Mauna Loa, Niwot Ridge, Barrow, and Alert. The nudging amount is stored on a monthly basis for each 10-degree latitude band, and used in the second step. In this second step, CH_4 is no longer constrained by observations, but instead the nudging amount calculated in the first step is applied as an emission in all scenarios in the lower 2 km.

Figure 5.7 presents the global and dateline monthly mean CH_4 concentrations and the deseasonalized growth rates obtained in the two runs of 'Base1', and their comparison with 'Background5' observations. Please note that we show here absolute CH_4 growth rates, and not variations with respect to 1990 as shown in Figure 5.4. Also note that the actual CH_4 growth rates in 'Base1' are plotted, unlike in Figures

5.3 and 5.4 and where differences between simulations were presented. CH_4 concentrations at the dateline were nudged in the first step to the concentration values indicated by 'Background5'. Therefore, the fact that the CH_4 dateline mean concentrations follow reasonably well the observations is a result of the nudging procedure. The global surface mean concentrations in the model show similar variations as the dateline mean, but with concentrations of 10 to 15 ppb higher. This is due to the fact that the dateline crosses the Paciffic Ocean, and is remote from CH_4 sources, while in the global mean both remote and polluted areas are included. The observed deseasonalised CH_4 growth rate is well reproduced in the model both by the dateline mean and by the surface mean. The modelled dateline growth rate is within 1 ppb/yr from the observed one, while the model global mean is within 2 ppb/yr. Both the surface mean and the dateline mean of the two steps from the model follow well the observed growth rate variations, with a slightly better performance of the dateline towards the end of the simulation.

In the first step, a correction is applied at every time-step on the CH_4 concentrations, based on the comparison between the modelled CH_4 concentrations at the dateline and the measured zonal mean background concentrations. In the second step, the same amount of monthly correction is applied on the CH_4 burden for every 10-degree latitude band. However, instead of adjusting the concentrations, the adjustment is made in the second step as an additional emission or sink in the lowest 2 km of the model. The global mean and dateline mean concentrations and growth rates of the second step are nearly identical to those of the first step. This shows that the procedure in which the correction is applied does not significantly influence the results, and that the simulations of the two steps give a similar performance in capturing the observed CH_4 growth rates.

Appendix B. Additivity between drivers of CH_4 variability

In Figure 5.3 we have shown the combined effect of the drivers for CH_4 variability assuming additivity between the different drivers. We verify this assumption by using results from the 'FixAll1' simulation, where all drivers of CH_4 were fixed to 1990 values. Figure 5.8 shows the combined effect of the 7 drivers for CH_4 variability found from the sum of individual drivers for the first simulation set (also shown in figure 5.4 and labeled 'All Orchidee'), and the combined effect found from the difference between 'Base1' and 'FixAll1'. The two global CH_4 growth rate curves nearly overlap each other, with differences less than 0.2 ppb/yr. This shows that indeed the assumption of additivity is valid.

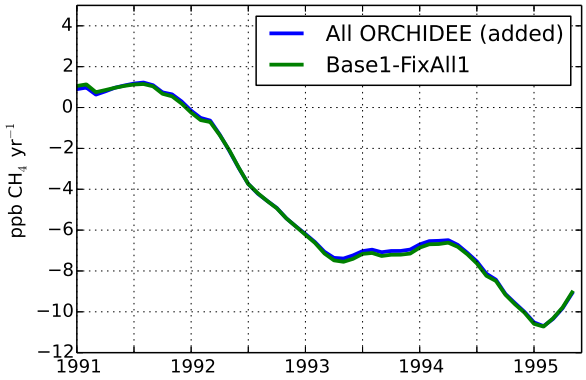

Figure 5.8: The combined effect of the 7 drivers of CH_4 variability on the global growth rate using ORCHIDEE emissions, assuming additivity (blue) and from the difference between 'Base1' and 'FixAll1'.

6

GENERAL CONCLUSIONS AND OUTLOOK

6.1 GENERAL CONCLUSIONS

This thesis has investigated in detail the processes affecting atmospheric CH_4 concentrations after the Mount Pinatubo eruption on 15 June 1991, and quantified their contribution to the observed variations in global CH_4 growth rate. The Pinatubo eruption was the largest eruption in the past century, and the single explosive stratospheric eruption since the NOAA network of continuous CH_4 measurements was established. The eruption determined significant changes in radiation, climate and atmospheric chemistry in the following years, providing an interesting test case for the processes driving CH_4 concentrations. The following research questions were addressed:

- What processes related to the Pinatubo eruption affected the CH_4 budget and what are their individual contributions to the observed CH_4 growth rate?
- What other processes than the volcanic eruption contributed to the observed CH_4 variability in the post-Pinatubo period?
- Are we able to simulate the observed CH_4 growth rate variations after the Pinatubo eruption?

In Chapter 3 we investigated the processes affecting the CH_4 growth rate after the Pinatubo eruption from a global perspective. Using a column chemistry model, we addressed the first and the third research questions, and quantified for the first time the combined effect of UV absorption by Pinatubo SO_2, sulfate aerosol scattering, stratospheric O_3 depletion, temperature and water vapour changes on global CH_4 concentrations (see Section 1.2.4). We also partially addressed the second research question by assessing the impact of anthropogenic emission changes in the years following the eruption.

The column chemistry model was coupled to the radiative transfer model TUV to evaluate the impact of changes in stratospheric O_3, SO_2 and sulfate aerosols on photolysis frequencies. While in most three-dimensional models CH_4 concentrations

are constrained to observations, in the column model we could perform transient simulations using CH_4 emissions. Therefore the feedback of CH_4 on its own lifetime could be taken into account. The model parameters were tuned such that the column model best represents global tropospheric chemistry budgets of CH_4, O_3 and CO, and the sensitivity of CH_4 lifetime to temperature, O_3 column and CH_4 concentrations.

Using this set-up, the column model reproduced reasonably well the long-term evolution of CH_4 and methyl chloroform. The Pinatubo eruption increased the CH_4 sink in the first year after the eruption by reducing UV levels in the troposphere and by decreasing tropospheric temperature and water vapour, leading to a decrease in OH levels and thus in the reaction rate between OH and CH_4. The depletion in stratospheric O_3, partly attributable to the Pinatubo eruption, peaked about two years after the eruption, leading to an increase in OH and in the CH_4 sink. Natural CH_4 emissions from wetlands were predicted to decrease due to the decrease in surface temperature in the two years after the eruption.

We simulated an initial increase in the CH_4 growth rate of 2 to 3 ppb yr^{-1} after the eruption, and a subsequent decrease of 7 ppb yr^{-1} due to the changes in chemistry and climate. We found an important contribution of 8 ppb yr^{-1} from stratospheric O_3 depletion. Other studied processes contributed by 2 to 5 ppb yr^{-1} to the overall effect, partially counteracting each other. An additional 5 ppb yr^{-1} decrease due to changes in anthropogenic emissions was found between 1991 and 1993, leading to a total decrease of 12 ppb yr^{-1} in the CH_4 growth rate in this period. While the magnitude of these changes are similar to observations, the timing of the decrease in CH_4 growth rate was modelled about 9 months later than observed.

Using a column model to represent global tropospheric chemistry such as described in Chapter 3 had several drawbacks. It was not possible to take into account atmospheric transport and regional differences in the drivers of CH_4 variability after Pinatubo. We could also not distinguish between clean and polluted regions with different chemical regimes, or take into account the local sensitivity of OH chemistry to a particular driver. These issues were addressed in Chapter 4 and 5 through the use of the global chemistry and transport model TM5.

To start the more advanced analysis, TM5 was used in Chapter 4 for the first time to quantify the impact of stratospheric sulfur on tropospheric photochemistry in a three-dimensional approach, contributing to answering our first research question. The coupling between aerosols and photolysis described in Chapter 2 enabled this assessment. Another novel development in Chapter 4 is the coupling between SO_2 and radiation, which allowed us to also estimate the impact of SO_2 on tropospheric photolysis.

Several adjustments were necessary to the default TM5 setup to obtain good performance of the model for Pinatubo SO_2 and sulfate aerosols. Firstly, 60 vertical layers were used instead of 34 to avoid large numerical errors due to a low vertical resolution in the stratosphere. Secondly, the modal representation of aerosols from the M7 microphysics module was modified according to previous studies to better

simulate the stratospheric sulfate aerosol size. To account for both stratospheric and tropospheric aerosols after the Pinatubo eruption, the default M7 setup was used below the 300 hPa level (∼9 km altitude), and the adjusted stratospheric setup was used above 300 hPa.

After these changes were implemented, we simulated the evolution of Pinatubo SO_2 and sulfate aerosols and obtained a good comparison with observations. Pinatubo aerosols were found to decrease tropospheric photolysis frequencies of O_3 and NO_2, and tropospheric OH concentrations by about 2% globally in the first two years after the eruption. Stratospheric sulfate was thus found to increase the CH_4 growth rate by 3.5 ppb yr^{-1} in the first year after the eruption and by 2 ppb yr^{-1} in the second year after the eruption. Due to the short lifetime of SO_2 of about one month, the SO_2 effect was found to be significant only in the northern tropical region in the first few months after the eruption, leading to an increase of 0.5 ppb yr^{-1} in the global CH_4 growth rate in the first year after the eruption. The calculated increase in the CH_4 growth rate in the second half of 1991 and early 1992 is in line with observational evidence of increased CH_4 concentrations in the atmosphere in this period.

In chapter 5 we revisited the three research question above. We attempted to simulate the evolution of the observed CH_4 growth rate during 1990 to 1995 using the three-dimensional model TM5 and to identify the processes contributing to the growth rate changes. Seven potential drivers of CH_4 variability were taken into account: stratospheric sulfur from the eruption, stratospheric O_3, changes in meteorology, emissions of CH_4 from wetlands, biomass burning and anthropogenic activity, and emissions of other species (CO, NMVOC, NO_X).

We found that variations in the CH_4 growth rate during the studied period were primarily determined by stratospheric aerosols from the eruption, changes in stratospheric O_3 levels, temperature and humidity, and variations in CH_4 emissions from wetlands, biogenic NMVOC emissions, and biomass burning emissions. Each of these processes caused variations of 2 to 6 ppb yr^{-1} in the CH_4 growth rate, and the effects partly counteracted each other. UV absorption by SO_2 emitted by the eruption, changes in the exchange between the stratosphere and the troposphere, and anthropogenic emissions were estimated to have had a smaller impact on the global CH_4 variability in the early 1990s, of less than 1 ppb yr^{-1}. We were able to reproduce a decrease in the CH_4 growth rate of about 10 ppb yr^{-1} after the Pinatubo eruption. However, the timing of the minimum CH_4 growth rate in the model occurred about 6 to 9 months later than in the observations. We did not find a recovery in CH_4 growth rate before the end of 1995, while the observations show that the growth rate partially recovers in 1993. In Section 6.2 we will discuss possible methods to better understand these differences between model and observations.

Interestingly, the simulated CH_4 growth rate changes in TM5 had a similar magnitude as obtained in the column model, and a similar timing. However, the attribution of the modelled CH_4 variability to the underlying drivers differed somewhat between the two approaches. By assuming an instant globally homogeneous distri-

bution of SO_2 in Chapter 3, the SO_2 impact on the CH_4 growth rate was found to be an increase of 3.5 ppb yr^{-1}, while in Chapter 4 the increase was only 1.1 ppb yr^{-1} in July 1991. The magnitudes of the effects of O_3 column changes and sulfate aerosols were also different between the two studies. While in the column model study the effect of O_3 column changes dominated, in the three-dimensional study it was found to have a similar magnitude compared to the effects of sulfate and meteorology. Finally, changes in anthropogenic emissions had a much smaller impact on the CH_4 growth rate in the period 1990 to 1995 in the simulations with TM5 compared to the column model. The decrease in the CH_4 growth rate in the column model was due to changes in emissions of short-lived gases such as NO_X, CO and NMVOC, rather than due to emissions of CH_4. The sensitivity of the CH_4 growth rate to short-lived gases might be overestimated in the column chemistry model because regional differences in the chemical regimes cannot be taken into account. Thus, the column model study was useful to make a first estimate of the effects of Pinatubo on the methane growth rate. However, three-dimensional effects cannot be neglected in explaining variations in the global growth rate of CH_4.

6.2 OUTLOOK

The evolution of SO_2 and stratospheric aerosols from the Pinatubo eruption was modelled in Chapter 4 as a first step in quantifying their impact on the CH_4 burden. The performance of TM5 in simulating their evolution is comparable to that of recent studies using climate and chemistry models (Aquila et al. 2012; Dhomse et al. 2014; English et al. 2013; Toohey et al. 2011). Further improving our results on Pinatubo aerosols might result from changing some specifications of the initial sulfur injection in the model. Note that we have tested the impact of injection height in Chapter 4 and have chosen the height resulting in the best latitudinal distribution of Pinatubo aerosols. The impact of injection amount and speciation into SO_2 and sulfate can be further tested. Recent studies on Pinatubo aerosol microphysics have inferred a lower SO_2 injection amount than previously estimated (Dhomse et al. 2014; Sheng et al. 2015). Aerosol measurements shortly after the eruption suggest that about 3 Tg SO_2 is already converted to sulfate within the eruption column (Guo et al. 2004a). Therefore, specifying a proportion of the sulfur emission as sulfate aerosol emission instead of SO_2 might improve the comparison between TM5 aerosols and observations.

To allow a good representation of the size distribution of volcanic aerosols within TM5, different setups of the modal aerosol representation were used above and below the 300 hPa level. Although this setup performed well in simulating both stratospheric and tropospheric aerosol optical depth, it might lead to unphysical behaviour of aerosols at the boundary between the two regimes, likely mainly affecting tropospheric aerosols on short time scales of the order of one week. Options to improve the transition between the two parameterizations can be further explored, for instance

by allowing coarse-mode particles to be transported above 300 hPa, though without interacting with accumulation-mode particles. Note that most sulfate aerosols will be sedimented out from the stratosphere before they would grow into coarse mode.

All known major drivers of CH_4 variability were taken into account in Chapter 5 in order to simulate the evolution of CH_4 concentrations after the Pinatubo eruption. Nevertheless, an additional decrease in the CH_4 burden of about 20 $Tg\,yr^{-1}$ in the northern tropical region was needed in our simulations during 1991 to 1994 to match the observations (see Section 5.3.2). Potential reasons for the mismatch between our simulations and the observations are: (i) significant unaccounted CH_4 emission changes in tropical wetlands, in combination with (ii) uncertainties in NMVOC emissions and chemistry, and (iii) not well-constrained biomass burning emissions.

The large difference between the two inventories used for CH_4 emissions from wetlands shows that further research is needed to improve our knowledge on wetland emissions, their inter-annual variability, and sensitivity to changes in hydrology and climate. This understanding is important for the prediction of the future evolution of CH_4 concentrations.

Furthermore, we found a significant impact of NMVOC emission variations on the CH_4 growth rate through their impact on OH. However, the sensitivity of OH to NMVOC emission changes has been shown to be overestimated in current chemistry schemes. We suggest that the use of an updated NMVOC chemistry scheme in TM5 could reduce this uncertainty. The impact of increased diffuse radiation due to the Pinatubo sulfate aerosol layer on biogenic NMVOC emissions was not included in the NMVOC emission inventory used here, and might lead to additional uncertainty in the magnitude of the effect of NMVOC emission changes.

Biomass burning affects CH_4 concentrations directly by emitting CH_4, and indirectly by emissions of CO, NO_X and NMVOC which affect OH concentrations. OH increases due to NO_X emissions and decreases due to CO emissions. Therefore, the overall effect of biomass burning on OH would depend on the relative emission factors for these compounds. Global biomass burning emissions for the early 1990s are available from the RETRO inventory (Schultz et al. 2008). The inter-annual variability in these emissions was inferred from national fire reports. For the tropical region such reports were not available, therefore IAV was inferred based on temperature, soil moisture and carbon pool data using the regional fire model Reg-FIRM. Therefore the IAV in tropical biomass burning for this period is quite uncertain. Biomass burning emissions for more recent years are better constrained by the use of satellite data (van der Werf et al. 2010).

We used a simple nudging technique to quantify the mismatch between simulated and observed CH_4 concentrations. This procedure adjusts the concentrations in each zonal band based on the comparison between the modelled CH_4 concentrations at the dateline and measured monthly mean CH_4 concentrations at background stations. We could therefore quantify the adjustments to the CH_4 burden needed in each

10-degree zonal band to match the observations. However, this procedure does not take into account potential sub-monthly transport between the different zonal bands. Therefore, the exact attribution of the adjustments to the simulated CH_4 burden to regional sources and sinks has some uncertainty. We suggest to use the simulated OH variability, that takes into account the photochemical changes after the eruption, to inversely estimate methane emissions. Such a study could help to better identify the exact regional CH_4 emission sources that might be responsible for the remaining differences between simulated and observed CH_4 concentrations.

By using a chemistry and transport model we were able to investigate the effect of observed variations in stratospheric O_3 and climate after the Pinatubo eruption on the CH_4 emissions and chemistry. Separating the effects of the eruption from other factors of natural variability was only possible for stratospheric sulfur in Chapter 4 by modelling interactively the evolution of SO_2 and sulfate. Because our model uses stratospheric O_3 and meteorological parameters based on observations, the exact magnitude of the impact of the eruption alone is difficult to quantify using a global chemistry and transport model. A climate model, including interactive emissions from vegetation and stratospheric O_3 chemistry, would be needed to fully separate the impact of the Pinatubo eruption on CH_4 through climate and stratospheric O_3 depletion from other factors of natural inter-annual variability, e.g. ENSO and the QBO.

As our modelling capabilities increase over time, more components of the Earth system can be studied interactively. The TM5 chemistry and transport model used in this thesis has been coupled to the EC-Earth climate model (van Noije et al. 2014), which is also coupled to the LPJ vegetation model. The combined model set-up would allow us to better assess the effect of the Pinatubo eruption on climate, and to distinguish its effect on CH_4 emissions and chemistry from other drivers of CH_4 variability. Both shortwave and longwave radiation schemes in EC-Earth have been coupled to the TM5/M7 aerosol fields. The coupling to shortwave radiation is necessary to infer the effect of Pinatubo on temperatures, while the longwave absorption by sulfate particles is essential for accurately simulating the impact of the eruption on atmospheric dynamics (Aquila et al. 2012; Young et al. 1994). In previous studies the coupling to longwave radiation has been shown to be important for the transport of the Pinatubo sulfate aerosols to the Southern Hemisphere, which is also not well captured in our model using ERA-Interim wind fields. Efforts to couple the LPJ emissions to TM5 are underway, which will enable quantifying the contribution of the Pinatubo climate perturbation to changes in CH_4 emissions from wetlands and biogenic NMVOC emissions. To fully separate the impact of the Pinatubo eruption on CH_4 and OH from other drivers of CH_4 variability, the effect on stratospheric O_3 would have to be simulated interactively in the TM5-EC-Earth system. This would require incorporating a stratospheric O_3 chemistry scheme in TM5.

The present study could be extended to assess the impact of other past volcanic eruptions or of potential future geo-engineering options on CH_4 concentrations and

the oxidizing capacity of the atmosphere. We have shown in Chapter 5 that several studied drivers of CH_4 concentrations have contributed significantly to the evolution of the CH_4 burden in the atmosphere. We have also shown that the overall effect of large volcanic eruptions on CH_4 depends on a delicate balance between these drivers, and it is difficult to make predictions on the effect of other volcanic eruptions based on the Pinatubo eruption alone. For example, the impact of an eruption on stratospheric O_3 depends on the abundance of O_3 depleting substances in the stratosphere, as well as on the exact injection height of the volcanic SO_2. Therefore, to quantify the impact of other past volcanic eruptions on tropospheric chemistry, a coupled chemistry-climate model with stratospheric O_3 chemistry would be needed. The significant burden of O_3-depleting substances at the time of the Pinatubo eruption led to a considerable decrease in stratospheric O_3. However, stratospheric O_3 was shown be less sensitive to stratospheric sulfate under lower loadings of O_3-depleting substances, and O_3 columns were shown to increase after a large volcanic eruption under preindustrial levels of O_3-depleting substances (Tie and Brasseur 1995; Tilmes et al. 2012). In contrast to the Pinatubo eruption, other past volcanic eruptions most probably decreased tropospheric OH levels and CH_4 removal rate, since scattering aerosols, decreased temperature and humidity, and increased O_3 columns all lead to decreased UV levels and OH. However, CH_4 emissions also decrease in response to the temperature decrease after a large volcanic eruption. The overall effect on CH_4 concentrations is unclear, and would strongly depend on the sensitivity of CH_4 emissions to a climate perturbation, which is highly uncertain. Furthermore, high-latitude volcanic eruptions were shown to have a smaller and shorter impact on global climate compared to low-latitude eruptions (Schneider et al. 2009). Therefore, the effect of a volcanic eruption on OH and CH_4 would also depend on the latitude of the eruption.

In this thesis we aimed to contribute to a better understanding of the drivers of CH_4 budget changes by studying the period after the Pinatubo eruption. The fact that we were able to reproduce the magnitude of the CH_4 perturbation after the eruption shows that we have a good understanding of the most important processes, although uncertainties remain and have been identified in this study.

A further step to improving our understanding of the CH_4 budget would be investigating the long-term evolution of past CH_4 concentrations. In Chapter 3, a transient run of the column chemistry model was performed. By considering changes in anthropogenic emissions alone, we simulated the evolution of CH_4 concentrations between 1890 and 2005, within 50 ppb of the observations. This experiment could be repeated using a three-dimensional model, and including other processes that were found to be important in the current study. Such long-term simulations would further improve our knowledge of the drivers of CH_4 variations in the atmosphere and our predictive capabilities of future CH_4 concentrations.

BIBLIOGRAPHY

J. M. J. Aan de Brugh. *Aerosol processes relevant for the Netherlands*. Phd thesis, Wageningen University, 2013.

J. M. J. Aan de Brugh, M. Schaap, E. Vignati, F. Dentener, M. Kahnert, M. Sofiev, V. Huijnen, and M. C. Krol. The European aerosol budget in 2006. *Atmospheric Chemistry and Physics*, 11:1117–1139, 2011.

R. J. Andres and A. D. Kasgnoc. A time-averaged inventory of subaerial volcanic. *Journal of Geophysical Research*, 103:25,251–25,261, 1998.

N. G. Andronova, E. V. Rozanov, F. Yang, M. E. Schlesinger, and G. L. Stenchikov. Radiative forcing by volcanic aerosols from 1850 to 1994. *Journal of Geophysical Research*, 104: 16,807–16,826, 1999.

A. Ansmann, I. Mattis, U. Wandinger, F. Wagner, J. Reichardt, and T. Deshler. Evolution of the Pinatubo Aerosol: Raman Lidar Observations of Particle Optical Depth, Effective Radius, Mass, and Surface Area over Central Europe at 53.4N. *Journal of Atmospheric Sciences*, 54: 2630–2641, 1997.

A. Ansmann, F. Wagner, U. Wandinger, I. Mattis, U. Gorsdorf, H.-D. Dier, and J. Reichardt. Pinatubo aerosol and stratospheric ozone reduction: Observations over central Europe. *Journal of Geophysical Research*, 101:18,775–18,785, 1996.

V. Aquila, L. D. Oman, R. Stolarski, A. R. Douglass, and P. A. Newman. The Response of Ozone and Nitrogen Dioxide to the Eruption of Mt. Pinatubo at Southern and Northern Midlatitudes. *Journal of the Atmospheric Sciences*, 70:894–900, 2013.

V. Aquila, L. D. Oman, R. S. Stolarski, P. R. Colarco, and P. A. Newman. Dispersion of the volcanic sulfate cloud from a Mount Pinatubo-like eruption. *Journal of Geophysical Research*, 117: D06216, 2012.

J. E. Barnes and D. J. Hofmann. Lidar measurements of stratospheric aerosol over Mauna Loa Observatory. *Geophysical Research Letters*, 24:1923–1926, 1997.

J. J. Bauman, P. B. Russell, and P. Hamill. A stratospheric aerosol climatology from SAGE II and CLAES measurements: 2. Results and comparisons, 1984 - 1999. *Time*, 108:1984–1999, 2003.

C. B. Bautista. The Mount Pinatubo disaster and the people of Central Luzon. In *Fire and Mud: Eruptions and Lahars of Mount Pinatubo, Philippines*, pages 151–161. University of Washington Press, Philippine Institute of Volcanology and Seismology, 1996.

S. Bekki and K. S. Law. Sensitivity of the atmospheric CH4 growth rate to global temperature changes observed from 1980 to 1992. *Tellus*, 49B:409–416, 1997.

S. Bekki and J. A. Pyle. A two-dimensional modeling study of the volcanic eruption of Mount Pinatubo. *Journal of Geophysical Research*, 99:18,861 – 18,869, 1994.

S. Bekki, R. Toumi, and J. A. Pyle. Role of sulphur photochemistry in tropical ozone changes after the eruption of Mount Pinatubo. *Nature*, 362:331–333, 1993.

S. Bekki, K. S. Law, and J. A. Pyle. Effect of ozone depletion on atmospheric CH4 and CO concentrations. *Nature*, 371:595–597, 1994.

S. Bekki, J. A. Pyle, W. Zhong, R. Toumi, J. D. Haigh, and D. M. Pyle. The role of microphysical and chemical processes in prolonging the climate forcing of the Toba Eruption. *Geophysical Research Letters*, 23:2669–2672, 1996.

F. A. Bender, A. M. L. Ekman, and H. Rodhe. Response to the eruption of Mount Pinatubo in relation to climate sensitivity in the CMIP3 models. *Climate Dynamics*, 35:875–886, 2010.

K. Bogumil, J. Orphal, T. Homann, S. Voigt, P. Spietz, O. C. Fleischmann, A. Vogel, M. Hartmann, H. Kromminga, H. Bovensmann, J. Frerick, and J. P. Burrows. Measurements of molecular absorption spectra with the SCIAMACHY pre-flight model: instrument characterization and reference data for atmospheric remote-sensing in the 230-2380 nm region. *Journal of Photochemistry and Photobiology A: Chemistry*, 157:167–184, 2003.

P. Bousquet, D. A. Hauglustaine, P. Peylin, C. Carouge, and P. Ciais. Two decades of OH variability as inferred by an inversion of atmospheric transport and chemistry of methyl chloroform. *Atmospheric Chemistry and Physics*, 5:2635–2656, 2005.

P. Bousquet, P. Ciais, J. B. Miller, E. J. Dlugokencky, D. A. Hauglustaine, C. Prigent, G. R. Van der Werf, P. Peylin, E.-G. Brunke, C. Carouge, R. L. Langenfelds, J. Lathière, F. Papa, M. Ramonet, M. Schmidt, L. P. Steele, S. C. Tyler, and J. White. Contribution of anthropogenic and natural sources to atmospheric methane variability. *Nature*, 443:439–43, 2006.

C. R. Burnett and E. B. Burnett. Observational results on the vertical column abundance of atmospheric hydroxyl: Description of its seasonal behavior 1977–1982 and of the 1982 El Chichon Perturbation. *Journal of Geophysical Research: Atmospheres*, 89:9603–9611, 1984.

T. M. Butler, I. Simmonds, and P. J. Rayner. Mass balance inverse modelling of methane in the 1990s using a Chemistry Transport Model. *Atmospheric Chemistry and Physics*, 4:2561–2580, 2004.

C. D. Camp, M. S. Roulston, A. F. Haldemann, and Y. L. Yung. The sensitivity of tropospheric methane to the interannual variability in stratospheric ozone. *Chemosphere - Global Change Science*, 3:147–156, 2001.

K. S. Carslaw, S. L. Clegg, and P. Brimblecombe. A Thermodynamic Model of the System HCl-HNO3-H2SO4-H2O, Including Solubilities of HBr, from <200 to 328 K. *J. Phys. Chem.*, 99: 11557–11574, 1995.

M. P. Chipperfield, W. J. Randel, G. E. Bodeker, M. Dameris, V. E. Fioletov, R. R. Friedl, N. R. P. Harris, J. A. Logan, R. D. McPeters, N. J. Muthama, T. Peter, T. G. Shepherd, K. P. Shine, S. Solomon, L. W. Thomason, and J. M. Zawodny. Global Ozone: Past and Future. In *Scientific Assessment of Ozone Depletion: 2002, Global Ozone Research and Monitoring Project–Report No. 47*, chapter 4. Geneva, 2003.

P. Ciais, C. Sabine, G. Bala, L. Bopp, V. Brovkin, J. Canadell, A. Chhabra, R. DeFries, J. Galloway, M. Heimann, C. Jones, C. L. Quéré, R. Myneni, S. Piao, and P. Thornton. Carbon and Other

Biogeochemical Cycles. In T. Stocker, D. Qin, G.-K. Plattner, M. Tignor, S. Allen, J. Boschung, A. Nauels, Y. Xia, V. Bex, and P. Midgley, editors, *Climate Change 2013: The Physical Science Basis. Contribution of Working Group I to the Fifth Assessment Report of the Intergovernmental Panel on Climate Change*, pages 465–570. Cambridge University Press, Cambridge, United Kingdom and New York, NY, USA, 2013.

S. B. Dalsøren and I. S. A. Isaksen. CTM study of changes in tropospheric hydroxyl distribution 1990–2001 and its impact on methane. *Geophysical Research Letters*, 33:L23811, 2006.

D. P. Dee, S. M. Uppala, A. J. Simmons, P. Berrisford, P. Poli, S. Kobayashi, U. Andrae, M. A. Balmaseda, G. Balsamo, P. Bauer, P. Bechtold, A. C. M. Beljaars, L. V. D. Berg, J. Bidlot, N. Bormann, C. Delsol, R. Dragani, M. Fuentes, A. J. Geer, L. Haimberger, S. B. Healy, H. Hersbach, E. V. Holm, L. Isaksen, and P. Kallberg. The ERA-Interim reanalysis: configuration and performance of the data assimilation system. *Quarterly Journal of the Royal Meteorological Society*, 137:553–597, 2011.

K. Denman, G. Brasseur, A. Chidthaisong, P. Ciais, P. Cox, R. Dickinson, D. Hauglustaine, C. Heinze, E. Holland, D. Jacob, U. Lohmann, S. Ramachandran, P. d. S. Dias, S. Wofsy, and X. Zhang. Couplings Between Changes in the Climate System and Biogeochemistry. In: Climate Change 2007: The Physical Science Basis. Contribution of Working Group I to the Fourth Assessment Report of the Intergovernmental Panel on Climate Change. Cambridge University Press, Cambridge, United Kingdom and New York, NY, USA, 2007.

F. Dentener, W. Peters, M. Krol, M. V. Weele, and P. Bergamaschi. Interannual variability and trend of CH4 lifetime as a measure for OH changes in the 1979–1993 time period. *Time*, 108, 2003.

T. Deshler. A review of global stratospheric aerosol: Measurements, importance, life cycle, and local stratospheric aerosol. *Atmospheric Research*, 90:223–232, 2008.

T. Deshler, B. J. Johnson, and W. R. Rozier. Balloonborne measurements of Pinatubo aerosol during 1991 and 1992 at 41N: vertical profiles, size distribution, and volatility. *Geophysical Research Letters*, 20:1435–1438, 1993.

A. E. Dessler, M. R. Schoeberl, T. Wang, S. M. Davis, K. H. Rosenlof, and J.-P. Vernier. Journal of Geophysical Research : Atmospheres. *Journal of Geophysical Research: Atmospheres*, 119: 12,588–12,598, 2014.

S. S. Dhomse, K. M. Emmerson, G. W. Mann, N. Bellouin, K. S. Carslaw, M. P. Chipperfield, R. Hommel, N. L. Abraham, P. Telford, P. Braesicke, M. Dalvi, C. E. Johnson, F. O'Connor, O. Morgenstern, J. a. Pyle, T. Deshler, J. M. Zawodny, and L. W. Thomason. Aerosol microphysics simulations of the Mt. Pinatubo eruption with the UKCA composition-climate model. *Atmospheric Chemistry and Physics Discussions*, 14:2799–2855, 2014.

R. R. Dickerson, S. Kondragunta, G. Stenchikov, K. L. Civerolo, B. G. Doddridge, and B. N. Holben. The Impact of Aerosols on Solar Ultraviolet Radiation and Photochemical Smog. *Science*, 278:827–30, 1997.

E. J. Dlugokencky, K. A. Masaire, P. M. Lang, P. P. Tans, L. P. Steele, and E. G. Nisbet. A dramatic decrease in the growth rate of atmospheric methane in the northern hemisphere during 1992. *Geophysical Research Letters*, 21:45–48, 1994.

E. J. Dlugokencky, E. G. Dutton, P. C. Novelli, P. P. Tans, K. A. Masarie, K. O. Lantz, and S. Madronich. Changes in CH4 and CO growth rates after the eruption of Mt. Pinatubo and their link with changes in tropical tropospheric UV flux. *Geophysical Research Letters*, 23:2761–2764, 1996.

E. J. Dlugokencky, S. Houweling, L. Bruhwiler, K. A. Masarie, P. M. Lang, J. B. Miller, and P. P. Tans. Atmospheric methane levels off: Temporary pause or a new steady- state? *Geophysical Research Letters*, 30:1992, 2003.

E. J. Dlugokencky, E. G. Nisbet, R. Fisher, and D. Lowry. Global atmospheric methane: budget, changes and dangers. *Phil. Trans. R. Soc. A*, 369:2058–2072, 2011.

S. D. Doiron, G. J. S. Bluth, C. C. Schnetzler, A. J. Krueger, and L. S. Walter. Transport of Cerro Hudson SO2 clouds. *Eos, Transactions American Geophysical Union*, 72:489–498, 1991.

P. Dunfield, R. Knowles, R. Dumont, and T. R. Moore. Methane production and consumption in temperate and subarctic peat soils: Response to temperature and pH. *Soil Biology and Biochemistry*, 25:321–326, 1993.

E. G. Dutton and J. R. Christy. Solar radiative forcing at selected locations and evidence for global lower tropospheric cooling following the eruptions of El Chichón and Pinatubo. *Geophysical Research Letters*, 19:2313–2316, 1992.

E. G. Dutton, P. Reddy, S. Ryan, and J. J. DeLuisi. Features and effects of aerosol optical depth observed at Mauna Loa, Hawaii: 1982–1992. *Journal of Geophysical Research*, 99:8295–8306, 1994.

L. Elterman. UV, Visible and IR Attenuation for Altitudes to 50 km. *Environmental Research Papers*, 285:AFCRL–68–0153, 1968.

J. M. English, O. B. Toon, and M. J. Mills. Microphysical simulations of large volcanic eruptions: Pinatubo and Toba. *Journal of Geophysical Research: Atmospheres*, 118:1880–1895, 2013.

D. M. Etheridge, L. P. Steele, R. J. Francey, and R. L. Langenfelds. Atmospheric methane between 1000 A. D. and present: Evidence of anthropogenic emissions and climatic variability. *Journal of Geophysical Research*, 103:15,979–15,993, 1998.

European Commission and Joint Research Centre (JRC)/Netherlands Environmental Assessment Agency (PBL). Emission Database for Global Atmospheric Research (EDGAR), release version 4.1 and 4.2, 2011.

M. Free and J. K. Angell. Effect of volcanoes on the vertical temperature profile in radiosonde data. *Journal of Geophysical Research*, 107:4101, 2002.

J. S. Fuglestvedt, J. E. Johnson, and I. S. A. Isaksen. Effects of reductions in stratospheric ozone on tropospheric chemistry through changes in photolysis rates. *Tellus*, 46B:172–192, 1994.

V. Gauci and S. J. Chapman. Simultaneous inhibition of CH4 efflux and stimulation of sulphate reduction in peat subject to simulated acid rain. *Soil Biology and Biochemistry*, 38:3506–3510, 2006.

V. Gauci, D. Fowler, S. J. Chapman, and N. B. Dise. Sulfate deposition and temperature controls on methane emission and sulfur forms in peat. *October*, pages 141–162, 2004.

V. Gauci, S. Blake, D. S. Stevenson, and E. J. Highwood. Halving of the northern wetland CH4 source by a large Icelandic volcanic eruption. *Journal of Geophysical Research*, 113: 1–8, 2008.

A. Gettelman, P. Hoor, L. L. Pan, W. J. Randel, M. I. Hegglin, and T. Birner. THE EXTRATROPICAL UPPER TROPOSPHERE AND LOWER STRATOSPHERE. *Reviews of Geophysics*, 49: RG3003, 2011.

GLOBALVIEW-CH4. Cooperative Atmospheric Data Integration Project - Methane. CD-ROM, NOAA ESRL, Boulder, Colorado [Also available on Internet via anonymous FTP to ftp://ftp.cmdl.noaa.gov, Path: ccg/ch4/GLOBALVIEW], 2009.

H. F. Graf, I. Kirchner, and I. Schult. Modelling Mt. Pinatubo Climate Effects. In G. Fiocco and D. Dua, editors, *NATO-ASI Series, Vol 142, The Mount Pinatubo Eruption*, pages 219–231. 1996.

A. Grant, A. T. Archibald, M. C. Cooke, and D. E. Shallcross. Modelling the oxidation of seventeen volatile organic compounds to track yields of CO and CO2. *Atmospheric Environment*, 44:3797–3804, 2010.

J.-U. Grooß and J. Russell III. Technical note: A stratospheric climatology for O3, H2O, CH4, NOx, HCl and HF derived from HALOE measurements. *Atmospheric Chemistry and Physics*, 5:2797–2807, 2005.

A. B. Guenther, P. R. Zimmerman, P. C. Harley, R. K. Monson, and R. Fall. Isoprene and Monoterpene Emission Rate Variability: Model Evaluations and Sensitivity Analyses. *Journal of Geophysical Research*, 98:12,609–12,617, 1993.

S. Guo, G. J. S. Bluth, W. I. Rose, I. M. Watson, and A. J. Prata. Re-evaluation of SO2 release of the 15 June 1991 Pinatubo eruption using ultraviolet and infrared satellite sensors. *Geochemistry Geophysics Geosystems*, 5, 2004a.

S. Guo, W. I. Rose, G. J. S. Bluth, and I. M. Watson. Particles in the great Pinatubo volcanic cloud of June 1991: The role of ice. *Geochemistry Geophysics Geosystems*, 5, 2004b.

J. Hansen, M. Sato, R. Ruedy, L. Nazarenko, A. Lacis, G. A. Schmidt, G. Russell, I. Aleinov, M. Bauer, N. Bell, B. Cairns, V. Canuto, M. Chandler, Y. Cheng, A. Del Genio, G. Faluvegi, E. Fleming, A. Friend, T. Hall, C. Jackman, M. Kelley, N. Kiang, D. Koch, J. Lean, J. Lerner, K. Lo, S. Menon, R. Miller, P. Minnis, T. Novakov, V. Oinas, J. Perlwitz, J. Perlwitz, D. Rind, A. Romanou, D. Shindell, P. Stone, S. Sun, N. Tausnev, D. Thresher, B. Wielicki, T. Wong, M. Yao, and S. Zhang. Efficacy of climate forcings. *Journal of Geophysical Research*, 110: D18104, 2005.

J. Hansen, R. Ruedy, M. Sato, and K. Lo. Global surface temperature change. *Reviews of Geophysics*, 48:RG4004, 2010.

S. He and G. R. Carmichael. Sensitivity of photolysis rates and ozone production in the troposphere to aerosol properties. *Journal of Geophysical Research*, 104:26,307–26,324, 1999.

E. L. Hodson, B. Poulter, N. E. Zimmermann, C. Prigent, and J. O. Kaplan. The El Niño–Southern Oscillation and wetland methane interannual variability. *Geophysical Research Letters*, 38:3–6, 2011.

C. D. Holmes, M. J. Prather, O. A. Sø vde, and G. Myhre. Future methane, hydroxyl, and their uncertainties: key climate and emission parameters for future predictions. *Atmospheric Chemistry and Physics*, 13:285–302, 2013.

S. Houweling, F. Dentener, and J. Lelieveld. The impact of nonmethane hydrocarbon compounds on tropospheric photochemistry radical. *Journal of Geophysical Research*, 103: 10,673–10,696, 1998.

V. Huijnen, J. Williams, M. van Weele, T. van Noije, M. Krol, F. Dentener, A. Segers, S. Houweling, W. Peters, J. de Laat, F. Boersma, P. Bergamaschi, P. van Velthoven, P. Le Sager, H. Eskes, F. Alkemade, R. Scheele, P. Nédélec, and H.-W. Pätz. The global chemistry transport model TM5: description and evaluation of the tropospheric chemistry version 3.0. *Geoscientific Model Development*, 3:445–473, 2010.

V. Huijnen, J. E. Williams, and J. Flemming. Modeling global impacts of heterogeneous loss of HO2 on cloud droplets, ice particles and aerosols. *Atmospheric Chemistry and Physics Discussions*, 14:8575–8632, 2014.

A. Jayaraman, S. Ramachandran, Y. B. Acharya, and B. H. Subbaraya. Pinatubo volcanic aerosol layer decay observed at Ahrnedabad (23N), India, using neodymium:yttrium/aluminium/garnet backscatter lidar. *Journal of Geophysical Research*, 100: 23,209–23,214, 1995.

D. E. Kinnison, K. E. Grant, P. S. Connell, D. A. Rotman, and D. J. Wuebbles. The chemical and radiative effects of the Mount Pinatubo eruption. *Journal of Geophysical Research*, 99: 25,705–25,731, 1994.

S. Kirschke, P. Bousquet, P. Ciais, M. Saunois, J. G. Canadell, E. J. Dlugokencky, P. Bergamaschi, D. Bergmann, D. R. Blake, L. Bruhwiler, P. Cameron-Smith, S. Castaldi, F. Chevallier, L. Feng, A. Fraser, M. Heimann, E. L. Hodson, S. Houweling, B. Josse, P. J. Fraser, P. B. Krummel, J.-F. Lamarque, R. L. Langenfelds, C. Le Quéré, V. Naik, S. O'Doherty, P. I. Palmer, I. Pison, D. Plummer, B. Poulter, R. G. Prinn, M. Rigby, B. Ringeval, M. Santini, M. Schmidt, D. T. Shindell, I. J. Simpson, R. Spahni, L. P. Steele, S. a. Strode, K. Sudo, S. Szopa, G. R. van der Werf, A. Voulgarakis, M. van Weele, R. F. Weiss, J. E. Williams, and G. Zeng. Three decades of global methane sources and sinks. *Nature Geoscience*, 6:813–823, 2013.

H. Kokkola, R. Hommel, J. Kazil, U. Niemeier, A.-I. Partanen, J. Feichter, and C. Timmreck. Aerosol microphysics modules in the framework of the ECHAM5 climate model–intercomparison under stratospheric conditions. *Geoscientific Model Development*, 2:97–112, 2009.

M. Krol and J. Lelieveld. Can the variability in tropospheric OH be deduced from measurements of 1,1,1-trichloroethane (methyl chloroform)? *Journal of Geophysical Research*, 108: 4125, 2003.

M. C. Krol and M. Van Weele. Implications of variations in photodissociation rates for global tropospheric chemistry. *Atmospheric Environment*, 31:1257–1273, 1997.

J.-F. Lamarque, T. C. Bond, V. Eyring, C. Granier, a. Heil, Z. Klimont, D. Lee, C. Liousse, a. Mieville, B. Owen, M. G. Schultz, D. Shindell, S. J. Smith, E. Stehfest, J. Van Aardenne, O. R. Cooper, M. Kainuma, N. Mahowald, J. R. McConnell, V. Naik, K. Riahi, and D. P. van Vuuren. Historical (1850–2000) gridded anthropogenic and biomass burning emissions of reactive gases and aerosols: methodology and application. *Atmospheric Chemistry and Physics*, 10:7017–7039, 2010.

K. S. Law and E. G. Nisbet. Sensitivity of the CH4 growth rate to changes in CH4 emissions from natural gas and coal. *Journal of Geophysical Research*, 101:14,387–14,397, 1996.

M. G. Lawrence, P. Joeckel, and R. von Kuhlmann. What does the global mean OH concentration tell us? *Atmospheric Chemistry and Physics*, 1:37–49, 2001.

J. Lelieveld, W. Peters, F. J. Dentener, and M. C. Krol. Stability of tropospheric hydroxyl chemistry. *Journal of Geophysical Research*, 107:D23, 4715, 2002.

H. Levy. Normal Atmosphere: Large Radical and Formaldehyde Concentrations Predicted. *Science*, 173:141–143, 1971.

H. Liao, Y. L. Yung, and J. H. Seinfeld. Effects of aerosols on tropospheric photolysis rates in clear and cloudy atmospheres. *Journal of Geophysical Research*, 104:23,697–23,707, 1999.

C. S. Long and L. L. Stowe. Using the NOAA/AVHRR to study stratospheric aerosol optical thicknesses following the Mt. Pinatubo Eruption. *Geophysical Research Letters*, 21:2215–2218, 1994.

L. Loulergue, A. Schilt, R. Spahni, V. Masson-Delmotte, T. Blunier, B. Lemieux, J.-M. Barnola, D. Raynaud, T. F. Stocker, and J. Chappellaz. Orbital and millennial-scale features of atmospheric CH4 over the past 800,000[thinsp]years. *Nature*, 453:383–386, 2008.

D. C. Lowe, M. R. Manning, G. W. Brailsford, and A. M. Bromley. The 1991-1992 atmospheric methane anomaly: Southern hemisphere 13C decrease and growth rate fluctuations. *Geophys. Res. Lett.*, 24:857–860, 1997.

S. Madronich. UV radiation in the natural and perturbed atmosphere. In M. Tevini, editor, *Einvironmental effects of UV (Ultraviolet) radiation*, pages 17 – 69. Lewis Publisher, Boca Raton, 1993.

M. P. McCormick, L. W. Thomason, and C. R. Trepte. Atmospheric effects of the Mt. Pinatubo eruption. *Nature*, 373:399–404, 1995.

J. R. Melton, R. Wania, E. L. Hodson, B. Poulter, B. Ringeval, R. Spahni, T. Bohn, C. a. Avis, D. J. Beerling, G. Chen, a. V. Eliseev, S. N. Denisov, P. O. Hopcroft, D. P. Lettenmaier, W. J. Riley, J. S. Singarayer, Z. M. Subin, H. Tian, S. Zürcher, V. Brovkin, P. M. van Bodegom, T. Kleinen, Z. C. Yu, and J. O. Kaplan. Present state of global wetland extent and wetland methane modelling: conclusions from a model inter-comparison project (WETCHIMP). *Biogeosciences*, 10:753–788, 2013.

L. M. Mercado, N. Bellouin, S. Sitch, O. Boucher, C. Huntingford, M. Wild, and P. M. Cox. Impact of changes in diffuse radiation on the global land carbon sink. *Nature*, 458:1014–1018, 2009.

R. A. Mercado, J. B. T. Lacsamana, and G. L. Pineda. Socioeconomic impacts of the Mount Pinatubo eruption. In *Fire and mud, eruptions and lahars of Mount Pinatubo, Philippines*, pages 1063–1069. University of Washington Press, Philippine Institute of Volcanology and Seismology, 1996.

S. Metzger, F. Dentener, S. Pandis, and J. Lelieveld. Gas/aerosol partitioning: 1. A computationally efficient model. *Journal of Geophysical Research: Atmospheres*, 107:ACH 16–1–ACH 16–24, 2002.

G. Monteil, S. Houweling, E. J. Dlugockenky, G. Maenhout, B. H. Vaughn, J. W. C. White, and T. Rockmann. Interpreting methane variations in the past two decades using measurements of CH4 mixing ratio and isotopic composition. *Atmospheric Chemistry and Physics*, 11:9141–9153, 2011.

S. A. Montzka, E. J. Dlugokencky, and J. H. Butler. Non-CO2 greenhouse gases and climate change. *Nature*, 476:43–50, 2011a.

S. A. Montzka, M. Krol, E. Dlugokencky, B. Hall, P. Jockel, and J. Lelieveld. Small Interannual Variability of Global Atmospheric Hydroxyl. *Science*, 331:67–69, 2011b.

G. Myhre, D. Shindell, F.-M. Bréon, W. Collins, J. Fuglestvedt, J. Huang, D. Koch, J.-F. Lamarque, D. Lee, B. Mendoza, T. Nakajima, A. Robock, G. Stephens, T. Takemura, and H. Zhang. Anthropogenic and Natural Radiative Forcing. In T. Stocker, D. Qin, G.-K. Plattner, M. Tignor, S. Allen, J. Boschung, A. Nauels, Y. Xia, V. Bex, and P. Midgley, editors, *Climate Change 2013: The Physical Science Basis. Contribution of Working Group I to the Fifth Assessment Report of the Intergovernmental Panel on Climate Change*, pages 659–740. Cambridge University Press, Cambridge, United Kingdom and New York, NY, USA, 2013.

T. Nagai, B. Liley, T. Sakai, T. Shibata, and O. Uchino. Post-Pinatubo Evolution and Subsequent Trend of the Stratospheric Aerosol Layer Observed by Mid-Latitude Lidars in Both Hemispheres. *Sola*, 6:69–72, 2010.

V. Naik, a. Voulgarakis, a. M. Fiore, L. W. Horowitz, J.-F. Lamarque, M. Lin, M. J. Prather, P. J. Young, D. Bergmann, P. J. Cameron-Smith, I. Cionni, W. J. Collins, S. B. Dalsøren, R. Doherty, V. Eyring, G. Faluvegi, G. a. Folberth, B. Josse, Y. H. Lee, I. a. MacKenzie, T. Nagashima, T. P. C. van Noije, D. a. Plummer, M. Righi, S. T. Rumbold, R. Skeie, D. T. Shindell, D. S. Stevenson, S. Strode, K. Sudo, S. Szopa, and G. Zeng. Preindustrial to present-day changes in tropospheric hydroxyl radical and methane lifetime from the Atmospheric Chemistry and Climate Model Intercomparison Project (ACCMIP). *Atmospheric Chemistry and Physics*, 13: 5277–5298, 2013.

C. G. Newhall, A. S. Daag, F. G. Delfin, R. P. Hoblitt, J. McGeehin, J. S. Pallister, M. T. Regalado, M. Rubin, B. S. Tubianosa, and R. A. Tamayo. Eruptive history of Mount Pinatubo. In *Fire and Mud: Eruptions and Lahars of Mount Pinatubo, Philippines*, pages 165–195. University of Washington Press, Philippine Institute of Volcanology and Seismology, 1996.

U. Niemeier, C. Timmreck, H.-F. Graf, S. Kinne, S. Rast, and S. Self. Initial fate of fine ash and sulfur from large volcanic eruptions. *Atmospheric Chemistry and Physics*, 9:9043–9057, 2009.

T. Ohara, H. Akimoto, J. Kurokawa, N. Horii, K. Yamaji, X. Yan, and T. Hayasaka. An Asian emission inventory of anthropogenic emission sources for the period 1980–2020. *Atmospheric Chemistry and Physics*, 7:4419–4444, 2007.

E. K. Oikonomou and A. O'Neill. Evaluation of ozone and water vapor fields from the ECMWF reanalysis ERA-40 during 1991–1999 in comparison with UARS satellite and MOZAIC aircraft observations. *Journal of Geophysical Research*, 111:D14109, 2006.

P. K. Patra, M. C. Krol, S. A. Montzka, T. Arnold, E. L. Atlas, B. R. Lintner, B. B. Stephens, B. Xiang, J. W. Elkins, P. J. Fraser, A. Ghosh, E. J. Hintsa, D. F. Hurst, K. Ishijima, P. B. Krummel, B. R. Miller, K. Miyazaki, F. L. Moore, S. O'Doherty, R. G. Prinn, L. P. Steele, M. Takigawa, H. J. Wang, R. F. Weiss, S. C. Wofsy, and D. Young. Observational evidence for interhemispheric hydroxyl-radical parity. *Nature*, 513:219–223, 2014.

J. P. Pinto, R. P. Turco, and O. B. Toon. Self-limiting physical and chemical effects in volcanic eruption clouds. *Journal of Geophysical Research: Atmospheres*, 94:11165–11174, 1989.

I. Pison, B. Ringeval, P. Bousquet, C. Prigent, and F. Papa. Stable atmospheric methane in the 2000s: key-role of emissions from natural wetlands. *Atmospheric Chemistry and Physics*, 13: 11609–11623, 2013.

U. Pöschl, R. von Kuhlmann, N. Poisson, and P. Crutzen. Development and Intercomparison of Condensed Isoprene Oxidation Mechanisms for Global Atmospheric Modeling. *Journal of Atmospheric Chemistry*, 37:29–52, 2000.

M. Prather, D. Ehhalt, F. Dentener, R. Derwent, E. Dlugokencky, E. Holland, I. S. A. Isaksen, J. Katima, V. Kirchhoff, P. Matson, P. M. Midgley, and M. Wang. Atmospheric Chemistry and Greenhouse Gases. In *Climate Change 2001: The Scientific Basis, Contribution of Working Group I to the Third Assessment Report of the Intergovernmental Panel on Climate Change*, pages 239–288. Cambridge Univ. Press, New York, 2001.

M. J. Prather. Numerical advection by conservation of second-order moments. *Journal of Geophysical Research: Atmospheres*, 91:6671–6681, 1986.

M. J. Prather, C. D. Holmes, and J. Hsu. Reactive greenhouse gas scenarios: Systematic exploration of uncertainties and the role of atmospheric chemistry. *Geophysical Research Letters*, 39:L098, 2012.

R. G. Prinn, J. Huang, R. F. Weiss, D. M. Cunnold, P. J. Fraser, P. G. Simmonds, A. McCulloch, C. Harth, P. Salameh, S. O'Doherty, R. H. J. Wang, L. Porter, and B. R. Miller. Evidence for Substantial Variations of Atmospheric Hydroxyl Radicals in the Past Two Decades. *Science*, 292:1882–1888, 2001.

R. G. Prinn, J. Huang, R. F. Weiss, D. M. Cunnold, P. J. Fraser, P. G. Simmonds, A. McCulloch, C. Harth, S. Reimann, P. Salameh, S. O'Doherty, R. H. J. Wang, L. W. Porter, B. R. Miller, and P. B. Krummel. Evidence for variability of atmospheric hydroxyl radicals over the past quarter century. *Geophysical Research Letters*, 32:L07809, 2005.

P. Quay, J. Stutsman, D. Wilbur, A. Snover, E. Dlugokencky, and T. Brown. The isotopic composition of atmospheric methane. *Global Biogeochemical Cycles*, 13:445–461, 1999.

J. W. Randel, F. Wu, J. Russell III, J. Waters, and L. Froidevaux. Ozone and temperature changes in the stratosphere following the eruption of Mount Pinatubo. *Geophysical Research Letters*, 100:16,753 – 16,764, 1995.

W. Read, L. Froidevaux, and J. W. Waters. Microwave limb sounder measurement of stratospheric SO2 from the Mt. Pinatubo volcano. *Geophysical Research Letters*, 20:1299–1302, 1993.

J. Reuder and H. Schwander. Aerosol effects on UV radiation in nonurban regions. *Journal of Geophysical Research*, 104:4065–4077, 1999.

B. Ringeval, N. de Noblet-Ducoudré, P. Ciais, P. Bousquet, C. Prigent, F. Papa, and W. B. Rossow. An attempt to quantify the impact of changes in wetland extent on methane emissions on the seasonal and interannual time scales. *Global Biogeochemical Cycles*, 24:GB2003, 2010.

F. Rohrer, K. Lu, A. Hofzumahaus, B. Bohn, T. Brauers, C.-C. Chang, H. Fuchs, R. Haseler, F. Holland, M. Hu, K. Kita, Y. Kondo, X. Li, S. Lou, A. Oebel, M. Shao, L. Zeng, T. Zhu, Y. Zhang, and A. Wahner. Maximum efficiency in the hydroxyl-radical-based self-cleansing of the troposphere. *Nature Geosci*, 7:559–563, 2014.

G. L. Russell and J. A. Lerner. A New Finite-Differencing Scheme for the Tracer Transport Equation. *Journal of Applied Meteorology*, 20:1483–1498, 1981.

P. B. Russell, J. M. Livingston, R. F. Pueschel, J. J. Bauman, J. B. Pollack, S. L. Brooks, P. Hamill, L. W. Thomason, L. L. Stowe, T. Deshler, E. G. Dutton, and R. W. Bergstrom. Global to microscale evolution of the Pinatubo volcanic aerosol derived from diverse measurements and analyses. *Journal of Geophysical Research*, 101:18,745 – 18,763, 1996.

S. P. Sander, R. R. Friedl, J. R. Barker, D. M. Golden, M. J. Kurylo, P. H. Wine, J. P. D. Abbatt, J. B. Burkholder, C. E. Kolb, G. K. Moortgat, R. E. Huie, and V. L. Orkin. Chemical Kinetics and Photochemical Data for Use in Atmospheric Studies. Jet Propulsation Laboratory, NASA, Pasadena, California, 2011.

B. D. Santer, T. M. L. Wigley, C. Doutriaux, J. S. Boyle, J. E. Hansen, P. D. Jones, G. A. Meehl, E. Roeckner, S. Sengupta, and K. E. Taylor. Accounting for the effects of volcanoes and ENSO in comparisons of modeled and observed temperature trends. *Journal of Geophysical Research*, 106:28,033–28,059, 2001.

S. M. Schauffler and J. S. Daniel. On the effects of stratospheric circulation changes on trace gas trends. *Journal of Geophysical Research*, 99:25,747–25,754, 1994.

D. P. Schneider, C. M. Ammann, B. L. Otto-Bliesner, and D. S. Kaufman. Climate response to large, high-latitude and low-latitude volcanic eruptions in the Community Climate System Model. *Journal of Geophysical Research: Atmospheres*, 114:D15101, 2009.

M. G. Schultz, A. Heil, J. J. Hoelzemann, A. Spessa, K. Thonicke, J. G. Goldammer, A. C. Held, J. M. C. Pereira, and M. van het Bolscher. Global wildland fire emissions from 1960 to 2000. *Global Biogeochemical Cycles*, 22:GB2002, 2008.

W. E. Scott, R. P. Hoblitt, R. C. Torres, S. Self, M. M. L. Martinez, and T. Nillos. Pyroclastic flows of the June 15, 1991, climactic eruption of Mount Pinatubo. In *Fire and mud: Eruptions and lahars of Mount Pinatubo, Philippines*, pages 545–570. University of Washington Press,

Philippine Institute of Volcanology and Seismology, 1996.

J.-X. Sheng, D. K. Weisenstein, B.-P. Luo, E. Rozanov, F. Arfeuille, and T. Peter. A perturbed parameter model ensemble to investigate 1991 Mt Pinatubo's initial sulfur mass emission. *Atmospheric Chemistry and Physics Discussions*, 15:4601–4625, 2015.

T. G. Shepherd, D. A. Plummer, J. F. Scinocca, M. I. Hegglin, V. E. Fioletov, M. C. Reader, E. Remsberg, T. von Clarmann, and H. J. Wang. Reconciliation of halogen-induced ozone loss with the total-column ozone record. *Nature Geosci*, 7:443–449, 2014.

D. T. Shindell, G. Faluvegi, D. S. Stevenson, M. C. Krol, L. K. Emmons, J.-F. Lamarque, G. Pétron, F. J. Dentener, K. Ellingsen, M. G. Schultz, O. Wild, M. Amann, C. S. Atherton, D. J. Bergmann, I. Bey, T. Butler, J. Cofala, W. J. Collins, R. G. Derwent, R. M. Doherty, J. Drevet, H. J. Eskes, A. M. Fiore, M. Gauss, D. A. Hauglustaine, L. W. Horowitz, I. S. A. Isaksen, M. G. Lawrence, V. Montanaro, J.-F. Müller, G. Pitari, M. J. Prather, J. A. Pyle, S. Rast, J. M. Rodriguez, M. G. Sanderson, N. H. Savage, S. E. Strahan, K. Sudo, S. Szopa, N. Unger, T. P. C. van Noije, and G. Zeng. Multimodel simulations of carbon monoxide: Comparison with observations and projected near-future changes. *Journal of Geophysical Research*, 111:D19306, 2006.

K. Sindelarova, C. Granier, I. Bouarar, A. Guenther, S. Tilmes, T. Stavrakou, J.-F. Müller, U. Kuhn, P. Stefani, and W. Knorr. Global dataset of biogenic VOC emissions calculated by the MEGAN model over the last 30 years. *Atmos. Chem. Phys. Discuss.*, 14:10725–10788, 2014.

B. J. Soden, R. T. Wetherald, G. L. Stenchikov, and A. Robock. Global Cooling After the Eruption of Mount Pinatubo: A Test of Climate Feedback by Water Vapor. *Science*, 296, 2002.

R. Spahni, R. Wania, L. Neef, M. van Weele, I. Pison, P. Bousquet, C. Frankenberg, P. N. Foster, F. Joos, I. C. Prentice, and P. van Velthoven. Constraining global methane emissions and uptake by ecosystems. *Biogeosciences*, 8:1643–1665, 2011.

R. W. Spencer and J. R. Christy. Precision Lower Stratospheric Temperature Monitoring with the MSU: Technique, Validation, and Results 1979–1991. *Journal of Climate*, 6:1194–1204, 1993.

G. L. Stenchikov, I. Kirchner, A. Robock, H.-F. Graf, J. C. Antuña, R. G. Grainger, A. Lambert, and L. Thomason. Radiative forcing from the 1991 Mount Pinatubo volcanic eruption. *Journal of Geophysical Research*, 103:13837–13857, 1998.

D. S. Stevenson, F. J. Dentener, M. G. Schultz, K. Ellingsen, T. P. C. van Noije, O. Wild, G. Zeng, M. Amann, C. S. Atherton, N. Bell, D. J. Bergmann, I. Bey, T. Butler, J. Cofala, W. J. Collins, R. G. Derwent, R. M. Doherty, J. Drevet, H. J. Eskes, A. M. Fiore, M. Gauss, D. A. Hauglustaine, L. W. Horowitz, I. S. A. Isaksen, M. C. Krol, J.-F. Lamarque, M. G. Lawrence, V. Montanaro, J.-F. Müller, G. Pitari, M. J. Prather, J. A. Pyle, S. Rast, J. M. Rodriguez, M. G. Sanderson, N. H. Savage, D. T. Shindell, S. E. Strahan, K. Sudo, and S. Szopa. Multimodel ensemble simulations of present-day and near-future tropospheric ozone. *Journal of Geophysical Research*, 111:D08301, 2006.

D. Stone, M. J. Evans, P. M. Edwards, R. Commane, T. Ingham, a. R. Rickard, D. M. Brookes, J. Hopkins, R. J. Leigh, a. C. Lewis, P. S. Monks, D. Oram, C. E. Reeves, D. Stewart, and D. E. Heard. Isoprene oxidation mechanisms: measurements and modelling of OH and HO2 over

a South-East Asian tropical rainforest during the OP3 field campaign. *Atmospheric Chemistry and Physics*, 11:6749–6771, 2011.

P. Telford, P. Braesicke, O. Morgenstern, and J. Pyle. Reassessment of causes of ozone column variability following the eruption of Mount Pinatubo using a nudged CCM. *Atmospheric Chemistry and Physics Discussions*, 9:5423–5446, 2009.

P. J. Telford, J. Lathiere, N. L. Abraham, A. T. Archibald, P. Braesicke, C. E. Johnson, O. Morgenstern, F. M. O'Connor, R. C. Pike, O. Wild, P. J. Young, C. N. Hewitt, and J. Pyle. Effects of climate-induced changes in isoprene emissions after the eruption of Mount Pinatubo. *Atmospheric Chemistry and Physics*, pages 7117–7125, 2010.

L. W. Thomason, L. R. Poole, and T. Deshler. A Global Climatology Of Stratospheric Aerosol Surface Area Density As Deduced From Stratospheric Aerosol and Gas Experiment II measurements: 1984–1994. *Journal of Geophysical Research*, 102:8967–8976, 1997.

L. W. Thomason, S. P. Burton, B.-P. Luo, and T. Peter. SAGE II measurements of stratospheric aerosol properties at non-volcanic levels. *Atmospheric Chemistry and Physics*, 8:983–995, 2008.

L. Thomason and T. Peter (Eds). SPARC: Assessment of Stratospheric Aerosol Properties (ASAP), SPARC Report No. 4. WCRP-124, WMO-No. 1295, 2006.

K. W. Thoning and P. P. Tans. Atmospheric Carbon Dioxide at Mauna Loa Observatory 2. Analysis of the NOAA GMCC Data, 1974-1985. *Journal of Geophysical Research*, 94:8549–8565, 1989.

X. Tie and G. Brasseur. The response of stratospheric ozone to volcanic eruptions: Sensitivity to atmospheric chlorine loading. *Geophysical Research Letters*, 22:3035–3038, 1995.

X. Tie, G. P. Brasseur, B. Briegleb, and C. Granier. Two-dimensional simulation of Pinatubo aerosol and its effect on stratospheric ozone. *Journal of Geophysical Research: Atmospheres*, 99:20545–20562, 1994.

M. Tiedtke. A comprehensive mass flux scheme for cumulus parameterization in large-scale models. *Mon. Weather Rev.*, 117:1779–1800, 1989.

S. Tilmes, D. E. Kinnison, R. R. Garcia, R. Salawitch, T. Canty, J. Lee-Taylor, S. Madronich, and K. Chance. Impact of very short-lived halogens on stratospheric ozone abundance and UV radiation in a geo-engineered atmosphere. *Atmospheric Chemistry and Physics*, 12:10945–10955, 2012.

C. Timmreck and H.-F. Graf. The initial dispersal and radiative forcing of a Northern Hemisphere mid-latitude super volcano: a model study. *Atmospheric Chemistry and Physics*, 6: 35–49, 2006.

C. Timmreck, H.-F. Graf, and I. Kirchner. A one and half year interactive MA / ECHAM4 simulation of Mount Pinatubo Aerosol. *Journal of Geophysical Research*, 104:9337–9359, 1999.

M. Toohey, K. Krüger, U. Niemeier, and C. Timmreck. The influence of eruption season on the global aerosol evolution and radiative impact of tropical volcanic eruptions. *Atmospheric Chemistry and Physics*, 11:12351–12367, 2011.

D. W. Valentine, E. A. Holland, and D. S. Schimel. Ecosystem and physiological controls over methane production in northern wetlands. *J. Geophys. Res.*, 99:1563–1571, 1994.

J. A. Van Aardenne, F. J. Dentener, J. G. J. Olivier, C. G. M. Klein Goldewijk, and J. Lelieveld. A High Resolution Dataset of Historical Anthropogenic Trace Gas Emissions for the Period 1890-1990. *Global Biogeochemical Cycles*, 15:909–928, 2001.

R. J. van der A, M. a. F. Allaart, and H. J. Eskes. Multi sensor reanalysis of total ozone. *Atmospheric Chemistry and Physics*, 10:11277–11294, 2010.

G. R. van der Werf, J. T. Randerson, L. Giglio, G. J. Collatz, M. Mu, P. S. Kasibhatla, D. C. Morton, R. S. DeFries, Y. Jin, and T. T. van Leeuwen. Global fire emissions and the contribution of deforestation, savanna, forest, agricultural, and peat fires (1997–2009). *Atmospheric Chemistry and Physics*, 10:11707–11735, 2010.

T. P. C. van Noije, P. L. Sager, A. J. Segers, P. F. J. van Velthoven, M. C. Krol, W. Hazeleger, A. G. Williams, and S. D. Chambers. Simulation of tropospheric chemistry and aerosols with the climate model EC-Earth. *Geoscientific Model Development*, 7:2435–2475, 2014.

C. Veldt. Updating and upgrading the PHOXA emission database to 1990, TNO report R 92-118/112322-23155. TNO-MW, Delft, 1992.

E. Vignati, M. Facchini, M. Rinaldi, C. Scannell, D. Ceburnis, J. Sciare, M. Kanakidou, S. Myriokefalitakis, F. Dentener, and C. O'Dowd. Global scale emission and distribution of sea-spray aerosol: Sea-salt and organic enrichment. *Atmospheric Environment*, 44:670–677, 2010.

E. Vignati, J. Wilson, and P. Stier. M7: An efficient size-resolved aerosol microphysics module for large-scale aerosol transport models. *Journal of Geophysical Research: Atmospheres*, 109: D22202, 2004.

A. Voulgarakis, V. Naik, J.-F. Lamarque, D. T. Shindell, P. J. Young, M. J. Prather, O. Wild, R. D. Field, D. Bergmann, P. Cameron-Smith, I. Cionni, W. J. Collins, S. B. Dalsøren, R. M. Doherty, V. Eyring, G. Faluvegi, G. A. Folberth, L. W. Horowitz, B. Josse, I. A. McKenzie, T. Nagashima, D. A. Plummer, M. Righi, S. T. Rumbold, D. S. Stevenson, S. a. Strode, K. Sudo, S. Szopa, and G. Zeng. Analysis of present day and future OH and methane lifetime in the ACCMIP simulations. *Atmospheric Chemistry and Physics Discussions*, 12:22945–23005, 2012.

A. Voulgarakis, V. Naik, J.-F. Lamarque, D. T. Shindell, P. J. Young, M. J. Prather, O. Wild, R. D. Field, D. Bergmann, P. Cameron-Smith, I. Cionni, W. J. Collins, S. B. Dalsøren, R. M. Doherty, V. Eyring, G. Faluvegi, G. A. Folberth, L. W. Horowitz, B. Josse, I. A. MacKenzie, T. Nagashima, D. A. Plummer, M. Righi, S. T. Rumbold, D. S. Stevenson, S. A. Strode, K. Sudo, S. Szopa, and G. Zeng. Analysis of present day and future OH and methane lifetime in the ACCMIP simulations. *Atmospheric Chemistry and Physics*, 13:2563–2587, 2013.

B. P. Walter, M. Heimann, and E. Matthews. Modeling modern methane emissions from natural wetlands 2. Interannual variations 1982–1993. *Journal of Geophysical Research*, 106: 34,207–34,219, 2001.

J. S. Wang, J. A. Logan, M. B. Mcelroy, B. N. Duncan, I. A. Megretskaia, and R. M. Yantosca. A 3-D model analysis of the slowdown and interannual variability in the methane growth rate from 1988 to 1997. *Global Biogeochemical Cycles*, 18:GB3011, 2004.

Y. Wang and D. J. Jacob. Anthropogenic forcing on tropospheric ozone and OH since preindustrial times. *Journal of Geophysical Research*, 103:31,123–31,135, 1998.

R. Wania, J. R. Melton, E. L. Hodson, B. Poulter, B. Ringeval, R. Spahni, T. Bohn, C. a. Avis, G. Chen, a. V. Eliseev, P. O. Hopcroft, W. J. Riley, Z. M. Subin, H. Tian, P. M. van Bodegom, T. Kleinen, Z. C. Yu, J. S. Singarayer, S. Zürcher, D. P. Lettenmaier, D. J. Beerling, S. N. Denisov, C. Prigent, F. Papa, and J. O. Kaplan. Present state of global wetland extent and wetland methane modelling: methodology of a model inter-comparison project (WETCHIMP). *Geoscientific Model Development*, 6:617–641, 2013.

K. T. Whitby. The physical characteristics of sulfur aerosols. *Atmospheric Environment (1967)*, 12:135–159, 1978.

O. Wild, X. I. N. Zhu, and M. J. Prather. Fast-J : Accurate Simulation of In- and Below-Cloud Photolysis in Tropospheric Chemical Models. *Journal of Atmospheric Chemistry*, 37:245–282, 2000.

K. Willeke and K. T. Whitby. Atmospheric Aerosols: Size Distribution Interpretation. *Journal of the Air Pollution Control Association*, 25:529–534, 1975.

J. E. Williams, J. Landgraf, A. Bregman, and H. H. Walter. A modified band approach for the accurate calculation of online photolysis rates in stratospheric-tropospheric Chemical Transport Models. *Atmospheric Chemistry and Physics*, 6:4137–4161, 2006.

J. E. Williams, A. Strunk, V. Huijnen, and M. van Weele. The application of the Modified Band Approach for the calculation of on-line photodissociation rate constants in TM5: implications for oxidative capacity. *Geoscientific Model Development*, 5:15–35, 2012.

D. J. Wilton, C. N. Hewitt, and D. J. Beerling. Simulated effects of changes in direct and diffuse radiation on canopy scale isoprene emissions from vegetation following volcanic eruptions. *Atmospheric Chemistry and Physics*, 11:11723–11731, 2011.

E. W. Wolfe and R. P. Hoblitt. Overview of the Eruptions. In C. G. Newhall and R. S. Punongbayan, editors, *FIRE and MUD: Eruptions and Lahars of Mount Pinatubo, Philippines*. University of Washington Press, Philippine Institute of Volcanology and Seismology, Quezon City, 1996.

R. E. Young, H. Houben, and O. B. Toon. Radiatively forced dispersion of the Mt . Pinatubo volcanic cloud and induced temperature perturbations in the stratosphere during the first few months following the eruption. *Geophysical Research Letters*, 21:367–372, 1994.

F. J. Zeleznik. Thermodynamic Properties of the Aqueous Sulfuric Acid Systems to 350 K. *J. Phys. Chem. Ref. Data*, 20:1157–1198, 1991.

T. X.-P. Zhao, P. K. Chan, and A. K. Heidinger. A global survey of the effect of cloud contamination on the aerosol optical thickness and its long-term trend derived from operational AVHRR satellite observations. *Journal of Geophysical Research: Atmospheres*, 118: 2849–2857, 2013.

ACKNOWLEDGMENTS

I would like to thank my supervising team, Maarten, Michiel, Twan and Thomas, first of all for thinking of this interesting interdisciplinary project that fitted me so well and for giving me the opportunity to work on it, although I had no knowledge about atmospheric chemistry when I started. Having you as supervisors was a very nice experience for me, as I could benefit from your vast knowledge and there was always someone there to help me when I needed it. Maarten, you have a contagious enthusiasm and every conversation with you leaves me with many new ideas. Michiel, thank you for your patience in the first years of my PhD when I learned a lot about atmospheric processes during our long discussions. Twan and Thomas, thank you for your valuable input and insightful comments.

I am happy that I had the opportunity to experience two working places with two different working environments during my PhD. I also had two very nice groups of colleagues who were always willing to help and who have taught me a lot. Thank you colleagues in APCG and CK for the interesting discussions during meetings and coffee breaks, and for giving me useful feedback on my work. The many dinners, parties and social gatherings we had together made me feel very welcome from the start.

Thank you Philippe and Sourish for being the friendly modelling help-desk whenever I needed some programming advice. Yvonne and Sandra, thank you for your help and support. I would also like to thank the TM5 community, collaborators from the SSiRC community and fellow methane researchers at Utrecht University for the fruitful scientific discussions and collaborations.

Thank you NWO for funding my research, and SURFsara for giving me access to the Cartesius supercomputer. Thank you Dorina Codaţ, Angela Berceanu and the ROTARY foundation for supporting me during my studies. I would also like to thank Daly Marciuc, who encouraged my interest in mathematics and helped me put the first building blocks of my scientific knowledge.

Elena, thank you for arranging that I am your office-mate before we even knew each other and for not having kicked me out yet. I had a lot of fun during our adventures in the Dutch wilderness. Elena and Sony, I enjoyed a lot our many coffee breaks with ‘fresh air’ and nice conversations. Sony, I am glad to have shared with you the joys and worries of approaching the finish line. Clifford, it was nice to have you as an office-mate during most of my PhD. Our conversations about future plans always motivated me. Thank you also Frans and Abhijit for your pleasant company in the office. I am happy to have been part of such a diverse group of PhD students. I would like to thank Supun, Guillaume, Sudhanshu, Joseph, Markella, Christiana,

Dewi, Bea, Carlos, Arjan, Dorota and Marion for sharing many nice moments at BBOS, BBQs and Christmas dinners, or spontaneous picnics in the park. Celia, Magdalena and the Earth, Wind and Choir, it was so nice to make music together after a long day of programming. Thank you friends from Rembrantkade 3, Anastasia, Tom, Aspa, Rafael and Maxim, for the good times we had exploring Utrecht and the Netherlands together.

Îţi mulţumesc, mamă, că m-ai sprijinit şi m-ai încurajat întotdeauna să-mi urmez visele. Finally, a big thank you to Vali, I am very grateful for your support during the difficult moments of my PhD. Thank you for your love and patience, and for always knowing how to bring up my mood.

ABOUT THE AUTHOR

Narcisa Bândă was born on June 23, 1986 in Satu Mare, Romania. She was a passionate problem solver from a very young age, participating in many mathematical competitions in Romania. In 2005 she enrolled in the bachelor studies in Mathematics at University of Bucharest, and one year later she also began following the courses in Physics at the same university. Her mathematics bachelor thesis on Noetherian rings reflected her early interest in theoretical mathematics. Her growing interest in more applied subjects, such as fluid mechanics and environmental science, led her to do her physics bachelor thesis on boundary layer height. In 2009, she left to Scotland to do a masters degree in Applied Mathematical Sciences with Climate Change Impacts Modelling at Heriot-Watt University in Edinburgh, which strengthened her numerical modelling skills and deepened her interest in climate research. During her dissertation project, she developed a two-dimensional shallow-water model under the guidance of prof. Gabriel Lord. In November 2010 she moved to Utrecht to pursue a PhD at the Institute for Marine and Atmospheric research Utrecht (IMAU) and the Netherlands Roral Meteorological Institute (KNMI), and the research results are presented in this thesis. Narcisa currently continues to work at IMAU, where she received a postdoc position on inverse modelling of carbon monoxide and carbon dioxide.

This document was typeset using `classicthesis` developed by André Miede.